UNIVERSITÀ DI PARMA

UNIVERSITA' DEGLI STUDI DI PARMA

DOTTORATO DI RICERCA IN

Scienze del Farmaco

CICLO XXXVII

Intranasal administration of advanced drug delivery systems encapsulating peptidic and biological drugs: in vitro, ex vivo and in vivo evaluation

Coordinatore:
Chiar.mo Prof. MARCO MOR

Tutore:
Chiar.mo Prof. FABIO SONVICO

Dottorando: FABIOLA GUARESCHI

Anni Accademici 2021/2022 – 2023/2024

Ai miei genitori e a Nicolò

Acknowledgements

First of all, I would like to thank my supervisor Prof. Fabio Sonvico, that contributed to my professional growth in these years, guiding me in the amazing world of pharmaceutical technology. Thank you for always giving me the best of your knowledge but at the same time leaving me the opportunity to express my opinion and put my ideas into practice.

I also would like to thank all the colleagues and Professors of the Advanced Drug Delivery Research Laboratory (ADDRes Lab) of Food and Drug Department at the University of Parma, especially Prof. Ruggero Bettini for giving me the opportunity to work in this laboratory and always being available to offer me valuable advice when needed. I would like to express a special thanks to all my colleagues from ADDRes Lab for supporting me every day, for sharing your ideas with me, helping me in difficult times and making me smile in the hardest moments. You are special people, and you have been like a family during these years.

Special thanks to Prof. Eride Quarta, my friend as well as an admirable Professor. Thank you for sharing your knowledge in managing the many projects we worked on together, for always giving me valuable advice and honest opinions, and for making each of our experiences abroad unforgettable.

Thanks to my friend and colleague Virginia Patterlini, for the professionalism, organization and efficiency demonstrated during the endless hours spent working together in the laboratory. Our complicity was certainly a fundamental factor in achieving each goal.

Thanks to Prof. Sara Nicoli and Prof. Silvia Pescina, for providing me with valuable advice necessary to continue my projects, as well as giving me essential materials to go on with my research.

I would also like to thank Prof. Annalisa Bianchera, for guiding me during the *in vitro* studies and for having transmitted her knowledge to me with dedication, professionalism and patience.

Thanks to Prof. Cristina Sissa and her team from SCVSA Department of the University of Parma, especially to Dott. Andrea Delledonne and Dott. Ilaria Ferraboschi, for the support they gave to me during the two-photon microscope analysis.

Many thanks to Prof. Elena Del Favero and Dott. Caterina Ricci for the support you gave me during the characterization phase of my formulations, and for giving me the opportunity to work together with you at the European Synchrotron Radiation Facility (ESRF) in Grenoble, at the Neutron Center in Budapest and in your laboratory placed at the University of Milan. Special thanks to Prof. Laura Cantù, thank you for the kindness and clarity with which you provided me with explanations on physics and for your exemplary professionalism, which will remain an indelible memory for me.

Thanks to Prof. Ravin Narain and his team, in particular Leslie Vanessa Snachez Castillo and Eleni Tsekoura, for the exciting project we worked at together, and the interesting results we reached.

Finally, I would like to express a special thanks to Prof. Ana Fortuna and her team from the Pharmacology Laboratory of the Pharmacy Department at the University of Coimbra, Portugal. You gave me the opportunity to explore the interesting field of pharmacology, giving me the opportunity to improve my knowledge, working in a field that was not properly my “comfort-zone”. Thank you for warmly welcoming me and always making me feel at home.

Summary

GENERAL INTRODUCTION

CHAPTER 1

CHAPTER 2

CHAPTER 3

List of Symbols and Acronyms

α	Alpha
Δ	Delta
Δρ	Contrast term
λ	Incident X-ray wavelength
µM	Micromolar
°	Plume angle
θ	Scattering angle
BBB	Blood-Brain-Barrier
BFT	Buried Food Test
BSA	Bovine serum albumin
$CaCl_2$	Calcium chloride
CaN	Calcineurin
C_{exp}	Experimental concentration
C_{nom}	Nominal concentration
CNS	Central Nervous System
COX-2	Cyclo-oxygenase-2
CPS	Conventional multidose preservative-free spray pump
CSA	Cyclosporine A
CSF	Cerebrospinal Fluid
CSS	Core-shell sphere
Ct	Cycle Threshold
CV	Coefficient of Variation
CXB	Celecoxib
Cy3	Cyanine3
CypA	Cyclophilin A
Da	Dalton
DAD	Diode array detection

DAPI	4’,6-diamidino-2-phenylindole
DI	Discrimination Index
DLS	Dynamic Light Scattering
Dmax	Maximum diameter
Dmin	Minimum diameter
D_2O	Deuterium oxide
DS	Dextran sulfate
DSD	Droplet Size Distribution
D_{V50}	Mean volume diameter
ECS	Extracellular Space
EE	Encapsulation Efficiency
f	Aperture diameter
FBS	Fetal bovine serum
FDA	Food and Drug Administration
H	Dynamic viscosity
HA	Hyaluronic acid
HCl	Hydrochloric acid
HL	High-Loading micelles
HPLC	High Performance Liquid Chromatography
HPMC	Hydroxypropylmethyl cellulose
HS	Hard sphere
IgG	Immunoglobulin G
IL-1	Interleukin-1
IL-2	Interleukin-2
IN	Intranasal
I(q)	Scattered intensity
IS	Internal Standard
KCl	Potassium chloride
LL	Low-Loading micelles
LLOQ	Lower Limit of Quantification
LPS	Lipopolysaccharide

MEM	Minimum Essential Medium
MERS-CoV	Middle East Respiratory Syndrome coronavirus
ML	Medium-Loading micelles
mMRT	Mucosal mean residence time
m.o.i	Multiplicity of infection
MOM	MuDT Oligo Mixture
N	Number of particles
NA	Numerical aperture
NaCl	Sodium chloride
NALT	Nose-associated lymphoid tissue
NaOH	Sodium hydroxide
NORT	Novel Object Recognition Test
NP	Nanoparticles
N2B	Nose-to-Brain
OFT	Open Field Test
OMP	Olfactory Marker Protein
OR	Odorant receptor
OR10R2	Odorant Receptor, family 10, subfamily R, member 2
ORN	Olfactory receptor neurons
PALS	Phase Analysis Light Scattering
PBS	Phosphate-buffered saline
PDI	Polydispersity Index
PEG	Poly(ethylene) glycol
PFA	Paraformaldehyde
PG	Plume geometry
P-gp	P-glycoprotein
PI	Preference Index
P(q)	Particle form factor
PVA	Poly(vinyl alcohol)
q	Scattering vettor
QC	Quality Control

RE	Relative Error
ROI	Regions of interest
rpm	Round per minute
SANS	Small Angle Neutron Scattering
SARS-CoV-2	Severe Acute Respiratory Syndrome Coronavirus 2
SAXS	Small Angle X-ray Scattering
SD	Standard deviation
SHG	Second Harmonic Generation
siRNA	Small interfering RNA
Sld	Scattering length density
SNES	Simulated Nasal Electrolyte Solution
SP	Spray Pattern
S(q)	Structure factor
TFA	Trifluoroacetic acid
TMC	Trimethyl chitosan
TNF-α	Tumor necrosis factor-alpha
TPEF	Two-photon excited fluorescence
TPGS	α-tocopheryl-polyethylene-glycol 1000 succinate
TPP	Tripolyphosphate
Triton-X100	Polyethylene glycol tert-octylphenyl ether
TST	Tail Suspension Test
V	Volume
WHT	Wire Hanging Test
X g	Gravitational force

List of Figures

General Introduction

Chapter 1

SUPPLEMENTARY MATERIAL

Chapter 2

SUPPLEMENTARY MATERIAL

Chapter 3

List of Tables

Chapter 1

SUPPLEMENTARY MATERIAL

Chapter 2

SUPPLEMENTARY MATERIAL

Chapter 3

Aim of the Thesis

The aim of this Doctoral Thesis is to evaluate the effectiveness of nasal therapies through different levels of study: *in vitro*, *ex vivo* and *in vivo*.

In this perspective, the nose is studied here as a potential effective deposition site for several therapeutic purposes, including antiviral activity and neuroprotection. These latter are experimentally demonstrated in this work *in vitro* and *in vivo*, respectively. Other applications, such as vaccination, are widely described in literature and contribute to broaden the range of therapies for which nasal administration represents an effective alternative to conventional and invasive route of administrations.

Considering that the nasal mucosa is the first anatomical section with which a drug interacts once administered to the nasal cavity, the main anatomical and functional features of this tissue are widely analyzed. The in-depth study of the nasal mucosa, done by exploiting an *ex vivo* animal model, has been done with the aim of understanding the main difference between the respiratory and the olfactory region in both anatomical and functional terms.

In addition to this, given that it is well known that the nasal mucosa can hinder the absorption of drugs due to its physiological features including the overlining mucus layer and the related mucociliary clearance, nanotechnology is described here as a tool to overcome these potential issues.

Nanosystems indeed, are widely leveraged in this work with the aim of overcoming the limits represented by physiological barriers, while on the other hand ensuring the stability of challenging cargoes such as peptides or genetic material, in order to effectively reach the target allowing for therapeutic effect.

Finally, this work aims at identifying the most suitable nasal device for each different therapeutic goal to be achieved, basing on the ability of the device to deliver the formulation to the desired area of the nose, responsible for drug absorption and effect.

GENERAL INTRODUCTION

This Chapter was partially taken from the following published Review: Sonvico, F., Colombo, G., Quarta, E., **Guareschi, F.**, Banella, S., Buttini, F., & Scherließ, R. "Nasal delivery as a strategy for the prevention and treatment of COVID-19," *Expert Opin. Drug Deliv.*, vol. 20, no. 8, pp. 1115–1130, 2023, doi: 10.1080/17425247.2023.2263363.

1. GENERAL INTRODUCTION

1.1 The nose as a target for drug delivery

The nasal route of administration has been widely explored in the last decades as a potentially effective alternative to the classic oral and parenteral routes for drug delivery.

Owing to its anatomical and physiological characteristics indeed, the nose represents an interesting deposition site for therapeutic agents. The external part of the nose presents two nostrils allowing the access to the two nasal cavities, that are separated by the septum [1]. The nasal cavities, each characterized by a volume of 7.5 mL [2], extend approximately 12-14 cm between the nostrils and the nasopharynx, that is the junction between the nose and the pharynx [1]. The nose is internally divided by inferior, middle and superior turbinates, consisting of three projections from the nasal walls [3] thank to which the total surface area of the nose is increased to 150 cm^2 [2 3] (**Figure 1**). This wide surface area not only allows a more efficient humidification of the inhaled air, but also represents the target for intranasally delivered drugs that can have a locally or a systemic effect [2].

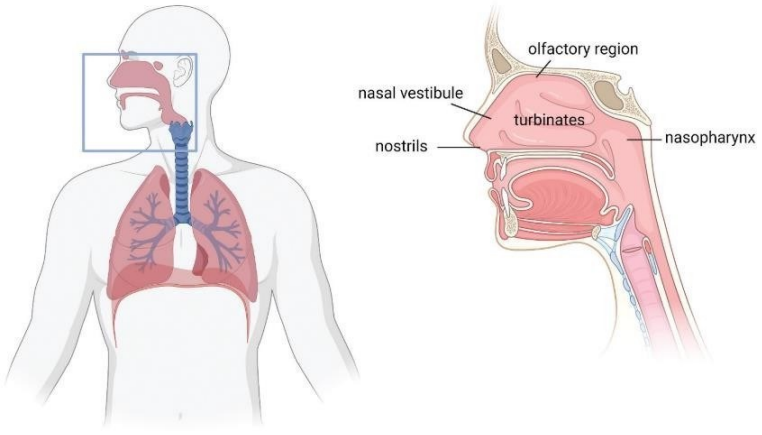

Figure 1 *– Anatomical features of the nose (right), that is part of the upper respiratory tract (left). Two nostrils open into the nasal cavity, that is internally divided by three turbinates. The olfactory epithelium is located in the upper part of the nasal cavity, near the superior turbinate. Figure reproduced from [4].*

The nasal mucosa is composed by three different epithelial cells: stratified squamous, pseudostratified columnar and transitional [5,6]. The anterior part of each cavity is mainly composed of stratified squamous and transitional epithelium, that are not characterized by cilia and

mostly not vascularized [2]. The posterior part of the nasal cavity is called "respiratory region" and consists of a columnar epithelium, characterized by cilia, Goblet cells secreting mucus and basal cells [3] (**Figure 2**). This region is highly vascularized and presents nerves and an extensive lymphatic network as well [3,7]. Finally, near the superior turbinate and adjacent to the nasal septum, is located the olfactory epithelium [7] (**Figure 1**), representing approximately 3-5% of the total area of the nasal surface [8]. Three different types of cells characterize the olfactory epithelium: olfactory sensory neurons, supporting cells and basal cells [9]. Olfactory neurons have their dendritic portion extending above the epithelial surface and terminating into the olfactory bulb [10]. Approximately 10-15 immotile cilia expressing odor receptors on their membrane protrude from the olfactory bulb, allowing the detection of inhaled odors [10]. Moreover, the axons of these olfactory neurons cross the basal lamina of the cells and join the axons belonging to other olfactory neurons, thus forming a network of nonmyelinated nerves into the lamina propria [9]. These nerve bundles pass through the cribriform plate separating the nasal cavity from the brain, and form the outer layer of the olfactory bulb [9] (**Figure 2**).

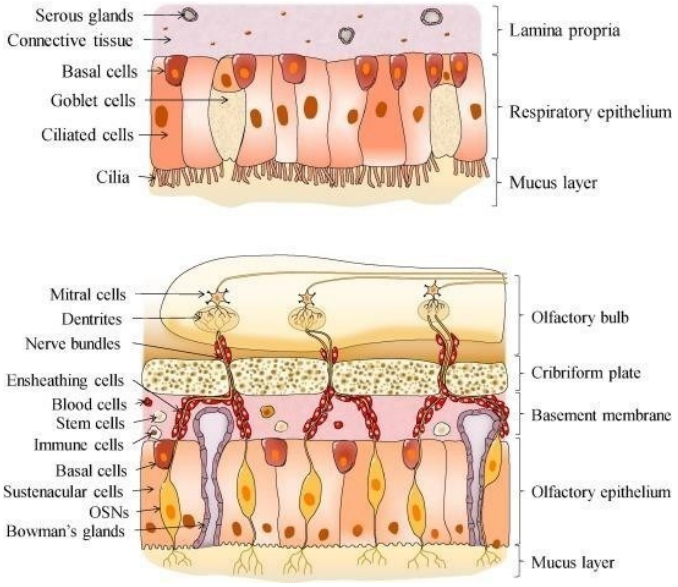

Figure 2 – *The different types of epithelia characterizing the nasal mucosa. The respiratory epithelium (above), mainly composed of goblet cells secerning mucus, basal cells and ciliated cells; the olfactory epithelium (below), presenting olfactory neurons, basal cells and supporting cells. Figure from* [11].

1.2 Advantages of nasal delivery compared to the classic routes of administration

It has been shown that the nasal administration of drugs has remarkable advantages compared to the classic routes of administration as the oral and the parenteral ones. These advantages include the rapid absorption due to the wide surface area and high vascularization of the nasal cavity,

allowing a high bioavailability of therapeutic molecules. This aspect is important because allows to significatively reduce the administered dose, contributing to prevent the risk of side effects [12]. Moreover, the nasal route of administration guarantees a rapid onset of action, and for this reason it is attractive in those cases in which a fast therapeutic effect is required (*e.g*. migraine, Parkinson rigidity, seizures, cardiovascular events) [13]. In addition to this, once a drug is intranasally administered, it does not undergo liver first pass metabolism or metabolism at the gastrointestinal level, thus avoiding the partial or total conversion of the drug into inactive metabolites and at the same time preventing the irritation of the gastrointestinal tract [12]. Noteworthy, the intranasal route is not invasive and it doesn't require needles for the administration, therefore it is associated to a reduced risk of infection and, as reported in literature, also to a reduced risk of overdose and infectious diseases transmission [12]. A pivotal aspect of nasal therapy is the ease of administration and the possibility of self-medication, an important aspect to optimize the patient compliance [12].

1.3 Therapeutic effects

1.3.1 Local effect

The nasal administration of drugs can be exploited when a localized therapeutic effect is required, for example to treat localized pathologic conditions such as rhinitis, sinusitis or allergic episodes [14]. Several drugs including corticosteroids, anti-histamines, anti-cholinergic and vasoconstrictors can be intranasally administered with this purpose, being formulated as solutions, gels, suspensions or emulsions [14].

In addition to this, it must be considered that the nasal cavity represents the access to a wide range of pathogens that can be directly driven into the nostril by the inhaled air causing infections both in the upper or in the deeper region of the respiratory tract, in some cases leading to severe complications. The first preventive measure to avoid this risk consists in avoiding the contact between the inhaled pathogens and the nasal mucosa. For this purpose, a number of nasal products acting as a barrier can be exploited to have a local protective effect and have experienced a significant success during COVID-19 pandemic [4]. These products, mostly marketed in the form of nasal sprays, can be exploited to prevent the spread of the infection when there is a high risk of transmission, for example in crowded places, schools and hospitals [4]. Moreover, these nasal products can also be used to reduce the severity and the duration of the symptoms caused by respiratory infection [15,16]. In this application, acting as a "second line" prevention, they can reduce the risk to have an increasing pathogen loading into the nasal cavity after when the infection has already occurred [4]. The therapeutic effect of these barrier products is considered passive, since it is mainly due to a non-specific mechanism of action; hence, these products can be useful in those

situations in which any pathogen's mutations can have a negative impact on the efficiency of the therapy [17]. Barrier nasal products are mainly marketed as medical devices; they can contain for example natural compounds such as carrageenans and bentonite, or chemical derivatives such as hydroxypropyl methyl cellulose, that in contact with the nasal secretions hydrate and form a protective gel layer on the mucosa. In addition to this, there are products containing compounds such as astodrimer sodium, that not only can form a barrier but are also able to interact with positively charged surface proteins of the pathogen, hindering their binding to the mucus and the underlying tissue [4].

In addition to the so called "barrier products" characterized by a non-specific mechanism of action, there is a number of molecules characterized by a known and specific antimicrobial activity that can be exploited to locally counteract the infection. Favipiravir, ivermectin and chlorpheniramine maleate are among the most studied for this purpose, especially starting from the pandemic period, due to their ability to hinder viral replication or its entry into the cells. More precisely, favipiravir inhibits viral RNA-dependent RNA polymerase and for this reason it is approved against influenza RNA-viruses [18]; to enhance the residence time of the treatment at the deposition site, this drug has been encapsulated into mucoadhesive chitosan/alginate nanoparticles [19]. Ivermectin has demonstrated antiviral properties *in vitro* against SARS-CoV-2, probably owing to the ability to inhibit the importin-α/β1-mediated nuclear entry of viral proteins, leading to the block of viral RNA replication [20]. Also in this case, it is reported in literature that the drug has been formulated as a mucoadhesive nanosuspension containing hydroxypropylmethyl cellulose (HPMC), poloxamer and alginate [21]. Finally, chlorpheniramine maleate demonstrated antiviral properties when formulated as a nasal spray [22], and the activity was attributed to the ability of the drug to hinder the viral entry into cells [23].

1.3.2 Nasal vaccines and systemic effect

The nose is considered a key component of the mucosal immune system of the upper respiratory tract [4]. Indeed, the nose-associated lymphoid tissue (NALT) is located at the level of the tonsils, but there are dendritic cells along the nasal epithelium that are specialized in taking up and processing antigenic materials [24]. The mucosal immune system, consisting of lymphoid tissues and dendritic cells, is considered the largest immunocompetent tissue in the human body [4]. The activation of this system by an antigen leads to a local and specific immune response, that successively can spread throughout the body following the "common mucosal immune system" [25]. The mucosal immune response consists in a combination of both a T-cell response and an IgA-based humoral response [26]. IgA are specific antibodies produced at the mucosal level and secreted on the mucosalexternal surface, where they interact with pathogens neutralizing them, thus preventing the

infections [27]. The presence and the activity of NALT makes the nose an ideal target for mucosal vaccination against airborne pathogens; however, it must be considered that the mucosal surfaces are constantly in contact with foreign bodies, and for this reason they can mediate both the mucosal immune activation and the induction of tolerance [25]. Therefore, the agent administered to stimulate the immune system has necessary to be of a particulate nature, in order to elicit a full immune response [28].

Nasal vaccination is characterized by remarkable advantages against the classic intramuscular injection; for example, it is not invasive and it does not require administration by healthcare professionals [4]. Moreover, it has been shown [29,30] that in some cases nasal vaccination allows to develop a stronger protection than that reached after a classic vaccination. More precisely, the superiority of nasal vaccination in terms of efficacy has been reported against those pathogens characterized by a high rate of mutations (*e.g.* influenza virus) [29,30].

Nasal vaccines can be formulated as liquids or powders taking into account the needs in terms of dosing and stability, for example in those cases in which the vaccine has to be administered to populations living in countries where cold-chain is not guaranteed and the transport is challenging [4].

Interestingly, before the pandemic period, only few nasal vaccines had been licensed and were available [31]. However, it was observed that the first developed vaccine against Severe Acute Respiratory Syndrome Corona Virus 2 (SARS-CoV-2) for parenteral use was unable to give rise to the expression and activation of neutralizing antibodies, pivotal to reduce infection severeness and viral spread [4]. This opened the discussion about the possibility of exploiting alternative routes of administration such as the nasal one [32], that led to have currently 8 nasal vaccines to prevent the SARS-CoV-2 infection in ongoing clinical study level [32–34] and six nasal vaccines approved in local markets [35].

Finally, in addition to the use as a target for nasal vaccination, the nasal route of administration has been studied over the recent decades as an effective and safe approach to reach a systemic effect of drugs [14]. This is possible thanks to the abundance of blood vessels characterizing the nasal mucosa, that can absorb the administered drug molecules [14]. Importantly, it has been reported that in some studies the nasal drug absorption turned out to be almost equal to the oral absorption [36].

1.3.3 Nose-to-Brain

It is well-known that drugs intended to treat neurological Central Nervous System (CNS) disorders have a pivotal prerequisite, consisting in the ability of crossing the Blood Brain Barrier (BBB) [37,38], a highly specialized brain endothelial structure [39]. BBB consists of layers of tightly packed cells located at the endothelial level of the brain capillaries that physiologically hinders the passage of mostly of

the molecules circulating in the bloodstream to the brain and the cerebrospinal fluid (CSF) [40].

As a consequence, the access of most of the therapeutic agents to CNS at therapeutic concentrations is strongly limited [41].

To overcome this issue, several strategies have been adopted, mostly extremely invasive since required neurosurgical procedures to direct inject the therapy in the brain's region of interest [42,43].

On the other hand, the Nose-to-Brain (N2B) delivery can be efficiently exploited as a non- invasive route allowing the delivery of intranasally administered drugs, comprehending peptides, directly to the CNS exploiting the olfactory "neuroepithelium" [44]. Indeed, the latter can be considered a natural and direct access to the brain [45] for both small and large molecules, since it is known that molecules intranasally administered are able to bypass the BBB and directly reach the CNS exploiting the olfactory and the trigeminal nerves located at the mucosal level [46], following an extracellular or a transcellular transport [47–52].

More precisely, there are four main pathways that allow the drug to reach the CNS. In the first case, the drug can be internalized into the olfactory neurons and transported along the axon; in the second case, the drug undergoes a paracellular transport exploiting the channels next to the olfactory nerves or the spaces between cells; in the third case, the drug crosses the basal epithelial cells following a transcellular transport [45,47–50,53]. The fourth case is represented by vascular pathway [46], consisting in the absorption of the drug into the systemic circulation exploiting the mucosal blood vessels; then, the drug is transported to the brain by crossing the BBB [54].

It is reported that the paracellular pathway is the dominant mechanism of transport among all the ones previously described [55]. Moreover, it allows the most rapid movement of active compounds from the nose to the brain (normally, less than 30 minutes); on the other hand, the other two mechanisms require a few hours or in some cases also days [49,56].

It has been hypothesized that the olfactory epithelium could allow the passage of drugs from the nasal cavity to the brain owing to the slow regeneration of the olfactory neurons (that takes around 1 month) and the coexistence of mature neurons; the result is that some parts of the olfactory epithelium show a partial absence of tight junctions and can be exploited as a passage for drugs [56]. In addition to this, the physiological bulk flow of the CSF into the brain contributes to drive the administered drugs to the CNS [49].

Once entered the CNS, the fate of a drug can be different basing on the cases. Indeed, the drug can accumulate selectively into one of the brain regions directly connected to the olfactory epithelium (*i.e.*, the piriform cortex, hypothalamus, amygdala) and/or distribute through the whole CNS [57].

1.4 Nanotechnology as a tool to overcome the limitations of nasal administration

1.4.1 Limitations affecting the nasal administration

Despite the remarkable advantages characterizing the intranasal administration described above, there are significant challenges associated with this innovative route.

First of all, nasal delivery is not applicable for all the drug molecules. Indeed, if a molecule is not sufficiently soluble in water it cannot be efficiently absorbed by the nasal mucosa [12]. This aspect becomes even more critical considering that the dose volume is limited to 25-200 µL per nostril, meaning that it is required a relatively high solubility of the drug to be administered in the desired amount [12]. Moreover, the extremely low volume administrable implies that nasal administration is limited just to drugs with high potency [13]. One other limitation is represented by the possible local irritation that some drugs can cause once in contact with the mucosa [12]; for this reason, nasal delivery is not considered suitable for chronic applications [12]. Moreover, the nasal mucosa is characterized by the presence of several enzymes including cytochrome P450, esterases and transferases [48,58–61] whose activity can cause the metabolic degradation of drugs [12].

Finally, there is a number of active compounds that, due to their intrinsic characteristics, are not able to permeate across the nasal mucosa due to their dimension, surface charge, lipophilicity and water solubility. This group of molecules includes for example peptides, proteins and nucleotides [13].

It must also be noted that the nasal mucosa is subjected to a continuous turnover of the overlying mucus layer, due to the mucociliary clearance. This system exploits the constant beat of the motile cilia to provide the transport of the mucus layer towards the nasopharynx [62] with a clearance $t_{1/2}$ of 20 minutes in humans [46]. This physiological function is essential to protect the respiratory tract from damages caused by inhaled pathogens [62]; however, being a non-specific mechanism, it can also provide the early removal of administered drug from the site of absorption or action. It follows that the chemical physical features of the drug play a pivotal role in the interaction with mucus laying on the surface of the mucosa. Indeed, the surface properties of the drug could represent a limitation for nasal delivery in those cases in which they favor the retention of the drug on the mucus layer and therefore its removal by mucociliary clearance.

Moreover, when nasal administration is exploited for N2B purposes, it must be considered that it is quite difficult to precisely deliver the drug on the olfactory region of the nasal epithelium; indeed, this latter is located in the roof of the nasal cavity, and this aspect makes it difficult to be reached by the administered drug [63,64].

1.4.2 Role of nanomedicine in nasal delivery

Nanomedicine offers a wide range of opportunities that can effectively be exploited to overcome the issues affecting the nasal delivery of drugs, described in the section above.

First, nanoparticle systems can be exploited to increase the drug apparent aqueous solubility [46], thus improving the absorption at the mucosal level. Moreover, nano-sized systems represent a platform to intranasally administer those molecules that, due to their features, could not be absorbed by the nasal epithelium as such. This group of drugs comprehends for example peptides, as well as biologics including RNA and DNA derivatives, that can be efficiently encapsulated into nanoparticle drug delivery systems and easily absorbed [65].

Additionally, the fact that high-potency drugs can be encapsulated often with high encapsulation efficiency, offers the opportunity of dramatically reducing the administered dose when exploiting nanocarriers for nasal delivery. This aspect is crucial from the point of view of the safety of the treatment, since the reduced dose is associated with a reduced risk of side effects including mucosal irritation. In addition, this allows the administration of low volume of product, thus bypassing one of the most critical aspects of the nasal delivery, that is the extremely low volume of dosages.

Noteworthy, nanosized (1-1000 nm) drug delivery systems guarantee the protection of the incapsulated drugs from chemical physical or enzymatic degradation to which they are exposed once in contact with the nasal environment [46]. This optimizes the efficiency of the therapy and allows to decrease the dose to reach the therapeutic effect.

Referring to a precise application of nasal delivery, namely N2B delivery, it becomes crucial to adopt strategies allowing the deposition of the drug specifically in a circumscribed anatomic region of the nose, *i.e.* the olfactory region. Despite the use of a suitable device such as a nasal atomizer, able to guarantee the deposition of the drug precisely in the upper part of the nose, remains pivotal to allow the N2B transport, nanotechnologies represent a valid opportunity to reach this goal [46]. Indeed, the nanoparticle surface can be modified to optimize the penetration across the mucus layer thus guaranteeing the mucosal absorption, or to improve the adhesion to the mucus layer thus avoiding mucociliary clearance [46].

The mucus layer (10–15 µm thick) lining on the surface of nasal epithelium is mainly composed of water (90-95%) and mucins (2-5 %) [66,67]. These latter glycoproteins provide to the mucus unique properties in terms of viscosity and elasticity [46] and contain high levels of sialic acids and sulfate residues. The overall negative charge provided by acid and sulfate groups is the main cause of the rigidity of the network [68], having a mesh spacing from 20 to 200-500 nm [69,70]. Moreover, the net negative charge allows the interaction between mucins and drugs through disulfide bridges, electrostatic attractive forces, hydrophobic interactions, hydrogen and Van der Waals bonds [71].

Surface-modified nanoparticles can be used as a suitable tool for enhancing mucoadhesion, for example exploiting polymeric excipients that, once in contact with mucus, can hydrate and then diffuse and entangle with mucin fibers [46]. Moreover, the adhesion to the mucus layer can also be improved by administering nanoparticles characterized by a positive surface charge (*e.g.*, chitosan nanoparticles [72]) to promote electrostatic interactions with the negative residues of mucus [46]. One other strategy may consists in the coating of the nanosystem with polymers (*e.g.*, poly(vinyl alcohol), PVA [73]) that allow to improve interaction with mucus probably, as it is reported, by hydrogen bonding and/or hydrophobic interactions with mucus components [46].

However, mucus represents a barrier that could hinder the interaction between the administered drug and the targeted tissue. Actually, the possibility that a particle has to cross the mucus layer depends on the interaction and size filtering properties of mucus itself [69]. In other words, mucopenetration can be achieved only if the physical chemical properties of the particle allow to avoid nonspecific particle-mucus interactions and at the same time to pass through the spaces characterizing the mucus mesh according to their size [46].

Some strategies have been proposed to bypass the issue represented by the filtering properties of mucus, including the synthesis of nanoparticles characterized by sufficiently small particle size coated with poly(ethylene) glycol (PEG) useful to minimize interactions with mucins thus leading to the direct contact with the underlying tissue [46].

Additional advantages that nanotechnology can bring include the possibility to precisely control the release kinetics of the encapsulated drug [46] and the possibility of modifying the surface of the nano-carrier to achieve a targeted drug delivery and limit the drug distribution to non- targeted sites, thus minimizing systemic side effects [46]. The remarkable advantages characterizing the nasal administration cited above and the wide range of therapeutic achievements that can be safely reached through this innovative route of administration have represented the basis of this thesis.

The aim of this work consisted of the deep exploration of the nasal route for drug delivery. Considering the physiological factors that can potentially represent an obstacle for drug absorption at the deposition site, nanotechnology was exploited as tool to overcome these issues.

The first chapter of this thesis entitled "*Cyclosporine A micellar nasal spray characterization and antiviral action against SARS-CoV-2*" regards the development of a TPGS micellar formulation encapsulating cyclosporine A (CSA). The formulation was fully characterized for physical/chemical features and its mucoadhesive properties have been tested on an *ex vivo* model of nasal mucosa. Then, the *in vivo* administration of the formulation in the form of a nasal spray was simulated using a human nasal cast exploiting different devices. Finally, the *in vitro* antiviral efficacy of micelles was tested exploiting different treatment protocols to simulate a preventive or healing treatment.

The second chapter of this thesis, entitled "*Therapeutic effect of cyclosporine A-loading TPGS micelles on a mouse model of LPS-induced neuroinflammation*" aimed to evaluate the *in vivo* therapeutic effects of the developed CSA-loading TPGS micelles against neuroinflammation, exploiting the Nose-to-Brain delivery. For this purpose, micelles were administered to CD-1 male mice injected with lipopolysaccharide (LPS) to induce neuroinflammation. Then, several selected behavioral tests have been used to assess the effect of CSA against depression, memory impairment and muscular weakness.

The third chapter of this thesis, entitled "*Application of rabbit nasal mucosa for ex vivo mucopenetration and mucoadhesion studies*" consists of an in-depth study of the nasal mucosa, realized by immunohistochemistry. The aim of this section was to highlight the main anatomical differences between the respiratory and the olfactory areas of the nasal mucosa, demonstrating the importance of using suitable drug delivery systems and devices to selectively allow the deposition of the drug on the olfactory region when a Nose-to-Brain delivery is desired. Once visualized the features of the nasal tissue, a chitosan-based nanoparticle formulation was used as model to explore the mucoadhesion and mucopenetration profiles using an *ex vivo* nasal mucosa exploiting the two-photons microscopy to analyze both the surface and the depth of the tissue.

REFERENCES

1. Kublik H, Vidgren MT. Nasal delivery systems and their effect on deposition and absorption. *Adv Drug Deliv Rev*. 1998;29(1):157-177. doi:10.1016/S0169-09X(97)00067-7
2. Suman JD. Current understanding of nasal morphology and physiology as a drug delivery target. *Drug Deliv Transl Res*. 2013;3(1):4-15. doi:10.1007/s13346-012-0121-z
3. Petruson B, Hansson H-A, Karlsson G. Structural and Functional Aspects of Cells in the Nasal Mucociliary System. *Arch Otolaryngol*. 1984;110(9):576-581. doi:10.1001/archotol.1984.00800350018006
4. Sonvico F., Colombo G., Quarta E., Guareschi F., Banella S., Buttini F., Scherließ R. Nasal delivery as a strategy for the prevention and treatment of COVID-19. *Expert Opin Drug Deliv*. 2023;20(8):1115-1130. doi:10.1080/17425247.2023.2263363
5. Adams DR. Transitional epithelial zone of the bovine nasal mucosa. *Am J Anat*. 1986;176(2):159-170. doi:10.1002/aja.1001760206
6. Boysen M. The surface structure of the human nasal mucosa. *Virchows Arch B*. 1982;40(1):279-294. doi:10.1007/BF02932871
7. Schipper NGM, Verhoef JC, Merkus FWHM. The Nasal Mucociliary Clearance: Relevance to Nasal Drug Delivery. *Pharm Res*. 1991;8(7):807-814. doi:10.1023/A:1015830907632
8. Morrison EE, Costanzo RM. Morphology of the human olfactory epithelium. *J Comp Neurol*. 1990;297(1):1-13. doi:10.1002/cne.902970102
9. Harkema JR, Carey SA, Wagner JG. The Nose Revisited: A Brief Review of the Comparative Structure, Function, and Toxicologic Pathology of the Nasal Epithelium. *Toxicol Pathol*. 2006;34(3):252-269. doi:10.1080/01926230600713475
10. Morrison E, Menco B. Morphology of the Mammalian Olfactory Epithelium: Form, Fine Structure, Function and Pathology.; 2003. doi:10.1201/9780203911457.ch2
11. Bourganis V, Kammona O, Alexopoulos A, Kiparissides C. Recent advances in carrier mediated nose-to-brain delivery of pharmaceutics. *Eur J Pharm Biopharm*. 2018;128:337-362. doi:10.1016/j.ejpb.2018.05.009
12. Behl CR, Pimplaskar HK, Sileno AP, DeMeireles J, Romeo VD. Effects of physicochemical properties and other factors on systemic nasal drug delivery. *Adv Drug Deliv Rev*. 1998;29(1-2):89-116. doi:10.1016/S0169-409X(97)00063-X
13. Touitou E, Illum L. Nasal drug delivery. *Drug Deliv Transl Res*. 2013;3(1):1-3. doi:10.1007/s13346-012-0111-1
14. Ghori, Muhammad U., Mahdi, Mohammed H., Smith, Alan M. and Conway BR. Nasal Drug Delivery Systems: An Overview. *Am J Pharmacol Sci*. 2015;3(5):110-119.

15. Ludwig M, Enzenhofer E, Schneider S, et al. Efficacy of a Carrageenan nasal spray in patients with common cold: a randomized controlled trial. *Respir Res*. 2013;14(1):124. doi:10.1186/1465-9921-14-124
16. Eccles R, Winther B, Johnston SL, Robinson P, Trampisch M, Koelsch S. Efficacy and safety of iota-carrageenan nasal spray versus placebo in early treatment of the common cold in adults: the ICICC trial. *Respir Res*. 2015;16(1):121. doi:10.1186/s12931-015-0281-8
17. Bentley K, Stanton RJ. Hydroxypropyl methylcellulose-based nasal sprays effectively inhibit in vitro SARS-CoV-2 infection and spread. *Viruses*. 2021;13(12). doi:10.3390/v13122345
18. Shiraki K, Daikoku T. Favipiravir, an anti-influenza drug against life-threatening RNA virus infections. *Pharmacol Ther*. 2020;209:107512. doi:10.1016/j.pharmthera.2020.107512
19. Djekic L. Novel Mucoadhesive Polymers for Nasal Drug Delivery. In: Pathak Y V, Yadav HKS, eds. *Nasal Drug Delivery: Formulations, Developments, Challenges, and Solutions*. Springer International Publishing; 2023:189-234. doi:10.1007/978-3-031-23112-4_11
20. Timani KA, Liao Q, Ye L, et al. Nuclear/nucleolar localization properties of C-terminal nucleocapsid protein of SARS coronavirus. *Virus Res*. 2005;114(1):23-34. doi:10.1016/j.virusres.2005.05.007
21. Zaki F.A, Shamardan E.E.S.B., Mohammed H.H., Abeer S.H., Alaa R., Rehab GH., Abdelmaksoud A.A. Clinical, Biochemical and Molecular Evaluations of Ivermectin Mucoadhesive Nanosuspension Nasal Spray in Reducing Upper Respiratory Symptoms of Mild COVID-19. *Int JNanomedicine*. 2021;16:4063-4072. doi:10.2147/IJN.S313093
22. Westover JB, Ferrer G, Vazquez H, Bethencourt-Mirabal A, Go CC. In Vitro Virucidal Effect of Intranasally Delivered Chlorpheniramine Maleate Compound Against Severe Acute Respiratory Syndrome Coronavirus 2. *Cureus*. 2020;12(9):e10501. doi:10.7759/cureus.10501
23. Xu W, Xia S, Pu J, et al. The antihistamine drugs carbinoxamine maleate and chlorpheniramine maleate exhibit potent antiviral activity against a broad spectrum of influenza viruses. *Front Microbiol*. 2018;9(NOV):1-13. doi:10.3389/fmicb.2018.02643
24. Davis SS. Nasal vaccines. *Adv Drug Deliv Rev*. 2001;51(1):21-42. doi:10.1016/S0169-409X(01)00162-4
25. Neutra MR, Kozlowski PA. Mucosal vaccines: the promise and the challenge. *Nat Rev Immunol*. 2006;6(2):148-158. doi:10.1038/nri1777
26. Janeway CA, Travers P, Walport M et al. The mucosal immune system. Immunobiology: the immune system in Health and disease 5th ed. (NY): Garland Science.
27. Ainai A, van Riet E, Ito R, et al. Human immune responses elicited by an intranasal

inactivated H5 influenza vaccine. *Microbiol Immunol*. 2020;64(4):313-325. doi:10.1111/1348-0421.12775

28. Csaba N, Garcia-Fuentes M, Alonso MJ. Nanoparticles for nasal vaccination. *Adv Drug Deliv Rev*. 2009;61(2):140-157. doi:10.1016/j.addr.2008.09.005
29. Belshe RB, Edwards KM, Vesikari T, et al. Live Attenuated versus Inactivated Influenza Vaccine in Infants and Young Children. *N Engl J Med*. 2007;356(7):685-696. doi:10.1056/nejmoa065368
30. Carter NJ, Curran MP. Live Attenuated Influenza Vaccine (FluMist®; Fluenz™). *Drugs*. 2011;71(12):1591-1622. doi:10.2165/11206860-000000000-00000
31. Xu H, Cai L, Hufnagel S, Cui Z. Intranasal vaccine: Factors to consider in research and development. *Int J Pharm*. 2021;609:121180. doi:10.1016/j.ijpharm.2021.121180
32. Alu A, Chen L, Lei H, Wei Y, Tian X, Wei X. Intranasal COVID-19 vaccines: From bench to bed. *eBioMedicine*. 2022;76. doi:10.1016/j.ebiom.2022.103841
33. Chavda VP, Vora LK, Pandya AK, Patravale VB. Intranasal vaccines for SARS-CoV-2: From challenges to potential in COVID-19 management. *Drug Discov Today*. 2021;26(11):2619-2636. doi:10.1016/j.drudis.2021.07.021
34. WHO. COVID-19 vaccine tracker and landscape. Available from: https://www.who.int/publications/m/item/draft-landscape-of -covid-19-candidate- vaccines.
35. Pilapitiya D, Wheatley AK, Tan H-X. Mucosal vaccines for SARS-CoV-2: triumph of hope over experience. *eBioMedicine*. 2023;92. doi:10.1016/j.ebiom.2023.104585
36. Rathbone, M. J., Hadgraft, J., & Roberts MS. Modified-release drug delivery technology. *Drugs and the Pharmaceutical Sciences*. Vol 126. 2002. doi:10.1016/j.ejpb.2003.10.011
37. Begley DJ. Delivery of therapeutic agents to the central nervous system: the problems and the possibilities. *Pharmacol Ther*. 2004;104(1):29-45. doi:10.1016/j.pharmthera.2004.08.001
38. Obermeier B, Daneman R, Ransohoff RM. Development, maintenance and disruption of the blood-brain barrier. *Nat Med*. 2013;19(12):1584-1596. doi:10.1038/nm.3407
39. Zlokovic B V. The Blood-Brain Barrier in Health and Chronic Neurodegenerative Disorders. *Neuron*. 2008;57(2):178-201. doi:10.1016/j.neuron.2008.01.003
40. Misra A, Kher G. Drug Delivery Systems from Nose to Brain. *Curr Pharm Biotechnol*. 2012;13(12):2355-2379. doi:10.2174/138920112803341752
41. Chen Y, Liu L. Modern methods for delivery of drugs across the blood–brain barrier. *Adv Drug Deliv Rev*. 2012;64(7):640-665. doi:10.1016/j.addr.2011.11.010
42. Pardridge WM. The blood-brain barrier: Bottleneck in brain drug development. *NeuroRx*. 2005;2(1):3-14. doi:10.1602/neurorx.2.1.3

43. Talegaonkar S, Mishra PR. Intranasal delivery: An approach to bypass the blood brain barrier. *Indian J Pharmacol*. 2004;36(3).
44. Samaridou E, Alonso MJ. Nose-to-brain peptide delivery – The potential of nanotechnology. *Bioorganic Med Chem*. 2018;26(10):2888-2905. doi:10.1016/j.bmc.2017.11.001
45. Pardeshi CV, Belgamwar VS. Direct nose to brain drug delivery via integrated nerve pathways bypassing the blood–brain barrier: an excellent platform for brain targeting. *Expert Opin Drug Deliv*. 2013;10(7):957-972. doi:10.1517/17425247.2013.790887
46. Sonvico F, Clementino A, Buttini F, et al. Surface-modified nanocarriers for nose-to-brain delivery: From bioadhesion to targeting. *Pharmaceutics*. 2018;10(1):1-34. doi:10.3390/pharmaceutics10010034
47. Djupesland PG, Messina JC, Mahmoud RA. The nasal approach to delivering treatment for brain diseases: An anatomic, physiologic, and delivery technology overview. *Ther Deliv*. 2014;5(6):709-733. doi:10.4155/tde.14.41
48. Hongbing Wu KH, Jiang X. From nose to brain: understanding transport capacity and transport rate of drugs. *Expert Opin Drug Deliv*. 2008;5(10):1159-1168. doi:10.1517/17425247.5.10.1159
49. Mistry A, Stolnik S, Illum L. Nanoparticles for direct nose-to-brain delivery of drugs. *Int J Pharm*. 2009;379(1):146-157. doi:10.1016/j.ijpharm.2009.06.019
50. Hanson LR, Frey WH. Intranasal delivery bypasses the blood-brain barrier to target therapeutic agents to the central nervous system and treat neurodegenerative disease. *BMC Neurosci*. 2008;9(3):S5. doi:10.1186/1471-2202-9-S3-S5
51. Malerba F, Paoletti F, Capsoni S, Cattaneo A. Intranasal delivery of therapeutic proteins for neurological diseases. *Expert Opin Drug Deliv*. 2011;8(10):1277-1296. doi:10.1517/17425247.2011.588204
52. Djupesland PG, Mahmoud RA, Messina JC. Accessing the Brain: The Nose may Know the Way. *J Cereb Blood Flow Metab*. 2013;33(5):793-794. doi:10.1038/jcbfm.2013.41
53. Illum L. Is nose-to-brain transport of drugs in man a reality? *J Pharm Pharmacol*. 2004;56(1):3-17. doi:10.1211/0022357022539
54. Dhuria S V, Hanson LR, Frey WH 2nd. Intranasal delivery to the central nervous system: mechanisms and experimental considerations. *J Pharm Sci*. 2010;99(4):1654-1673. doi:10.1002/jps.21924
55. Samaridou E, Alonso MJ. Nose-to-brain peptide delivery – The potential of nanotechnology. *Bioorganic Med Chem*. 2018;26(10):2888-2905. doi:10.1016/j.bmc.2017.11.001

56. Ruigrok MJR, de Lange ECM. Emerging Insights for Translational Pharmacokinetic and Pharmacokinetic-Pharmacodynamic Studies: Towards Prediction of Nose-to-Brain Transport in Humans. *AAPS J*. 2015;17(3):493-505. doi:10.1208/s12248-015-9724-x
57. Carmichael ST, Clugnet M-C, Price JL. Central olfactory connections in the macaque monkey. *J Comp Neurol*. 1994;346(3):403-434. doi:10.1002/cne.903460306
58. Cuschieri A. Enzyme histochemistry of the olfactory mucosa and vomeronasal organ in the mouse. *J Anat*. 1974;118(Pt 3):477-489.
59. Thiebaud N, Veloso Da Silva S, Jakob I, et al. Odorant Metabolism Catalyzed by Olfactory Mucosal Enzymes Influences Peripheral Olfactory Responses in Rats. *PLoS One*. 2013;8(3):1-13. doi:10.1371/journal.pone.0059547
60. Hu J, Sheng L, Li L, et al. Essential Role of the Cytochrome P450 Enzyme CYP2A5 in Olfactory Mucosal Toxicity of Naphthalene. *Drug Metab Dispos*. 2014;42(1):23-27. doi:10.1124/dmd.113.054429
61. Ding X, Xie F. Olfactory Mucosa: Composition, Enzymatic Localization, and Metabolism. *Handbook of Olfaction and Gustation*. John Wiley & Sons, Ltd; 2015:63-92. doi:10.1002/9781118971758.ch3
62. Marttin E, Schipper NGM, Coos Verhoef J, Merkus FWHM. Nasal mucociliary clearance as a factor in nasal drug delivery. *Adv Drug Deliv Rev*. 1998;29(1-2):13-38. doi:10.1016/S0169-409X(97)00059-8
63. Quintana DS, Guastella AJ, Westlye LT, Andreassen OA. The promise and pitfalls of intranasally administering psychopharmacological agents for the treatment of psychiatric disorders. *Mol Psychiatry*. 2016;21(1):29-38. doi:10.1038/mp.2015.166
64. Quintana DS, Westlye LT, Alnæs D, et al. Low dose intranasal oxytocin delivered with Breath Powered device dampens amygdala response to emotional stimuli: A peripheral effect-controlled within-subjects randomized dose-response fMRI trial. *Psychoneuroendocrinology*. 2016;69:180-188. doi:10.1016/j.psyneuen.2016.04.010
65. Wahlich J, Desai A, Greco F, et al. Nanomedicines for the delivery of biologics. *Pharmaceutics*. 2019;11(5):1-14. doi:10.3390/pharmaceutics11050210
66. Lai SK, Wang Y-Y, Wirtz D, Hanes J. Micro- and macrorheology of mucus. *Adv Drug Deliv Rev*. 2009;61(2):86-100. doi:10.1016/j.addr.2008.09.012
67. Xu Q, Ensign LM, Boylan NJ, et al. Impact of Surface Polyethylene Glycol (PEG) Density on Biodegradable Nanoparticle Transport in Mucus ex Vivo and Distribution in Vivo. *ACS Nano*. 2015;9(9):9217-9227. doi:10.1021/acsnano.5b03876
68. Lai SK, Wang Y-Y, Hanes J. Mucus-penetrating nanoparticles for drug and gene delivery to mucosal tissues. *Adv Drug Deliv Rev*. 2009;61(2):158-171. doi:10.1016/j.addr.2008.11.002

69. Sigurdsson HH, Kirch J, Lehr C-M. Mucus as a barrier to lipophilic drugs. *Int J Pharm*. 2013;453(1):56-64. doi:10.1016/j.ijpharm.2013.05.040

70. Cone RA. Barrier properties of mucus. *Adv Drug Deliv Rev*. 2009;61(2):75-85. doi:10.1016/j.addr.2008.09.008

71. Sosnik A, das Neves J, Sarmento B. Mucoadhesive polymers in the design of nano-drug delivery systems for administration by non-parenteral routes: A review. *Prog Polym Sci*. 2014;39(12):2030-2075. doi:10.1016/j.progpolymsci.2014.07.010

72. Clementino AR, Pellegrini G, Banella S, et al. Structure and Fate of Nanoparticles Designed for the Nasal Delivery of Poorly Soluble Drugs. *Mol Pharm*. 2021;18(8):3132-3146. doi:10.1021/acs.molpharmaceut.1c00366

73. Yang M, Lai SK, Yu T, et al. Nanoparticle penetration of human cervicovaginal mucus: The effect of polyvinyl alcohol. *J Control Release*. 2014;192:202-208. doi:10.1016/j.jconrel.2014.07.045

CHAPTER 1

CYCLOSPORINE A MICELLAR NASAL SPRAY CHARACTERIZATION AND ANTIVIRAL ACTION AGAINST SARS-COV-2

Cyclosporine A micellar nasal spray characterization and antiviral action against SARS-CoV-2

*Fabiola Guareschi[1], Elena Del Favero[2], Caterina Ricci[2], Laura Cantù[2], Martina Brandolini[3], Vittorio Sambri[3,4], Sara Nicoli[1], Silvia Pescina[1], Davide D'Angelo[1], Irene Rossi[5], Francesca Buttini[1,6], Ruggero Bettini[1,6], Fabio Sonvico[1,6] **

[1]*ADDRes Lab, Department of Food and Drug, University of Parma, Parco Area delle Scienze 27/a, 43124 Parma, Italy*

[2]*Department of Medical Biotechnology and Translational Medicine, University of Milan, Via Fratelli Cervi 93, 20054 Milan, Italy*

[3]*Unit of Microbiology, The Great Romagna Hub Laboratory, Piazza della Liberazione 60, 47522 Pievesestina, Italy*

[4]*Department of Experimental, Diagnostic and Specialty Medicine—DIMES, Alma Mater Studiorum—University of Bologna, Via Massarenti 1, 40138 Bologna, Italy*

[5]*Nanopharm Ltd, Franklin House, Grange Road, Cwmbran NP44 3WY, United Kingdom*

[6]*Interdepartmental Center for Innovation in Health Products, Biopharmanet_TEC, University of Parma, Parco Area delle Scienze 27/A, 43124 Parma, Italy*

Published in December 2023, ***European Journal of Pharmaceutical Sciences***

ABSTRACT

The upper airways represent the point of entrance from where Severe Acute Respiratory Syndrome Coronavirus 2 (SARS-CoV-2) infection spreads to the lungs. In the present work, α-tocopheryl-polyethylene-glycol succinate (TPGS) micelles loaded with cyclosporine A (CSA) were developed for nasal administration to prevent or treat the viral infection in the very first phases. The behavior of the micelles in presence of simulated nasal mucus was investigated in terms of stability and mucopenetration rate, evidencing long-term stability and fast diffusion across the glycoproteins matrix. Moreover, the spray characteristics of the micellar formulation and deposition profile in a silicon nasal model were studied using three nasal spray devices. Results allowed to identify the nasal spray pump (BiVax, Aptar) able to provide the wider and uniform deposition of the nasal cavity. The cyclosporine A micelles antiviral activity against SARS-CoV-2 was tested on the Omicron BA.1 variant using Vero E6 cells with protocols simulating treatment before, during and after the infection of the upper airways. Complete viral inactivation was observed for the cyclosporine-loaded micelles while a very low activity was evidenced for the non-formulated drug, suggesting a synergistic activity of the drug and the formulation. In conclusion, this work showed that the developed cyclosporine A-loaded micellar formulations have the potential to be clinically effective against a wide spectrum of coronavirus variants.

1. INTRODUCTION

Severe acute respiratory syndrome coronavirus 2 (SARS-CoV-2) belongs to the coronavirus genus, which comprehends 26 [1] known species divided in four genera (Alpha, Beta, Gamma and Delta CoV) [2]. However, only Alpha and Beta Coronaviruses can infect humans, leading to mild to severe respiratory infections [2]. SARS-CoV-2 is a Betacoronavirus, discovered for the first time in Wuhan, China, at the end of 2019 and it since spread dramatically rapidly all over the world [3,4]. This led to a pandemic which caused a significatively higher number of infected people and larger diffusion than the previously Severe Acute Respiratory Syndrome (SARS-CoV) and Middle East Respiratory Syndrome (MERS-CoV) coronaviruses appeared in 2002 and 2012, respectively [3]. The infection can cause the manifestation of various symptoms comprehending fever and cough, but in the most severe cases, the rapid viral replication can lead to a strong immune response, consisting in a high release of cytokines. This cytokine "storm" can rapidly lead the patient to death, since it provokes acute respiratory distress syndrome and respiratory failure [5,6]. Despite SARS-CoV-2 can infect all the human population regardless of the age and gender, older men with coexisting illnesses appears to be the fraction most exposed to the risk of developing a severe respiratory disease requiring hospitalization and often causing death [7].

Due to its unique virological features, SARS-CoV-2 shows a high transmissibility. In particular, the transmission often occurs early since registered viral load in the upper airways has been found to be already very high when the first symptoms occur; this correlates with a high risk of nasopharyngeal virus shedding at the beginning of the infection [8,9]. The airborne transmission of the virus from an infected person occurs through liquid droplets incorporating the virus during speech. Furthermore, together with the larger droplets, smaller and more numerous aerosol particles are produced. These latter can persist in the air for a long period of time and finally inhaled by someone thus leading to a starting infection [10,11]. Therefore, after the starting infection of the epithelial cells located in the upper respiratory tract, the virus quickly migrates to the deeper airways and finally reaches the alveolar epithelial tissue in the lungs [3].

Vaccination is certainly one of the most effective tools to control and prevent the spread of viral pandemics [12,13], but the genetic variability of the coronaviruses complicates the development of effective vaccination able to prevent the infection of all the viral variants [1]. For this reason, a broad spectrum of drugs is currently being studied for their anti-viral properties against coronaviruses. Cyclosporine A belongs to this group, since already in 2011 it was demonstrated to be effective at suppressing coronaviruses on a broad spectrum [14]. One peculiar viral replication feature of SARS-CoV-2 is that the virus exploits the activity of the intracellular cyclophilin A (CypA) when infecting the host cell. This highly-expressed protein provides the cloaking of the viral replication

intermediates, thus preventing the viral nucleic acid from being detected by the innate immune cellular sensors [15]. The mechanism of action of cyclosporine A consists precisely in the inhibition of CypA, [1,14] therefore hindering the viral cloaking step and leading to a restoration of the normal innate immunity processes including the expression of antiviral genes that block the viral infection [15]. In addition to this, CSA can also be exploited to limit the excessive release of pro-inflammatory cytokines in patients infected with SARS-CoV-2 by creating a complex with CypA and calcineurin (CaN). In this complex, the phosphorylation activity of CaN, normally involved in the release of several pro-inflammatory cytokines, is inhibited [16–18]. Results from cell culture experiments have demonstrated that CSA strongly inhibits the replication of SARS-CoV, manifesting the antiviral activity only at the early stage of viral replication and at a relatively higher concentration (16 μM) if compared to that required to inhibit the replication of other RNA viruses (0.5 – 3 μM) [14,19].

However, the peptide nature, the relatively high molecular weight (1202.635 Da), the low aqueous solubility (~ 5 μg/mL in phosphate buffered saline) [20,21] and the high lipophilicity attested by a log P value of 3, [22] make the formulation of CSA challenging.

One strategy to formulate CSA proposed in the past is represented by oil-based surfactant-containing dosage forms [23]. However, these formulations when applied on mucosal tissues, such as the eye for instance, evidenced low tolerability causing local inflammatory responses, as irritation and hyperemia [24,25]. Furthermore, it is suggested that because of the high affinity of the drug for the oily phase of pharmaceutical emulsions, in most cases these formulations show poor bioavailability [25]. A possible valid alternative to emulsions is represented by micelles, able to increase the solubility of this hydrophobic peptide drug. Micelles are nanosystems relatively easy to prepare and characterized by high scalability which demonstrated to be able to improve the drug solubility and cellular uptake [26,27]. Despite ocular administration of CSA, also in micellar formulations, has been extensively studied, [27–30] to the best of our knowledge, CSA-loaded micelles have not yet been tested for intranasal administration as antiviral agents against SARS-CoV-2. However, it is reported in literature that a nasal spray containing nitric oxide has been used to efficiently reduce the SARS-CoV-2 viral RNA concentration in patients infected with the virus, confirming the efficacy of the intranasal approach to allow the clearance of the virus [31,32].

Therefore, the aim of this study was to formulate and characterize cyclosporine A loaded micelles produced using a vitamin E derivative, *i.e.* α-tocopherol polyethylene glycol 1000 succinate (TPGS) and to evaluate their antiviral activity *in vitro* against SARS-CoV-2, in view of a clinical application via intranasal administration.

2. MATERIALS AND METHODS

2.1 Materials

The vitamin E-derived surfactant α-tocopherol polyethyleneglycol succinate (TPGS, MW 1513 g/mol) was a kind gift from PMC ISOCHEM (Vert-Le-Petit, France). Cyclosporine A (CSA, MW 1202.61 g/mol) was obtained from Metapharmaceutical (Barcelona, Spain). Deuterium oxide (D_2O) and mucin from porcine stomach type II were from Sigma Aldrich (Saint Louis, USA). Sodium chloride (NaCl) was obtained from VWR International (Leuven, Belgium). Calcium chloride ($CaCl_2$) was purchased from Fluka Chemika (Buchs, Switzerland). Potassium chloride (KCl) was provided by A.C.E.F (Fiorenzuola d'Arda, Italy). Acetonitrile, trifluoroacetic acid and the other solvents were of HPLC grade. Ultrapure water was purified by reverse osmosis (MilliQ, Millipore, Molsheim, France).

2.2 Methods

2.2.1 Preparation of the blank and drug-loaded micelles

The micelles were prepared following the method described previously by Pescina *et al.* [33]. For the preparation of the blank micelles, TPGS (20 mM, 3% w/v) was solubilized in a NaCl solution (9 g/L). The system was kept under magnetic stirring at 300 rpm until the complete dissolution of the TPGS. Importantly, the solution was prepared in a closed amber glass vessel to preserve TPGS from possible photodegradation.

The drug-loaded micelles were prepared by adding to the previously prepared blank micelles the CSA powder, accurately weighed on an aluminum weighing boat. More precisely, different amounts of CSA (1 mg, 2.5 mg and 5 mg) were used to prepare 10 mL of the Low-Loading (LL, 0.1 mg/mL), Medium-Loading (ML, 0.25 mg/mL) and High-Loading (HL, 0.5 mg/mL) micelles.

Then, the system was subjected to sonication in an ultrasound bath (USC 300-T, VWR International, Radnor, PA, USA) for 2 minutes to favor the complete detachment of the powder from the weighing boat. Finally, the micelles were maintained under magnetic stirring at 300 rpm (AREX-6 Digital, VELP Scientific, Usmate, Italy) overnight. To separate the eventual non-encapsulated drug, as a precipitate, the micelles were subjected to centrifugation (NEYA-16R, Remi Elektrotechnik, Vasai, India) at 9,500 rpm for 10 minutes at 25°C. The supernatant was finally collected and stored at 25°C in amber glass vessels.

2.2.2 Characterization and stability study

2.2.2.1 Particle size, PDI and surface Zeta Potential

The particle size and the polydispersity index (PDI) of both the blank and drug-loaded micelles were determined by dynamic light scattering (DLS) using Malvern Zetasizer Nano ZS (range 0.3 nm – 10

µm, Malvern Instruments Ltd., Malvern, UK). For each DLS measurement, 1 mL of the formulation was analyzed without dilution using a disposable polystyrene cuvette. Measurements were performed at the temperature of 25°C and at a scattering angle of 173°. The refractive index and the viscosity of the dispersant were 1.33 and 0.8872 mPa·s, respectively. The refractive index of the material was set at the value of 1.00. Before analysis, the sample was equilibrated for 30 seconds. Analyses were repeated three times for each sample, with 15 sub-runs for measurement to increase data and correlation and reported as cumulative unimodal/multimodal fitting (sample dependent) and Z-average mean particles size.

The samples were also analyzed for zeta-potential using a patented laser interferometric technique called M3-PALS (Phase analysis Light Scattering), with the same instrument (Zetasizer Nano ZS, Malvern Instruments Ltd., Malvern, UK) and the same parameter set for particle size and PDI analysis. Analyses were performed using a disposable folded capillary cell, at 25°C, and recorded three times for each sample, with 100 runs for measurement.

The characterization of the produced micelles was done at time zero and after every month for 7 months, keeping the samples stored at 25°C in closed amber glass vessels.

DLS was also employed to evaluate any changes in terms of size before and after actuation of the micellar formulation from the nasal devices tested. To do this, the formulation was sprayed into 2 mL Eppendorf® tubes (Eppendorf AG, Hamburg, Germany) after being loaded into each nasal device tested. Then, the sample was collected and analyzed by DLS as described above.

2.2.2.2 Density

The densities of TPGS micellar formulations were assessed at 22°C with a density meter (DMA5000, Anton Paar, Graz, Austria) allowing an accuracy of 7×10^{-6} g/cm³. Samples (1.5 mL) were inserted into the measuring U-capillary cell by means of two syringes, tightly connected at its ends, and were equilibrated for 15 minutes at each temperature before data collection.

2.2.2.3 Viscosity

Dynamic viscosity, η, was measured for the blank, HL, ML and LL micelles by a controlled shear rate MCR102 Rheometer and data were analyzed using the Rheocompass™ software version 1.25 (Anton PaarGraz, Austria). Rotational measurements were carried out without diluting the samples,which were analyzed by a CC27 geometry (27 mm diameter, 1.13 mm gap). Measurements were performed both at 25°C and at 37°C to simulate the physiological nostril temperature, for a shear rate ranging from 10 to 1000 s^{-1}. All the analyses were performed in triplicate.

2.2.2.4 Cyclosporine A quantification method

The method used to quantify the amount of solubilized drug in the drug-loaded micelles was previously validated for precision and accuracy [34]. Briefly, CSA was quantified using a HPLC-UV system consisted of a pump (Model LC-10 AS, Shimadzu, Japan) and an ultraviolet detector (Model SPD-10A, Shimadzu, Japan). The mobile phase was a mixture acetonitrile: water with 0.1% trifluoroacetic acid in 65:35 (v/v) ratio, pumped at 1.6 mL/min. The column used to analyze cyclosporine A was a reverse-phase Nova-Pack C18 cartridge (150×3.9 mm, 4 µm, Waters, Milford, MA, USA) equipped with a guard column (4×3.0 mm, Security Guard™ Cartridge, Phenomenex, USA) thermostated at 65°C. The injection volume was 100 µL and absorbance was monitored at 230 nm. Using these conditions, cyclosporine A retention time was about 4 minutes. The CSA stock solution was prepared by dissolving a weighed amount of CSA in acetonitrile. The dilutions of the stock were then prepared in mobile phase.

Several calibration curves were built to cover different concentration ranges: 3 – 90 µg/mL, used for the quantification of the drug loaded into the micelles; and 0.1 – 3 µg/mL and 1 – 10 µg/mL, exploited for the *ex vivo* mucoadhesion study. Each stock dilution of these two latter calibration curves was then diluted with water to generate two additional calibration curves in the ranges of 0.77 - 7.69 µg/mL and 0.08 – 2.3 µg/mL. These curves were used for the CSA quantification in samples deriving from the mucoadhesion experiments, which were diluted in an aqueous medium. The quantification of the solubilized drug was done at time 0 and after every month for 7 months, keeping the samples stored at 25°C in closed amber glass vessels.

2.2.2.5 SAXS and SANS analysis

Small Angle X-ray (SAXS) and Neutron (SANS) scattering measurements were carried at the high brilliance beamline ID02 of the European Synchrotron Radiation Facility (ESRF, Grenoble, France), experiment DOI: 10.15151/ESRF-ES-653835676 and on Yellow Submarine diffractometer at the Budapest neutron center (Hungary), experiment CERIC_20217127. The magnitude of the scattering vector q is defined as $q = (4\pi/\lambda) \sin(\theta/2)$ with θ being the scattering angle and λ the incident X-ray wavelength. SANS measurements were carried out in the q-range between 0.4–4.0 nm^{-1}, with a fixed value of the incident wavelength (λ = 0.488 nm, Δλ/λ = 20%) and two sample-to-detector distances (1.1 and 5.2 m). The measurements were conducted at room temperature of 20°C. Samples were loaded in quartz cells of 2 mm thickness (Hellma analytics GmbH & Co. KG, Müllheim, Germany). To obtain the intensity of scattering in absolute units, a standard procedure of calibration to water was performed after subtracting the background and scattering in the solvent (D_2O) which were measured in separate experiments. SAXS measurements were performed using

polycarbonate capillaries of 2 mm thickness (ENKI, Concesio, Italy) as sample containers. The measured two-dimensional SAXS patterns were corrected for detector artefacts, normalized to absolute intensity scale and azimuthally averaged to obtain the intensity profile I(q) as a function of q, in the range ($0.7\ nm^{-1}<q<6nm^{-1}$). Spectra were recorded at several positions of the capillary's length to test radiation damage that might be induced by X-ray exposure. For each static measurement, at least 5 spectra were averaged after excluding any possible radiation damage. The averaged background signal was subtracted from each averaged sample intensity profile.

The analysis of the I(q) profiles was performed assuming that for a monodisperse homogeneous micellar solution as $I(q) = NV^2 2\Delta\rho^2 P(q)S(q)$ where N is the number of particles per unit volume V, $\Delta\rho$ is the contrast term between the particles and the medium. P(q) is the form factor of the micelles, giving information on their size and shape, while S(q) is the solution structure factor, that depends on the spatial distribution of interacting micelles, becoming constant, $S(q) = 1$, for dilute solutions of non-interacting micelles [35].

The mucin–micelle interaction was investigated by observing the diffusion of CSA-loaded micellar solution (40 µL) put in contact with mucin (20 µL, c = 15% w/v) in the polycarbonate capillary placed in a horizontal sample holder. SAXS intensities at different positions in the capillary were measured. Simulated Nasal Electrolyte Solution (SNES, described in **section 2.2.3**) was used as buffer for both micelles and mucin solution. Spectra of the solution in different horizontal positions have been acquired over time, thus monitoring the evolution of the diffusion of the particles the first acquirable measurement, at t=200 seconds, to t=1500 seconds. As a reference, the diffusion of SNES alone in mucin has been measured.

2.2.3 Ex vivo mucoadhesion study

The mucoadhesive properties of the micelles subjected to a constant Simulated Nasal Electrolyte Solution (SNES) flow were investigated exploiting the rabbit nasal mucosa by means of an "inclined plane apparatus". The apparatus consisted of an inclined plane with an angle of inclination of 45° on which a glass Petri dish was located and used to position the tissue and collect samples. With this test, the mucoadhesive properties of the HL micelles were investigated and compared to those of a CSA suspension (0.5 mg/mL).

SNES consisted of an aqueous solution containing calcium, sodium and potassium ions at the same concentrations present in the human nasal fluid [36,37]. It was prepared by dissolving sodium chloride (8.77 mg/mL), potassium chloride (2.98 mg/mL) and calcium Chloride (0.45 mg/mL) in ultrapure water [38]. After the complete dissolution of the salts, the pH was adjusted to 6.5 with hydrochloric acid 1M. The nasal mucous membranes were isolated from fresh rabbit heads kindly provided by

Bertoni Carni S.r.l. (Busana, Reggio-Emilia, Italy), stored in ice, and used within four hours from animal death. The heads were sectioned longitudinally, then the whole mucosa and the respective portion of supporting cartilage were taken using a scalpel. Successively, the mucosa was punched to obtain 8 mm diameter circular portions of tissue. The tissue was then placed on absorbent paper soaked in physiological solution in a closed plastic Petri before testing.

The mucosal tissue was fixed with the double-sided tape (Tesafix® 4934, KaiserKraft, Stuttgart, Germany) within the glass Petri dish on a horizontal plane and treated with 20 µL of the HL micellar formulation or the CSA suspension. After 5 minutes, the Petri dish was positioned on the inclined plane apparatus so that the SNES flowed over the tissue running from its upper edge to the bottom of the Petri dish, where it could be collected for analysis. To do this, the SNES was flowed at 100 µL/min with the aid of a syringe pump (Harvard Apparatus, Holliston, USA) equipped with a plastic syringe having an internal diameter of 19 mm and a needle of 0.8x40 mm, conditioned for at least 15 minutes before starting the experiments. Samples were collected every 5 minutes for 30 minutes and mixed with 500 µL of mobile phase. Then, samples were centrifuged (NEYA-16R, Remi Elektrotechnik, Vasai, India) at 9,500 rpm for 10 minutes at 25°C and the supernatant was analyzed by HPLC. At the end of the thirty minutes-experiment, the drug adhered to the tissue was extracted with an extracting fluid consisting of a mixture of acetonitrile and 1% acetic acid at a volume ratio of 87:13 respectively. The tissue was kept in the extracting fluid (1 mL) overnight at ambient temperature, then was sonicated and centrifuged (NEYA-16R, Remi Elektrotechnik, Vasai, India) at 12,500 rpm for 15 minutes at 25°C; 500 µL of the supernatant were withdrawn and mixed with ultrapure water (150 µL) and finally analyzed with HPLC. Moreover, 1 mL of acetonitrile was used to collect and dissolve the drug that had eventually adhered to the Petri dish; the samples were centrifuged at 9,500 rpm for 10 minutes at 25°C and the supernatant was collected and analyzed by HPLC in triplicate. The percentage of mucoadhesion was calculated considering the theoretical amount of drug deposited on the nasal mucosa as 100%, from which a cumulative curve was built by subtracting the drug amount found in the withdrawal at each time point.

Finally, a mucosal mean residence time (mMRT) was calculated from data applying **Equation 1** [39], obtained from a classic method for the calculation of the mean residence time in pharmacokinetics reported in literature [40].

$$\mathrm{mMRT} = \frac{\mathrm{AUMC}_{0\to\infty}}{\mathrm{AUC}_{0\to\infty}} \qquad \textbf{(1)}$$

In **Equation 1** reported above, AUC is the area under the curve describing the percentage of residual CSA adhering to the nasal mucosa over time, while AUMC is the area under the first moment curve. The AUC and AUMC were calculated by the trapezoidal method with exponential extrapolation, and

these were used to calculate the mMRT.

2.2.4 *In vitro* studies

2.2.4.1 Cell line and culture conditions

Vero E6 cell cultures (American Type Culture Collection, ATCC CRL-1586) were grown in Minimum Essential Medium (MEM) supplemented with L-glutamine (2 mM), penicillin (100 U/mL), streptomycin (100 µg/mL) (complete culture medium) and heat inactivated fetal bovine serum (FBS) (10% v/v), as recommended [41]. Cells were incubated at 37 °C in a humidified, 5% CO_2 atmosphere-enriched chamber until use. For compound treatment studies, cells were seeded in 96-well plates and cultured in MEM containing FBS (2% v/v). Cell culture medium and supplements were all purchased from EuroClone (Milan, Italy).

2.2.5 Antiviral Activity Studies

2.2.5.1 Virus propagation and titration

The inhibitory effect of pure CSA, blank and CSA-loaded micelles on viral replication was tested against Omicron subvariant BA.1, technically referred to as lineage B.1.1.529.BA.1. The viral strain was isolated from a residual clinical specimen conferred to the Unit of Microbiology, Greater Romagna Area Hub Laboratory (Cesena, Italy), for routine diagnostic purposes and sequenced as part of the project for monitoring the prevalence and distribution of SARS-CoV-2 variants in Italy, promoted by the Italian National Institute of Public Health (ISS, Rome, Italy). Before being used for this study, the sample underwent an anonymization procedure, in order to adhere to the regulations issued by the local Ethical Board (AVR-PPC P09, rev.2; based on Burnett *et al.* [42]). In brief, a specific volume of clinical specimen (500 µL) was used to infect a cell monolayer at confluency. After a one-hour adsorption, the culture was maintained in FBS MEM (2% v/v) and incubated for 72 hours. Both the original clinical samples and the viral strains were analyzed employing the FilmArray Respiratory Panel (Biomerieux, Marcy l'Etoile, France), testing negative forother respiratory viruses. After isolation on Vero E6 cells, the viral strain was in turn sequenced usingCleanPlex SARS-CoV-2 Flex (Paragon Genomics, Inc., Hayward, CA, USA) and Illumina MiSeq (Illumina Inc., San Diego, CA, USA) (Genomics, n.d.) to reconfirm the lineage identification providedfor diagnostic purposes. Sequenced reads were aligned and compared with the reference genomicsequence of SARS-CoV-2 Wuhan-Hu-1 isolate (Access: NC_045512, Version: NC_045512.2) using SOPHiA DDM platform software (SOPHiA Genetics, Lausanne, Switzerland), for determination of the consensus sequence, variant calling and lineage assignment. The viral strain was titrated using the endpoint dilution method [43]. In brief, serial 10-fold dilutions (from 10^{-1} to 10^{-10}) in FBS MEM (2% v/v) were used to infect confluent monolayers of cells in a 96- well plate. After 72 hours cells werefixed and stained by means of a

formaldehyde solution (4% v/v) in crystal violet. Absence or presence of cytopathic effect at each dilution was assessed by comparison of each well with virus control and cell control wells. Viral titres, expressed as $TCID_{50}$/mL, were calculated with the Reed and Muench formula based on eight replicated for dilution [44].

2.2.5.2 Cell treatment and viral replication inhibition assay

The day prior to treatment and infection, Vero E6 cells were seeded at a density of 2×10^6 cells per plate in 96-well plates and allowed to attach for 16 to 24 hours at 37 °C, 5% CO_2. On the day of infection, each tested compound stock solution was freshly diluted in cell culture medium containing FBS (2% v/v). CSA was tested at concentrations ranging from 2 µM to 64 µM (2, 4, 8, 16, 32 and 64 µM) [14]. Each CSA-loaded micellar formulation was diluted accordingly, in order to obtain the same CSA concentrations. Similarly, the blank micelles were diluted to obtain the same concentration of TPGS micelles as the drug-loaded samples. In order to better determine at which level the viral replication cycle was inhibited, cells were subjected to different treatment regimens, which can be distinguished into single- and multiple-treatment regimens. The first category includes: pre-treatment 1 hour before infection (*protocol A*), simultaneous treatment and infection (*protocol B*), treatment 2 hours post-infection (*protocol C2*) and treatment 6 hours post-infection (*protocol C6*). The second category, on the other hand, includes: pre-treatment 1 hours before infection followed by treatment 2 hours post-infection treatment (*protocol D*), three treatments post-infection (*protocol E*) and pre-treatment 1 hour before infection followed by three treatments post-infection (*protocol F*). In any case, each treatment lasted one hour and in the multi-treatment regimens, treatments were repeated one hour apart. Antiviral efficacy was tested against two different virus concentrations: 0.005 m.o.i. (*i.e.,* multiplicity of infection) and 0.0005 m.o.i. In both cases, infected cultures were incubated for one hour at 37 °C to allow viral adsorption. Treated and infected cultures were incubated at 37 °C, 5% CO_2 for 72 hours. For each treatment protocol, a cell culture was infected directly with the virus suspension at the two tested concentrations to assess viral replication in the absence of any potential inhibition.

2.2.5.3 SARS-CoV-2 nucleic acid quantification

Viral replication in treated and untreated cell cultures was evaluated by qRT-PCR by comparing the Ct values of each treated sample and its corresponding untreated control obtained after 72 hours of incubation. For this purpose, the Allplex SARS-CoV-2 Extraction-Free system (Seegene Inc., Seoul, South Korea) was used (Seegene Inc., n.d.). It consists of a real-time qRT-PCR multiplex assay based

on the use of TaqMan probes, which allows the simultaneous detection of four target genes, namely E gene, RdRP/S gene and N gene. Sample preparation, reaction setup and analysis were performed accordingly to the manufacturer instructions. Briefly, 15 µL of the sample was diluted 1:4 in 45 µL of RNAse-free water in a 96-well PCR plate and hence an exact volume of the dilution (5 µL) was transferred to another plate with 16 µL of PCR master mix, containing the following compounds: 5 µL of MOM (MuDT Oligo Mixture, with dNTPs, oligos, primers and TaqMan 5' fluorophore/3' Black Hole Quencher probes), 5 µL of enzymes, 5 µL of RNase-free water and 1 µL of an exogenous internal control for every reaction. A positive and a negative control were included in each run. The assay was run on a CFX96 real-time thermal cycler (Bio-Rad, Feldkirchen, Germany). The amplification process includes cDNA denaturation at 95°C for 10 seconds, primers annealing at 60°C for 15 seconds and elongation at 72°C for 10 seconds (44 cycles). Fluorescent signals were acquired after every amplification cycle. Results analysis and targets quantification were performed with 2019-nCoV Viewer from Seegene Inc. (Seoul, South Korea). By comparing the Ct values referred to the N gene of each treated sample and its corresponding untreated control, the percentage of infectivity reduction was calculated as follows (**Equation 2**), approximating 100% of infectivity reduction to treated sample Ct value at time 0 and 0% of infectivity reduction to the Ct value obtained from the untreated controls:

$$Viral\ Infectivity\ reduction\ (\%) = \frac{Treated\ sample\ Ct\ value\ 72h - Untreated\ control\ Ct\ value\ 72h}{Treated\ sample\ Ct\ value\ t{=}0 - Untreated\ control\ Ct\ value\ 72h} \cdot 100 \qquad \textbf{(2)}$$

2.2.6 Cytotoxicity study

Cells treated with the same treatment protocols described in ***Section 2.2.5*** but not infected were used to assess cytotoxicity. For this purpose, the blank and drug-loaded micellar formulations (HL, ML, LL; diluted to a CSA concentration in the range of 2-64 µM) as well as the pure CSA powder (2-64 µM) were tested.

To quantify cell viability, after the incubation period, the cell monolayers were fixed and stained using a 4% formaldehyde solution in crystal-violet; absorbance was read at 595 nm. For each tested compound concentration, the percentage of viable cells for each tested concentration was calculated, setting the mean absorbance value of the cell control wells (neither treated, nor infected cells) as 100% viability. The tested formulation and relative dilutions were considered cytotoxic when lead to a cell viability lower than 80%.

2.2.7 Spray characterization

Three different nasal devices were provided by Aptar Pharma (Le Vaudreuil, France) and used for spray characterization and deposition in the nasal cast assessment: an amber glass vial equipped with CPS preservative-free spray pump, 70 µL/single spray (device A), a Bidose system BDSI V3 device, 100 µL/single spray (device B) and a BiVax system, 250 µL/single spray (device C) assembled using a standard kit BDSI (references 2457_010 et 2457_140) (**Figure S1, Supplementary Material**). Droplet Size Distribution (DSD) of the aerosol emitted from the selected devices was carried out employing Malvern Spraytec (Malvern Panalytical Ltd, Malvern, UK) in open bench configuration. The nasal spray was actuated at 3 cm and 6 cm with the plume cutting perpendicularly the laser beam. Data collected were analyzed in terms of transmittance, volume diameter of the 10^{th}, 50^{th} and 90^{th} percentile of the distribution and width of the droplets distribution obtained (span). Three replicates per distance for each device were performed.

The plume of the formulation sprayed from the selected pump was characterized also employing a pulsed laser technique using Patternate software version 1.3.1 (Oxford Lasers, Didcot, UK).

For Spray Pattern (SP) the laser beam was positioned at 3 cm and 6 cm from the pump nozzle. The laser cut the plume horizontally whilst high-speed images were recorded. SP allowed to collect the following spray characterization parameters: minimum diameter (Dmin), maximum diameter (D_{max}), ovality ratio $\frac{Dmax}{Dmin}$ and area (π x $\frac{Dmin}{2}$ x $\frac{Dmax}{2}$). Three replicates per distance for each device were performed. For Plume Geometry (PG) the laser beam was positioned at a distance to allow for the capture of the whole plume emitted from the device nozzle. The laser beam cut vertically the plume while high-speed images were recorded. PG allowed to analyze the following parameters: plume angle (°), plume length (cm) and plume width (cm). The plume width was taken at a plume length of 6 cm. Three replicates per device were carried out for PG.

The screened nasal devices were automated actuated for spray characterization employing Vereo® actuator (NSx, Proveris Scientific Corporation, MA, USA). The method for automated actuation employed was previously developed and validated by Aptar Pharma (**Table S1, Supplementary Material**).

2.2.8 Deposition study on a nasal cast

The deposition profile of the developed micelles was studied using a silicone nasal cavity model by Koken® (Model LM-005 Koken ltd., Tokyo, Japan) (**Figure S2, Supplementary Material**). For these studies, as for the mucoadhesion studies, the micellar formulation with the highest drug content (HL micelles) was selected since it was considered the best candidate for a possible *in vivo* administration.

For each kind of device (**Figure S1, Supplementary Material**), the experiments were performed in triplicate. The experiments were performed in absence of any simulated inhalation flow, and each device was actuated once into the left nostril at a 45° angle considering the palate as reference.

Device **A** was filled with 5 mL of micellar formulation, primed four times before the analysis, and inserted 12 mm into the nostril. Device **B** was filled with 250 µL of micellar formulation and inserted 7 mm into the nostril without being primed, according to the manufacturer instructions. Device **C** was filled with 300 µL of micellar formulation, primed once according to the manufacturer and inserted 7 mm into the nostril. In order to identify the areas in which the micellar formulation was deposited, we used for each analysis about 0.6 g of the color finding past Sargel® (Arkema, Exton, PA, U.S.A), which in contact with the water present in the formulation becomes pink [45].

A digital camera equipped with a 16-50 mm lens (Sony α 5100, Sony, Tokyo, Japan; 24.3 megapixels APS-C sensor) was used to capture the images, keeping the nasal cast 15 cm apart from the camera; to standardize photographic conditions a photographic set was used with a white background and the same light condition for all the pictures. To balance the ambient light, the experiments were performed in a dark room, using a LED light as the only light source, kept at a fixed distance from the nasal cast. The positions and distance between the camera and the cast were maintained fixed. The camera was set with an exposure time of 1/250 s, the ratio of focal length to effective aperture diameter (f) was 4.5, with a focal distance of 16 mm and ISO 250. For each analysis, 1 minute elapsed between the actuation of the device and the imaging. Each device was weighed before and after each actuation in order to know how much formulation was dispensed.

The pictures were elaborated using the ImageJ software (U.S. National Institute of Health, Bethesda, MD, USA) to analyze the deposition area and identify the deposition regions. For this purpose, the nasal cavity was divided into four regions of interest (ROI): the vestibule, the middle-upper turbinate, the lower turbinate and the throat (**Figure S2, Supplementary material**). The images acquired one minute after spraying were converted to an 8-bit color image and the conversion of the number of pixels into mm^2 was realized by using a graduated scale positioned near the nasal cast during the analysis. The threshold level range was fixed between 0 and 109 for all the acquired images.

2.2.9 Statistical Analysis

Differences were analyzed using one-way ANOVA and Tukey HSD Post Hoc test (α=0.05) using KaleidaGraph software (ver. 4.5, Synergy Software, Reading, PA, USA) and were considered statistically significant when $p < 0.05$.

3. RESULTS

3.1 Characterization of the blank and CSA-loaded micelles

As shown in **Table 1**, all the produced micelles showed a particle size below 15 nm, low values of polydispersity index (PDI) and an almost neutral surface. The density of the micellar formulation was in all the cases slightly above the value of 1 g/cm^3, with a tendency to slightly increase with increasing CSA loading. The CSA-loading encapsulation efficiency for low-loading (LL, 0.1 mg/mL), medium-loading (ML, 0.25 mg/mL) and high-loading (HL, 0.5 mg/mL) CSA micelles was in all cases higher than 95% without statistically significant differences. Despite showing the rheological behavior of a dilatant fluid (shear thickening), at low shear the viscosity calculated at 25°C was basically the same for all the developed micelles, turning out to be slightly above 1 mPa·s. No differences were found between the blank and the three types of CSA-loaded micelles, and the amount of CSA present in the formulations does not seem to have any impact on the viscosity. The viscosity of the micelles was also analyzed at 37°C to simulate the nasal environment, but again no differences were evidenced apart from the expected slight decrease in viscosity values. The viscosity flow curves of the micellar formulation at 25°C and at 37°C are reported in **SupplementaryMaterial** (**Figure S3**).

The presence of CSA in the micellar structure appears to slightly but consistently reduce their average hydrodynamic radius of around 10% compared to the value of blank micelles (**Table 1**). The results of the characterization made on the micellar formulation over 7 months after the first characterization are collected in **Supplementary Material Table S2**.

Table 1 *– Physico-chemical characterization of blank and 0.1, 0.25, 0.5 mg/mL CSA-loaded micelles at time 0 (n=3)*

	Size [nm]	PDI	Zeta Potential [mV]	Density [g/cm^3]	Encapsulation Efficiency [%]	Viscosity (25°C) [mPa·s]
Blank	13.2 ± 3.2	0.08	-2 ± 0	1.0061012 §	--	1.24 ± 0.06
LL micelles (0.1 mg/mL)	11.7 ± 0.5	0.07	-2 ± 1	1.0061056 §	99.49 ± 8.37	1.26 ± 0.07
ML micelles (0.25 mg/mL)	11.4 ± 0.1	0.06	-1 ± 1	1.0061630 §	98.15 ± 5.60	1.27 ± 0.06
HL micelles (0.5 mg/mL)	11.7 ± 0.2	0.12	-1 ± 1	1.0062672 §	97.40 ± 2.69	1.25 ± 0.07

§ the SD of the results is below 0.000005

A structural analysis of micelles was performed by Small Angle Neutron Scattering (SANS) performing experiments on both blank and CSA-loaded micellar formulations. The intensity spectra measured at room temperature are reported in **Figure 1**. The background-subtracted scattered intensity I(q) can be expressed as **Equation 3**:

$$I(q) = NV^2 2\Delta\rho^2 P(q)S(q) \quad \textbf{(3)}$$

where N is the number of particles per unit volume V, $\Delta\rho$ is the contrast term between the particles and the medium, P(q) and S(q) are the particle form factor and the structure factor, describing the size, the shape and interactions between particles, respectively. **Figure 1A** reports the intensity spectra of blank micelles along a dilution line (TPGS concentration from 30 mg/mL to 1.5 mg/mL, *i.e.* up to 1:20 dilution), to verify the stability of the micelles and to enucleate information on the particles' size and shape. The features of SANS curves are similar, although a depression of the intensity profile in the low-q region is visible in high concentration samples. This trend is characteristic for interacting particles, experiencing steric repulsions, which vanish at low concentration. In the non-interacting regime (concentration below 6 mg/mL) the intensity curves are superimposable, indicating that micelles are physically stable, with identical size and shape. Structural details were obtained fitting the curves to a core−shell sphere model combined with a hard-sphere structure factor, as already reported in the literature for TPGS micelles [46]. The fit is reported for the sample diluted 1:20 (1.5 mg/mL) in **Figure 1A** and the parameters are reported in the **Supplementary Material**. Micelles display a hydrophobic core of 7 nm (diameter) surrounded by a hydrophilic shell with a thickness of 2.9 nm. The calculated overall size of the micelles, around 13 nm, is in good agreement with DLS data. The amphiphilic nature of TPGS leads in water to the

formation of a micellar structure composed of an inner lipophilic core encapsulating the lipophilic drug and responsible for its solubilization, and an outer hydrophilic shell involved in the interaction with the biological surfaces upon administration [27].

Interestingly, the addition of cyclosporine A results in an increase of inter-particle interaction. In fact, the intensity profile at low q lowers accordingly to the amount of loaded CSA, as shown in **Figure 1B**. This increase of steric repulsion between micelles at a constant solution concentration indicates that micelles become closer and more numerous, *i.e.* smaller. As for blank micelles, SANS curves of CSA-loaded micelles were fitted to a core–shell sphere model combined with a hard-sphere structure factor [46] and results are reported in **Supplementary Material**. In agreement with DLS data, results indicate an overall reduction of the size of the CSA-loaded micelles. Analysis of the SANS spectra reveals that the size of the micelle core decreases from 7 to 6.4 nm, while the hydrophilic shell keeps a constant thickness (2.9 nm).

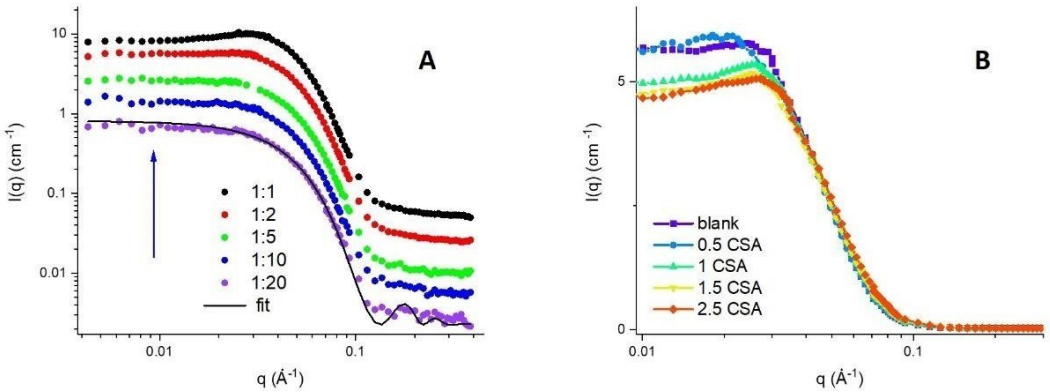

Figure 1 *– SANS spectra of micelles at room temperature. A) blank micelles at different dilution, starting from 30 mg/mL w/v. The fit of the most diluted system is reported (black solid line). B) micelles (15 mg/mL), at different CSA loading, as reported in the legend (CSA concentrations in mg/mL). The intensity is reported in linear scale to highlight the effect of the structure factor in the low q region*.

3.2 SAXS mucodiffusion study

The stability of the micellar structure when in contact with mucus and the propensity of micelles to permeate and cross a mucus layer were investigated by SAXS, observing the interaction of micelles with mucin. Mixed mucin-micelles samples were prepared by mixing 40 µL of HL micelles formulation (30 mg/mL) with 20 µL of a mucin type II solution 5% w/v. The scattered intensity profiles of the mixed samples, reported in **Supplementary Material**, can be reconstructed by the mere sum of the intensity contribution of micelles and mucin, revealing that the micelles are stable in the glycoprotein network and do not interact with mucin. The propensity of the micelles to penetrate into a mucus layer after contact was investigated by observing the diffusion process of

the micelles in a layer of mucin, as sketched in **Figure 2G**, exploiting the shorter acquisition time of SAXS measurements (1 s) with respect to SANS (2.5 hours). For these diffusion experiments, an already published protocol was used [47]: 40 µL of HL micelles formulation (30 mg/mL) were carefully put in contact with 20 µL porcine mucin (15% w/v) in a polycarbonate capillary (2 mm diameter), placed in a horizontal sample holder. SAXS intensities at different positions in the capillary were measured at different time delays (200, 800 and 1500 seconds). Results obtained for Simulated Nasal Electrolyte Solution (SNES) alone and CSA-loaded micelles are reported in **Figure 2**. The graphs (**Figure 2 A-C**, SNES in mucin and **Figure 2 D-F**, micelles in mucin) represent the evolution of the systems over time, after 200, 800 and 1500 s. The red curves are acquired in the mucin section of the capillary, as can be confirmed by the similarities with the pure mucin curve (reported in black on top) while blue curves represent the spectra acquired in the SNES or micelles section. The spectrum of pure micelles, is reported for comparison, presenting intensity minima and maxima (black line on the bottom of the graphs, **D-F**). The mixing kinetic of the two samples is appreciable, from a state in which the two main components, *i.e.* mucins and SNES or micelles, are clearly separated (Panel **A**, **D**) to the final state in which components are homogeneously mixed (Panel **C**, **F**).

To highlight the effective micelles permeation into the mucus, spectra acquired at a fixed position (2.4 mm from the samples contact interface) in the mucin section are reported in **Figure 2G** at different delays. The transition from a mucin-like spectrum toward a mixed micelle-mucin spectrum is clearly visible. This indicates the ability of the micelles to enter easily into mucin (15% w/v concentration). A similar behavior has been observed for the diffusion of a sample of SNES alone into mucin, as reported in **Supplementary Material**. Results indicate that micelles are able to enter and percolate together with water into mucin, with a diffusion time of the order of 10 µm/s, comparable with the one observed using SNES alone.

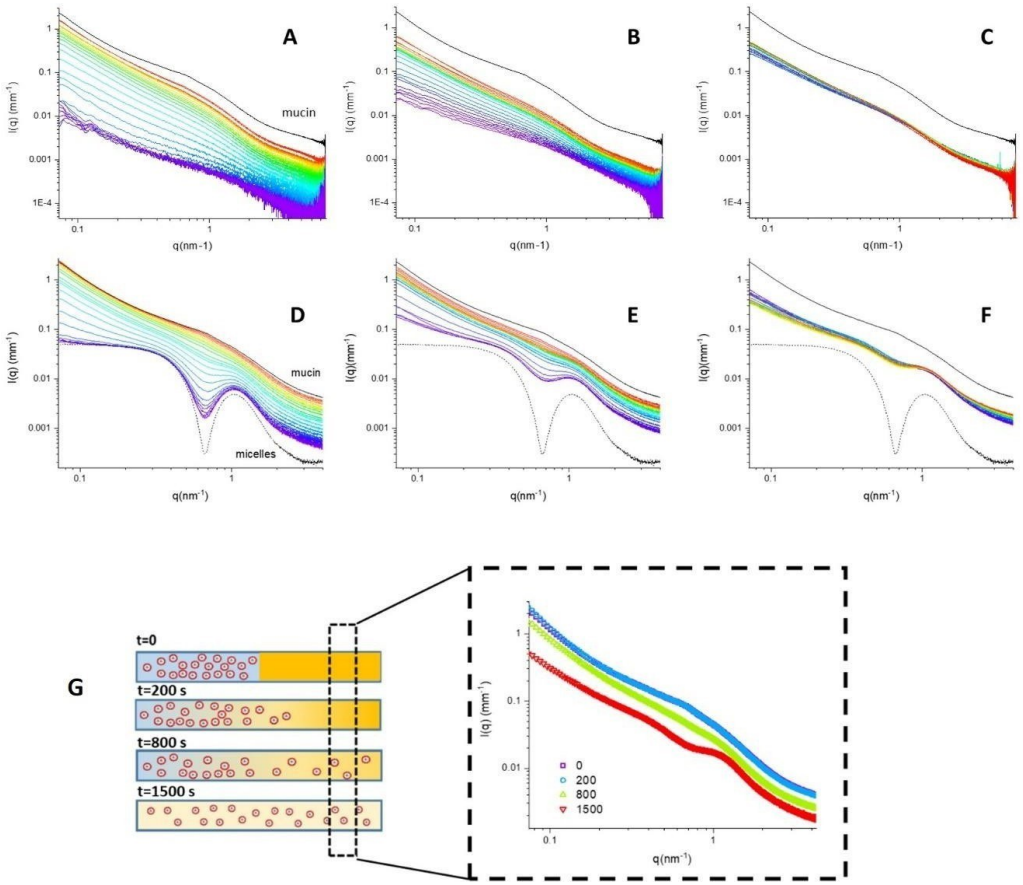

Figure 2 *– A-C) SNES diffusion in mucin during time. SAXS spectra at different positions in the horizontal capillary at three delays (from left to right: 200, 800, 1500 s). D-F) Micelles diffusion in mucin. SAXS spectra of micelles at different positions in the horizontal capillary at three delays (from left to right: 200, 800, 1500 s). G) sketch of the experimental set up and time evolution of the SAXS spectra acquired at 2.4 mm distance from the mucin/micelles contact interface (as indicated by the dotted square) over time (from t=0 to t=1500 s).*

3.3 *Ex vivo* mucoadhesion study

The HL micelles were compared to a CSA suspension for the tendency to adhere to the nasal tissue exploiting an excised rabbit mucosa positioned on an inclined plane apparatus.

The HL micelles resulted significatively less bioadhesive than the water suspension of CSA at the same concentration, used as control. After 30 minutes indeed, it has been shown that only 26% of the CSA belonging to the micellar formulation adhered to the fresh rabbit mucosa. As can be seen from **Figure 3**, most of the micellar formulation deposited on the nasal mucosa was removed already during the first 5 minutes of the experiment, with a dramatic fall in percentage of CSA adhering to the nasal mucosa. Then, from 5 to 30 minutes, the percentage of CSA adhering to the mucosa decreased very slowly.

The 0.5 mg/mL CSA suspension showed a different behavior, demonstrating to be more mucoadhesive than the micellar suspension, as can be seen from **Figure 3**. In this case, 89% of the

drug initially deposited on the mucosa adhered to the tissue even after 30 minutes. Exploiting the collected data, the mucosal mean residence time (mMRT) was calculated for both the micellar formulation and the drug suspension. The mMRT of the micelles turned out to be significatively lower than that of the drug suspension. More precisely, the micellar mMRT was 42.9 ± 8.8 minutes, while the mMRT of the drug suspension was 163.8 ± 28.6 minutes.

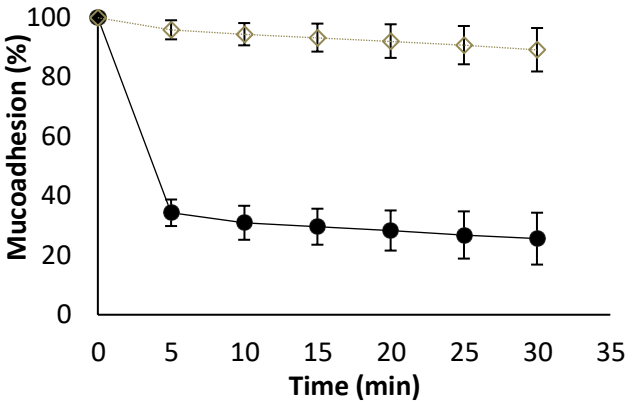

Figure 3 *– Ex vivo mucoadhesion study on rabbit's nasal mucosa. Comparison between the mucoadhesive properties exhibited by the micelles loaded with 0.5 mg/mL CSA (black circles) and those exhibited by a 0.5 mg/mL CSA suspension (gray empty diamonds) used as reference. (n=6).*

3.4 Cytotoxicity study on Vero E6 cells

The cell viability of the Vero E6 cell cultures treated with CSA alone was completely comparable to that of the untreated ones, so none of the pure CSA concentration tested proved to be cytotoxic for Vero E6 cells. The LL micelles appeared extremely cytotoxic at the three upper concentrations tested, *i.e.* 16 µM, 32 µM and 64 µM containing respectively 3.81 mM, 7.63 mM and 15.25 mM TPGS. The same cytotoxicity profile was demonstrated for the blank micelles at the corresponding TPGS concentrations.

Similarly, the ML micelles were cytotoxic at the tested CSA concentrations of 32 µM and 64 µM (TPGS concentration: 3.05 and 6.10 mM respectively). Finally, as regards the HL micelles, only the CSA concentration of 64 µM (15.25 mM TPGS) provoked cytotoxicity. In all the experiments, the same cytotoxicity profile was demonstrated when testing the blank micelles at the TPGS concentrations corresponding to the CSA-loaded formulations, indicating that the surfactant is the component responsible for the observed toxicity.

3.5 Antiviral activity of the developed micelles against SARS-CoV-2

The ability of the CSA-loaded micelles to prevent and/or block SARS-CoV-2 replication was tested *in vitro* on Vero E6 cells and compared to the antiviral activity of both CSA solution and blank

micelles. Cytotoxic formulations, *i.e.* those that reduced the cell viability below 80%, were excluded from the evaluation. Cells were treated following different protocols, based on different treatment timing (pretreatment, treatment contextual to the infection, post-treatment 2 hours or 6 hours after the infection) and treatment repetitions (single or multiple treatments). This approach was aimed at understanding which stage of viral replication is targeted by CSA and which is the most advantageous mode of administration of micelles in view of a possible *in vivo* intranasal administration.

As shown in **Figure 4**, we found that, overall, the CSA-loaded micelles performed significatively better than both CSA solution and the blank micelles, attaining in most cases a percentage of viral inhibition higher than 100%. The results obtained by working with two different viral loads, *i.e.* 0.005 and 0.0005 m.o.i. (multiplicity of infection, *i.e.* the ratio of the number of virus particles to the number of target cells) were in good agreement even if the efficiency of the drug-loaded micelles turned out to be higher when a lower viral amount was used, as expected. Here below, we present the results obtained working with 0.005 m.o.i. while **Supplementary Material** contains a comment on the results obtained by treating cells with 0.0005 m.o.i. (**Figure S7**). **Table 2** reports the concentration of TPGS in the micellar solutions tested.

Table 2 *– Composition of the micellar solutions used for the determination of the antiviral activity.*

CSA (μM)	TPGS (mM)		
	HL	ML	LL
32	1.525	-	-
16	0.763	1.525	-
8	0.381	0.763	1.907
4	0.191	0.381	0.953
2	0.095	0.191	0.477

In the case of the pre-treatment protocol (one hour treatment before the infection, **Figure 4A**) both HL and ML micelles showed a maximum antiviral activity of about 70%, significatively better if compared to both CSA solution and blank micelles. Regarding the micelles with the lowest CSA loading (LL micelles), in this protocol the results obtained by using the blank and the drug loaded micelles were similar. In general, the blank micelles, used as reference, showed a variable antiviral action, with values however significantly lower than those obtained with the corresponding loaded micelles. The CSA controls, in which the drug solution was used, turned out to be ineffective against SARS-CoV-2 at all the concentrations tested.

When a treatment contextual to the infection was used (one hour treatment in presence of the virus), in most cases the loaded micelles turned out to perform significatively better than the CSA

alone and the blank micelles controls (**Figure 4B**). All the drug-loaded formulations showed a similar trend, consisting in an increasing antiviral activity with increasing CSA concentrations, leading to values above 90% of viral inhibition for HL, ML, and LL at 32, 8 and 4 μM, respectively. In particular, among all the CSA-loaded micelles, the LL formulation showed the highest antiviral activity (107%) when used at a CSA concentration of 8 μM.

CSA solution used at concentration between 2 and 16 μM were significantly less effective if compared to the loaded micelles. The CSA solution only showed an antiviral activity comparable to that of the drug-loaded micelles when applied at the highest concentration tested which was 32 μM. It must be underlined that this was the only case in which we registered a 100% antiviral efficiency for the non-formulated CSA.

The blank micelles used as reference, although showing an appreciable effect (7-79%), sometimes even higher than CSA solution, turned out to be in all the cases significantly less effective than the corresponding drug loaded micelles.

When applied post-infection (one hour treatment two hours after the infection, **Figure 4C**), all the drug-loaded micelles turned out to be significatively more effective at hindering viral replication if compared to both the blank micelles and the CSA solution. HL and ML micelles showed a similar behavior, turning out to be more effective at the lowest CSA concentration tested, 2 μM. More precisely, the HL micelles exhibited a 102% viral inhibition, while the ML micelles exhibited a 111% viral inhibition. The LL micelles effectiveness was proportional to the CSA concentration, with a peak in correspondence of the 8 μM drug concentration (101%). When applied two hours after the infection at the highest concentration tested (corresponding to 32 μM), the CSA solution inhibited the SARS-CoV-2 replication up to 45%. A certain antiviral activity was also evidenced at a drug concentration of 16 μM, at which the viral replication was inhibited by 21%. Under this concentration, no antiviral effect was observed for the raw peptide.

Blank micelles highlighted a certain antiviral activity (38-66%) significantly lower than the drug-loaded micelles. When a delayed treatment protocol was used (one hour treatment six hours after the infection, **Figure 4D**), the lowest percentages of viral inhibition for all the three different developed micellar formulations were obtained (77% at 32 μM, 73% at 16 μM, 73% at 8 μM for HL, ML and LL micelles, respectively). The not-formulated CSA demonstrated a 42% viral inhibition at 32 μM, and a 25% viral inhibition at 16 μM. Its effectiveness dramatically decreased with lower concentrations becoming totally ineffective for concentrations below 8 μM. Nevertheless, in all the cases the drug- loaded micelles performed significatively better than the CSA raw material and in most cases than the blank micelles, with the only exception of CSA concentration of 2 μM, where blank micelles performed better than HL and ML micelles, but with antiviral efficacy below 40%.

When treatment was applied twice pre- and post-infection (one hour treatment before the

infection and a posttreatment two hours after the infection, **Figure 4E**), all the developed CSA-loaded micellar formulations showed significatively improved values of viral inhibition if compared to both the peptide solution and the blank micelles at all the CSA concentrations tested.

The HL and ML micelles showed a similar trend consisting of a very high antiviral activity, never going under 90%, with highest values at 2 μM (122% for HL and of 135% for ML micelles).

The behavior showed by the LL micelles was slightly different, *i.e.* consisted in a peak of activity (116%) at 8 μM but lower values at decreasing CSA concentrations, however never going under 100% inhibition. Antiviral effect of drug-loaded micelles was consistent.

The CSA showed a maximum of 39% of antiviral activity when tested at the highest concentration (32 μM), but below 16 μM no antiviral effect was observed. For all the blank formulations higher antiviral activity was detected compared to the one obtained by using the peptide solution; however, the inhibition never exceeded the value of 74%.

In the case of repeated post-treatments (one hour treatment repeated two, four and six hours after the infection, **Figure 4F**) the developed CSA-loaded micellar formulations provided an overall performance quite similar to the previous condition. The HL and ML micelles showed high antiviral activity in all the conditions tested (never under 70%), with highest values recorded at 2 μM (109% for HL and 106% for ML micelles). The results obtained using the LL micelles were slightly different, showing the highest activity (106%) at 8 μM but lower values at decreasing CSA concentrations, however never going under 93% inhibition. Again, for CSA solution and blank micelles antiviral activity (max. 28% for CSA solution and 88% for blank micelles) was invariably lower than the one obtained for the corresponding drug-loaded micelles at all the concentrations tested.

Finally, when a pre-treatment was associated with repeated post-treatments (one hour treatment before infection and repeated treatments two, four and six hours after the infection, **Figure 4G**) the two previous conditions data (**Figure 4E** and **4F**) were confirmed. Indeed, all the drug-loaded micelles performed significatively better than the non-formulated drug and the control blank formulation. The antiviral activity observed from the HL and ML micelles was again very high (always above 90%) with the highest value (116% for the HL and 121% for the ML micelles) recorded at 2 μM CSA concentration. LL micelles peak of antiviral activity (115%) was observed at the highest CSA concentration tested (8 μM). CSA solution and blank micelles antiviral activity (max. 25% for CSA solution and 84% for blank micelles controls) was lower than the one obtained for the corresponding drug-loaded micelles at all the concentrations tested. The results of the statistical analysis performed on data obtained by the *in vitro* studies are collected in **Supplementary Material** (**Tables S4-S17**).

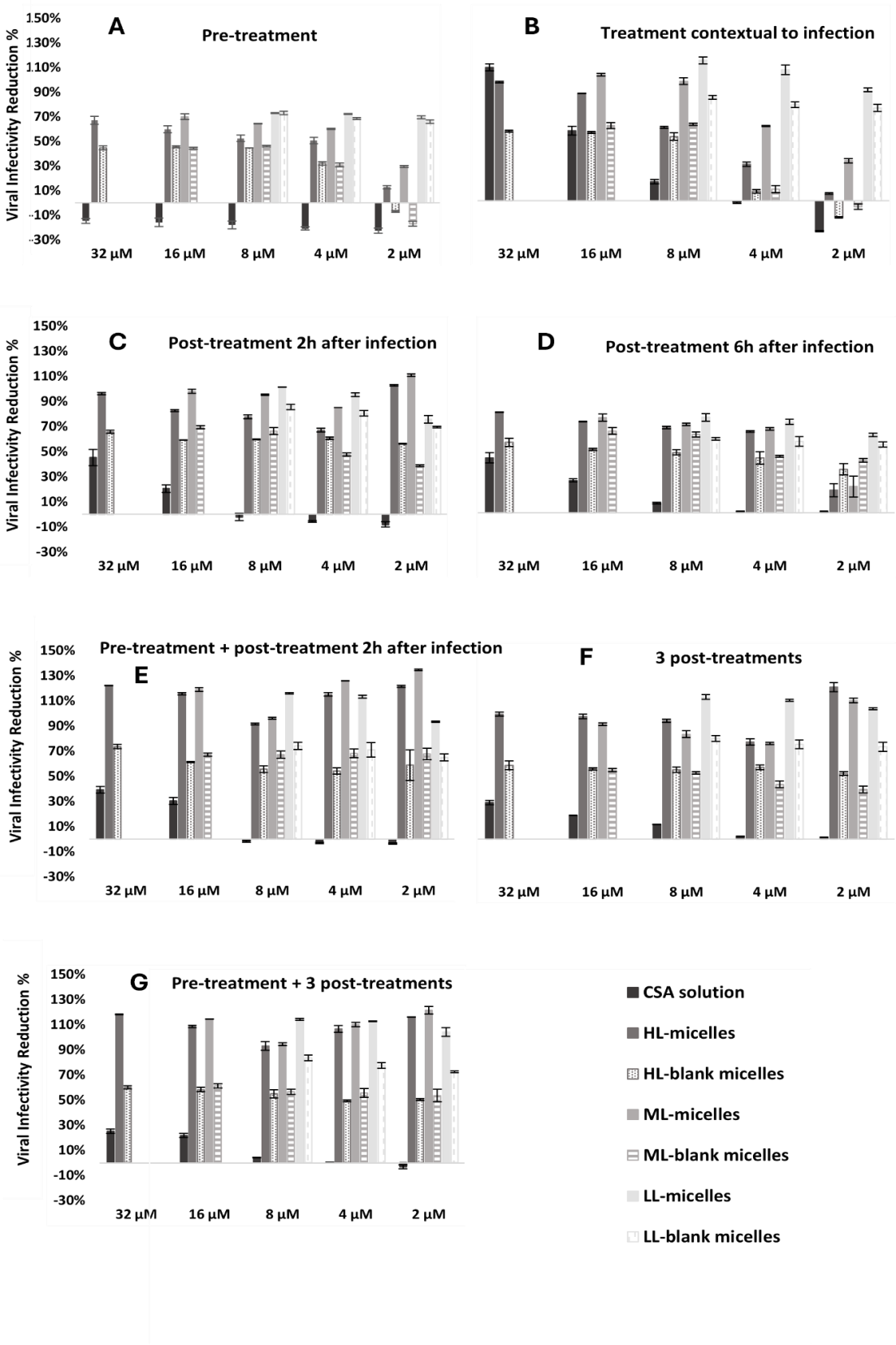
A
Pre-treatment
B
Treatment contextual to infection
C
Post-treatment 2h after infection
D
Post-treatment 6h after infection
E
Pre-treatment + post-treatment 2h after infection
F
3 post-treatments
G
Pre-treatment + 3 post-treatments
Viral Infectivity Reduction %
150%
130%
110%
90%
70%
50%
30%
10%
-10%
-30%
32 µM
16 µM
8 µM
4 µM
2 µM
CSA solution
HL-micelles
HL-blank micelles
ML-micelles
ML-blank micelles
LL-micelles
LL-blank micelles

Figure 4 *- Antiviral activity of the HL micelles, ML micelles and LL micelles compared to the raw CSA and the blank formulations. Each graph represents the results obtained by treating the infected cells with one of the seven different protocols tested: treatment 1h before infection (protocol A), treatment contextual to the infection (protocol B), post-treatment 2h after the infection (protocol C), post-treatment 6h after the infection (protocol C6), pre-treatment 1h before the infection followed by a post-treatment 2h after the infection (protocol D), 3 post-treatments spaced 1h apart (protocol E), pre-treatment 1h before the infection followed by 3 post-treatments spaced 1h apart (protocol F).*

3.6 Spray characterization

The HL formulation was loaded into three different devices, namely a conventional multidose preservative-free spray pump (CPS, device **A**) and innovative Bidose (device **B**) and BiVax (device **C**) nasal devices, to assess the potential nasal application of the micelles system developed.

The integrity of the micelles delivered by the three devices was studied employing DLS. As reported in **Table 3**, the BiVax device was the one which reported comparable size and PDI with the bulk formulation, whereas, particularly with the conventional spray pump, a slight increase in size and PDI was observed, indicating more polydispersity of the sample analyzed with a very moderate tendency to aggregation of the sprayed micelles. A negligible increase in Zeta Potential was observed as well for all sprayed samples analyzed, regardless of the nasal device employed.

Table 3 *– Integrity of the HL micelles formulation delivered by the three nasal devices*

	Size [nm]	PDI	Zeta Potential [mV]
HL micelles 0.5 mg/mL (before firing)	11.3 ± 0.1	0.08	-1.5 ± 0.2
HL micelles 0.5 mg/mL (fired by BiVax)	11.5 ± 0.1	0.08	-3.7 ± 0.3
HL micelles 0.5 mg/mL (fired by Bidose)	11.9 ± 0.1	0.20	-3.5 ± 0.9
HL micelles 0.5 mg/mL (fired by CPS spray pump)	12.2 ± 0.4	0.22	-3.8 ± 0.7

The spray emitted from the three devices was then characterized in terms of droplet size distribution (DSD), spray pattern (SP) and plume geometry (PG).

DSD (**Figure 5**) analyzed at 3 and 6 cm from the laser beam showed comparable size for the droplets emitted by the Bidose (**B**) and BiVax (**C**) systems mean volume diameter (D_{v50}) of 30.4 ± 1.9 µm and 34.6 ± 1.2 µm, at 3 cm respectively, and D_{v50} of 42.8 ± 2.0 µm and 42.3 ± 4.8 µm, at 6 cm respectively), whereas the CPS nasal pump (**A**) reported larger droplets (D_{v50} of 45.6 ± 0.6 µm at 3 cm and 49.1 ± 1.1 µm). Span was also higher for the droplets generated by CPS pump showing a wider droplet distribution in comparison of the other two nasal devices. This will determine a tendency of higher deposition in the anterior region of the nose for CPS nasal pump. However, the percentage of droplets below 10 µm was < 3% for all three systems employed, ideal to avoid

deposition into the throat targeting just the nasal cavity, namely the primary entry and infection site of the virus.

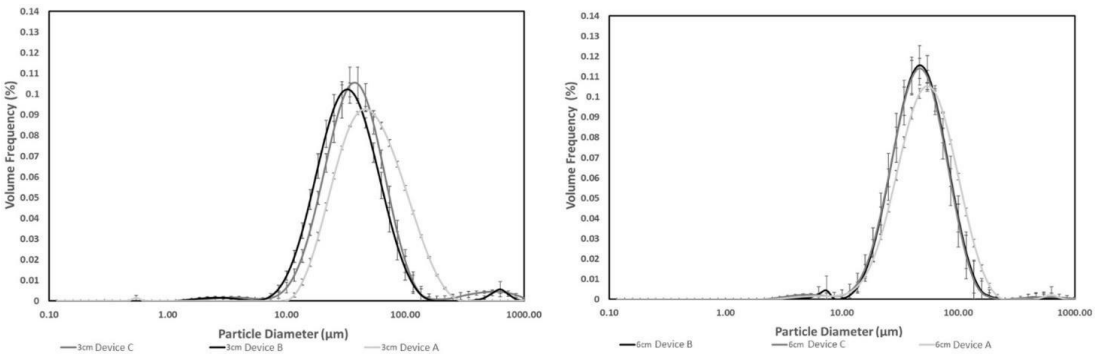

Figure 5 *– DSD at 3 and 6 cm from the laser beam for the three nasal devices employed (A: CPS spray pump, B: Bidose System BDSI V3 and C: BiVax System).*

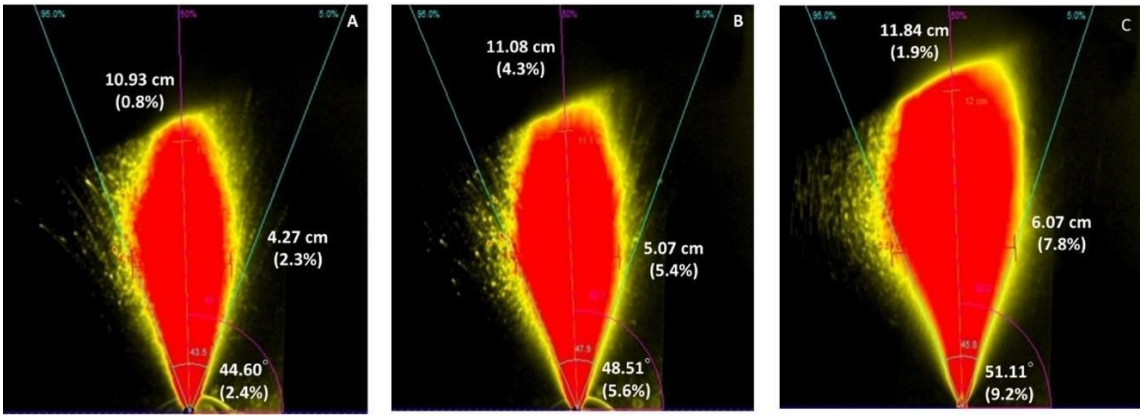

Figure 6 *– PG of the spray emitted from the three nasal devices employed (A: CPS spray pump, B: Bidose System BDSI V3 and C: BiVax System).*

Plume geometry (PG) and spray pattern (SP) were measured for all three devices. PG did not display any relevant difference between the spray emitted by the systems (**Figure 6**). The main effect observed on the shape of the plume was correlated with the volume delivered by a single actuation of the different devices: 70 µL for the conventional spray pump, 100 µL for the Bidose and 250 µL for BiVax. The latter showed the largest plume minimum and maximum diameter by SP at both distances evaluated (**Table 4**), whereas the spray area increased proportionally to the volume delivered by a single shot (BiVax ≥ Bidose > CPS nasal pump). However, the effect of the spray volume was predominant for BiVax in comparison to CPS nasal pump and Bidose, which behaved more similarly.

Table 4 *– SP at 3 and 6 cm from the laser beam for the three nasal devices employed (A: CPS spray pump, B: Bidose System BDSI V3 and C: BiVax System).*

Device	Distance	Dmin (cm)	Dmax (cm)	Ovality ratio	Area (cm^2)
CPS spray pump (A)	3 cm	2.9 ± 3.4	4.5 ± 4.1	1.6 ± 1.0	9.6 ± 6.0
	6 cm	4.1 ± 1.1	5.6 ± 5.2	1.3 ± 4.4	17.5 ± 3.3
Bidose (B)	3 cm	3.0 ± 7.8	4.7 ± 2.2	1.6 ± 9.5	9.5 ± 11.7
	6 cm	4.4 ± 11.7	6.3 ± 6.4	1.4 ± 7.8	21.6 ± 18.2
BiVax (C)	3 cm	4.0 ± 12.7	5.4 ± 4.3	1.4 ± 12.7	16.3 ± 14.5
	6 cm	6.5 ± 2.2	8.3 ± 3.6	1.3 ± 3.1	44.0 ± 6.8

3.7 Formulation deposition in a nasal cast

The characterization studies demonstrated the high rate of mucopenetration of micelles developed in this work as well as their potential for nasal application.

The three different devices were then used to deliver the HL formulation and thus originate different deposition profiles within the nasal cavity. The study aimed to select the device most suitable for intranasal administration of micelles loaded with CSA to counteract SARS-CoV-2 infection in the upper airway.

The deposition study performed on the silicon nasal cast highlighted that the three different devices tested performed in a significantly different manner. As can be seen from **Figure 7**, the BiVax System nasal atomizer (device **C**) allowed to reach the highest deposition area (45.52 ± 3.09 %) into the nasal cavity. A statistically significant lower total deposition area (32.42 ± 2.68 % and 25.85 ± 7.39 %) was obtained by using the Bidose System BDSI V3 (device **B**) and CPS spray pump (device **A**), respectively. These results were in line with the spray characterization results collected, which showed a similar spray pattern for devices **A** (CPS nasal pump) and **B** (Bidose System), in comparison to the one of BiVax (device **C**).

As illustrated in **Figure 7** below, when devices **A** and **B** were used, the micellar formulation mainly deposited in the ventral region of the nose, called *vestibulum*, and to a lower extent but in similar percentages in the middle-upper and lower turbinate. More precisely, the ratio between the deposition in the *vestibulum* and that in the middle-upper or inferior turbinate was 3:1. On the other hand, when using device **C** (BiVax) the distribution of the administered micellar formulation

appeared more homogeneously distributed on the nasal cavity surface. Indeed, the deposition was comparable between the *vestibulum*, the middle-upper turbinate and the lower turbinate. In all the three cases, the deposition at the throat level was minimal, as also observed in the DSD results, and the statistical analysis did not show any significant differences between devices **A**, **B** and **C**. After each spray, the behavior of the administered formulation was carefully observed, and no dripping was evidenced for the devices tested.

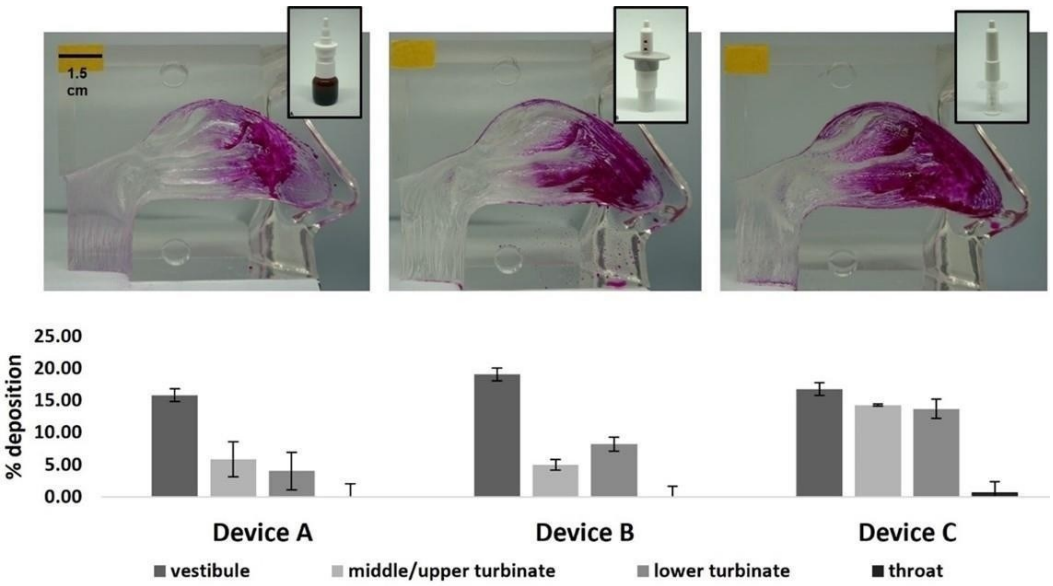

Figure 7 *– the different distribution profile of the HL micelles obtained by administering the micellar formulation into a simulated nasal cavity using the three different nasal devices tested. Above, a visual representation of the nasal areas reached by the formulation once sprayed into the nostril. Below, a graphical representation of the distribution of the micellar formulation into the different regions of the nasal cavity that are vestibulum, middle/upper turbinate, lower turbinate and throat*.

4. DISCUSSION

The developed CSA-loaded micelles turned out to be perfectly in line with those already reported in literature by Pescina *et al.* [33] and Ghezzi *et al.* [27] and proposed for ocular administration, showing a particle size of ~15 nm, null surface charge and low PDI, confirming that the obtained systems were monodispersed [48]. The encapsulation efficiency of cyclosporine A at the concentrations tested was always nearly complete (above 97%) attesting that TPGS leads to a higher improvement of the drug encapsulation if compared to other non-ionic amphiphilic polymers, such as Solutol® HS15 and poloxamer 407. This aspect was highlighted in recent works attesting that the solubility of cyclosporine A in 20 mM TPGS is six-fold higher than that in 20 mM Solutol® HS15, [27] and 8-fold higher than that in 20 mM poloxamer 407 [49]. In this work, the drug was encapsulated into the micelles at three different concentrations to evaluate whether the encapsulation efficiency could vary as the drug concentration increased. The choice to remain in the loading range between 0.1 mg/mL (equivalent to 83 µM) and 0.5 mg/mL (equivalent to 416 µM) was due to the high potency of the drug, which has proven to be effective in counteracting the replication of coronaviruses at concentrations between 2µM and 64µM [14].

However, we didn't observe any decrease in terms of encapsulation efficiency with increasing drug concentration. Moreover, the amount of the drug encapsulated did not appear to have an impact on the particle size and the polydispersity index as well as on the viscosity of the formulation which was around 1 mPa·s in all the formulations at 25°C. Although it was reported in literature that the ability to encapsulate CSA within micelles of TPGS can be even 10 times that used in this work [27], the drug content of our formulations was kept low, using 0.5 mg/mL as maximum concentration (except in SANS studies). This choice was motivated by the known immunosuppressive activity of CSA [1], which is obviously to be avoided when this drug is administered intranasally to have an antiviral action against SARS-CoV-2. As regards the stability, all the micelles showed a good stability profile with steady particle size, PDI and drug content during storage up to 7 months; in particular, HL micelles showed a slightly better stability if compared to the ML and LL micelles. Considering this factor as well as the fact that HL, by containing the highest drug concentration, would allow to reduce the volume to be administered potentially *in vivo*, we identified HL as the best candidate for the future *in vivo* studies, therefore decided to test only them to evaluate the mucoadhesion profile and behavior when sprayed with nasal spray.

As highlighted by SAXS and SANS analysis, the presence of CSA in the micellar core affected the size and shape of the self-aggregating micelles even in small amount (few molecules per micelle). The CSA-loaded systems rearrange, as a function of CSA loading, in micelles with a slightly smaller spherical hydrophobic core (size from 7 to 6.4 nm) surrounded by a hydrophilic shell of constant

thickness (2.9 nm).

Quite interestingly, the CSA-loaded micelles formulations were demonstrated to be stable in simulated mucus, suggesting that they are not inclined to interact with mucin glycoproteins neither by electrostatic interaction nor by hydrogen bonding. This is a feature attributable to the almost neutral surface of the micelles, allowing to avoid the possible electrostatic interaction of the micelles with the negatively charged sialic acid residues characterizing the mucins [50]. Moreover, we observed a poor tendency of the micelles to stick to the mucus layer on the *ex vivo* model used, obtaining highly reproducible results regardless of the variability that naturally characterizes the biological tissues.

The poor tendency of the micelles to stick to the mucus layer could also be attributed to the PEGylated hydrophilic surface of micelles provided by TPGS. In fact, PEG surface modification has been demonstrated to be able to reduce protein surface adhesion in a number of nanomaterials [51–55], as well as to avoid interactions with mucin glycoproteins in the mucus layer [54].

These structural features suggest a mucopenetration ability of the formulation, that could provide an escape strategy from the physiological process of muco-ciliary clearance, thus increasing the retention time in the nasal cavity. For this reason, the propensity of the developed micelles to penetrate mucus was tested and confirmed by diffusion results obtained by SAXS and successively by *ex vivo* mucoadhesion studies on rabbit nasal mucosa. Results indicate that micelles are able to enter and permeate together with water into a viscous mucin solution (15% w/v), used as mucus model, with a diffusion speed of the order of 10 µm/s, comparable with the one observed using a simulated nasal fluid alone. This was further explained by the fact that the very small particle size (about 12 nm) and the almost spherical shape can ensure that the micelles are not retained by the size filter consisting of the mucin fiber mesh, which porosity has been indicated between 50 and 1800 nm [56,57].

The suitability of the micellar formulation for intranasal application was further confirmed by the administration of the micellar formulation in a nasal cast using different devices. The good distribution profile obtained and the absence of dripping regardless of the kind of device confirmed that the developed micelles could actually be exploited as an intranasal treatment. In particular, giving the more homogeneous distribution between the regions of the nose and the greater covered surface area obtained using the BiVax nasal atomizer (device **C**) as well as the best stability results obtained in terms of micelles size and PDI after administration, we believe that this is the most suitable device to guarantee greater protection against SARS-CoV-2 infection in the upper airways. Indeed, it should be considered that the nasal cavity represents a very large surface to which the virus can adhere after being inhaled giving rise to a starting infection. Considering that the greater the covered nasal surface, the higher the protective activity of the micellar formulation,

the BiVax nasal atomizer was preferred to the other two tested nasal devices, because it has been shown to be able to distribute the micellar formulation more deeply in the nasal cavity leading to the greatest surface coverage, justified by the spray characterization results which showed a larger plume diameter and area for this nasal device which led to the greater and more homogenous cover of the nasal cavity.

Concerning the antiviral effect of the formulations tested, all the drug-loaded micelles showed significantly higher antiviral efficacy than pure CSA and the blank formulations. The only exception was represented by the LL micelles used to pre-treat infected cells. In this specific case indeed, the activity of the blank and the drug-loaded micelles did not differ, probably due to the very low concentration of CSA.

By comparing the results obtained with different treatment protocols, it was found that the best approaches to hinder the viral replication consist in a post-treatment 2 hours after infection or protocols in which repeated treatments are combined pre- or post-infection, simulating a repeated administration, a quite common and realistic situation for nasal medicinal products.

Concerning the three different formulations tested, the results obtained by testing the HL and ML micelles could be commented parallelly, since showed a similar behavior which was slightly different from that obtained by testing the LL micelles. In fact, when the ML and HL micelles were tested at the lowest CSA concentration (2 µM), the inhibition of the SARS-CoV-2 replication turned out to be the most effective, resulting greater than 100% in all the cases. On the contrary, the same results in terms of antiviral efficiency were obtained when the LL micelles were used at the highest CSA concentration, *i.e.* 8 µM. This difference could be attributed to a potential role of TPGS which, at each CSA concentration tested, was proportionally more abundant in the LL micelles, due to the lower drug content. This hypothesis is supported by the fact that by testing the blank micelles we observed a noticeable antiviral activity, even if significatively lower than that of the loaded micelles. In particular, a linear correlation between the blank micellar concentration used and the Cycle Threshold (Ct) value was found, indicating a reduction in the viral activity and replication. Firstly, given the surfactant properties of the polymer, we can attribute the antiviral activity of the blank micelles to the ability of TPGS to alter the fluidity of the viral envelop, by interpolation between phospholipids [58,59]. Another possible mechanism has been reported by researchers from the University of Alabama at Birmingham (Birmingham, AL, USA). Their data, published as pre-print [60] demonstrated the capacity of water-soluble tocopherol derivatives, (specifically TPGS and, albeit to a lesser extent, also Vitamin E succinate) to inhibit the transcriptional activity of SARS-CoV-2 RNA-dependent RNA polymerase.

However, despite the blank micelles had also shown this kind of activity, we exclude that the effect

belonged only to the presence of TPGS, but hypothesized a synergistic action of TPGS with CSA, since the percentages of infectivity reduction were significatively higher for almost all the drug-loaded micelles tested than for the blank micelles.

Indeed, when the non-formulated CSA was used as control, its effectiveness was dramatically lower than that shown when loaded into the micellar structure. In most cases, pure CSA antiviral activity did not exceed 50% which however was registered only working at the highest drug concentration, *i.e.* 32 µM. An exception occurred when pure CSA was present with the virus at the moment of the infection, where an inhibition up to 100% was attained. This is consistent with data reported in literature [1,14], attesting that CSA mainly acts on the very first phases of infection by altering the organization of the viral intracellular membranes exploited to generate the viral replication complex, which normally forms early after the cell penetration. However, this action seemed to prevail on another CSA antiviral action reported in literature, which consists in the hindering of the N protein's folding and its subsequent binding with the viral genome to assemble the viral progeny [61].

On the contrary, CSA encapsulated in a micellar formulation based on TPGS underwent a significative improvement of its antiviral activity even at the lowest concentration tested, 2 µM. This is due to the presence of TPGS, that can have a series of actions enabling a more effective antiviral activity: 1) improvement of CSA solubility, making the peptide more available at molecular level; 2) enhanced CSA cell penetration, an effect related to the surface-active properties of TPGS; 3) potential hindering of the receptor-ligand interactions normally exploited by the virus to infect cells [62–64], allowing the CSA micellar formulation to be effective at inhibiting SARS-CoV-2 infection even when used as a pre-treatment. Furthermore, we can also hypothesize that the well-known activity of TPGS as P-glycoprotein (P-gp) efflux inhibitor [65] could contribute to the result, since it has been demonstrated in CaCo-2 [66], that CSA transport is modulated by these systems. Finally, the antioxidant activity of TPGS could be exploited in the most severe cases of infection, since it undergoes degradation leading to the release of vitamin E [67] which can help to avoid the worsening of the disease. It is known indeed, that the viral infection causes an alteration of the balance between the production of oxidants and antioxidants leading to an oxidative stress responsible for serious complications [6].

When the ML micelles and HL micelles were applied on cells 6 hours after infection, the antiviral activity was lower than the cases in which were applied following the other approaches. Our hypothesis was that after 6 hours from the infection, the replicative cycle of the virus is in an advanced phase, with the virus completely penetrated the cell starting its replication. At that point, as also reported in literature [14], neither the peptide drug, nor the TPGS could interfere with the viral replication leading to a complete inhibition of the infection. However, it must be underlined

that despite the reduced antiviral activity demonstrated in this case by all the drug-loaded micelles, the effectiveness of the latter always demonstrated to be greater than that of the blank micelles and in most cases also of the non-formulated CSA, with the only exception represented by the cases in which the loaded micelles were diluted so as to work at concentrations of CSA of 2 μM: in these cases the level of efficacy of the drug loaded micelles was comparable to that of the blank micelles. By making a general overview of the collected data, it can be appreciated that in several cases the viral inhibition corresponded to or exceeded the 100% value, indicating that viral replication was completely blocked. Values exceeding 100% were due to the fact that, after the replication of the virions had been blocked by the treatment, the virions remained in solution and started to degrade. The extent to which the virus degrades and therefore how much the percentage could be higher than 100 is a totally random factor. However, we noted a direct proportion between the concentration of the micelles and the percentage of viral inhibition, leading to confirming the hypothesis that the micelles were able to degrade the virus in solution.

Concerning the spray characteristics and deposition in the nasal cavity, anyone of the three devices tested did affect the physical properties of the micelles, preserving their size and surface charge. Sprays did not appear to differ in a significant manner in terms of emitted droplet size distribution, spray angle and spray plume characteristics. However, the device BiVax provided a significantly better coverage of the nasal cast both in terms of overall surface area covered and distribution over different region of interest such as upper and lower turbinates. This was attribute to a higher surface spray area that was correlated with the larger emitted volume (250 μL against 100 and 70 μL for BiDose and CPS device, respectively). This result is in agreement with the observations of Kundoor and Dalby [45], that using the same cast, found that spray pumps delivering 100 μL had significantly greater nasal deposition area than nasal spray pumps delivering 50 μL. However, the deposition observed were mainly in the vestibule part of the nasal cavity, demonstrating that the choice of an optimal combination between device and formulation is required in order to develop a nasal product truly effective against a viral infection. In fact, the penetration of the formulation and coverage of nasal anatomical structures such as the turbinates involved in the filtration and entrapment of the particulate carried by inhaled air appears critical to prevent or treat early SARS-CoV-2 infections.

5. CONCLUSIONS

All the CSA-loaded micellar formulation developed in the present work showed high industrial scalability due to their simple and fast production method, and to the possibility of an easy sterilization by filtration. At the same time, the formulation was stable for at least 7 months at ambient temperature. Moreover, the low particle size, the almost neutral surface and the high rate of mucopenetration make them ideal for intranasal administration. The high drug encapsulation efficiency of the TPGS micelles was also exploited in our research to increase the low solubility of cyclosporine A, an immunosuppressant drug tested in this work for its potential as antiviral agent. The results obtained in an *in vitro* model of infection of SARS-CoV-2 Omicron variant highlighted that the drug-loaded micelles provided an excellent viral replication inhibition for single and repeated treatments pre-infection and up to 6 hours post-infection. In addition, CSA-loaded micelles performed better than CSA alone or the blank formulation at inhibiting the SARS-CoV-2 replication. Particularly, it was evidenced that also the micelle-forming excipient, the vitamin E derivative TPGS, plays a critical role in enhancing CSA inhibition of the viral replication, probably itself having an antiviral action through nonspecific mechanisms. Finally, the *in vivo* administration of the highest drug-loaded micellar formulation was simulated using a silicone human nasal cast after the *in vitro* characterization of the spray emitted by different systems, which allowed to identify a device able to deposit the micellar formulation homogeneously within the nasal cavity once intranasally administered, potentially providing a more effective protection against an incipient infection.

SUPPORTING INFORMATION

The Supporting Information is available free of charge.

Isothermal stability of micelles at 25°C over 7 months; dynamic viscosity calculated at both 25°C and 37°C; Fitting parameters for SANS data; *in vitro* antiviral activity against 0.0005 m.o.i; *p* values obtained by the statistical analysis.

AKNOWLEDGEMENTS

E.D.F. acknowledges the UniMi support (PSR2021_DEL_FAVERO). The authors are grateful for beam-time allocation and financial support to ESRF (DOI: 10.15151/ESRF-ES-653835676) and to CERIC (CERIC_20217127). This work benefited from the use of the SasView application for SANS and SAXS analysis.

DECLARATION OF COMPETING INTEREST

The authors declare no conflict of interest.

AUTHOR CONTRIBUTIONS

Conception and design, FG, FS; analysis and interpretation of the data, FG, FS, EDF, CR, LC, MB, IR; drafting of the paper, FG, FS, EDF, CR, IR; revising it critically for intellectual content, FS, SP, SN, EDF, CR; final approval of the version to be published, DD, FB, RB. All authors agree to be accountable for all aspects of the work.

DATA AVAILABILITY STATEMENT

The data supporting this work are accessible upon reasonable request from the corresponding author.

REFERENCES

1. Liu C, von Brunn A, Zhu D. Cyclophilin A and CD147: novel therapeutic targets for the treatment of COVID-19. *Med Drug Discov*. 2020;7:100056. doi:10.1016/j.medidd.2020.100056
2. Gorbalenya AE, Baker SC, Baric RS, et al. The species Severe acute respiratory syndrome-related coronavirus: classifying 2019-nCoV and naming it SARS-CoV-2. *Nat Microbiol*. 2020;5(4):536-544. doi:10.1038/s41564-020-0695-z
3. Hu B, Guo H, Zhou P, Shi ZL. Characteristics of SARS-CoV-2 and COVID-19. *Nat Rev Microbiol*. 2021;19(3):141-154. doi:10.1038/s41579-020-00459-7
4. Wu JT, Leung K, Leung GM. Nowcasting and Forecasting the Potential Domestic and International Spread of the 2019-nCoV Outbreak Originating in Wuhan, China: A Modeling Study. *Obstet Gynecol Surv*. 2020;75(7):399-400. doi:10.1097/01.ogx.0000688032.41075.a8
5. Mehta P, McAuley DF, Brown M, Sanchez E, Tattersall RS, Manson JJ. COVID-19: consider cytokine storm syndromes and immunosuppression. *Lancet*. 2020;395(10229):1033-1034. doi:10.1016/S0140-6736(20)30628-0
6. Laforge M, Elbim C, Frère C, et al. Tissue damage from neutrophil-induced oxidative stress in COVID-19. *Nat Rev Immunol*. 2020;20(9):515-516. doi:10.1038/s41577-020-0407-1
7. Chen N, Zhou M, Dong X, et al. Epidemiological and clinical characteristics of 99 cases of 2019 novel coronavirus pneumonia in Wuhan, China: a descriptive study. *Lancet*. 2020;395(10223):507-513. doi:10.1016/S0140-6736(20)30211-7
8. Lirong Zou FR, Huang M, Lijun Liang, Huitao Huang ZH, et al. SARS-CoV-2 viral load in upper respiratory specimens of infected patients. *N Engl J Med*. 2020;382(12):1177-1179. doi:10.1056/nejmc2000231
9. Wölfel R, Corman VM, Guggemos W, et al. Virological assessment of hospitalized patients with COVID-2019. *Nature*. 2020;581(7809):465-469. doi:10.1038/s41586-020-2196-x
10. Stadnytskyi V, Bax CE, Bax A, Anfinrud P. The airborne lifetime of small speech droplets and their potential importance in SARS-CoV-2 transmission. *Proc Natl Acad Sci U S A*. 2020;117(22):11875-11877. doi:10.1073/pnas.2006874117
11. Bleier BS, Ramanathan M, Lane AP. COVID-19 Vaccines May Not Prevent Nasal SARS-CoV-2 Infection and Asymptomatic Transmission. *Otolaryngol Neck Surg*. 2020;164(2):305-307. doi:10.1177/0194599820982633
12. Chavda VP, Vora LK, Pandya AK, Patravale VB. Intranasal vaccines for SARS-CoV-2: From challenges to potential in COVID-19 management. *Drug Discov Today*. 2021;26(11):2619-2636. doi:10.1016/j.drudis.2021.07.021

13. Chavda VP, Baviskar KP, Vaghela DA, Raut SS, Bedse AP. Nasal sprays for treating COVID-19: a scientific note. *Pharmacol Reports*. 2023;75(2):249-265. doi:10.1007/s43440-023-00463-7
14. de Wilde AH, Zevenhoven-Dobbe JC, van der Meer Y, et al. Cyclosporin A inhibits the replication of diverse coronaviruses. *J Gen Virol*. 2011;92(11):2542-2548. doi:10.1099/vir.0.034983-0
15. Mamatis JE, Pellizzari-Delano IE, Gallardo-Flores CE, Colpitts CC. Emerging Roles of Cyclophilin A in Regulating Viral Cloaking. *Front Microbiol*. 2022;13(February):1-8. doi:10.3389/fmicb.2022.828078
16. Sweeney ZK, Fu J, Wiedmann B. From chemical tools to clinical medicines: Nonimmunosuppressive cyclophilin inhibitors derived from the cyclosporin and sanglifehrin scaffolds. *J Med Chem*. 2014;57(17):7145-7159. doi:10.1021/jm500223x
17. Schreiber SL, Crabtree GR. The mechanism of action of cyclosporin A and FK506. *Immunol Today*. 1992;13(4):136-142. doi:10.1016/0167-5699(92)90111-J
18. Peel M, Scribner A. Cyclophilin inhibitors as antiviral agents. *Bioorganic Med Chem Lett*. 2013;23(16):4485-4492. doi:10.1016/j.bmcl.2013.05.101
19. Pfefferle S, Schöpf J, Kögl M, et al. The SARS-Coronavirus-host interactome: Identification of cyclophilins as target for pan-Coronavirus inhibitors. *PLoS Pathog*. 2011;7(10). doi:10.1371/journal.ppat.1002331
20. Lallemand F, Perottet P, Felt-Baeyens O, et al. A water-soluble prodrug of cyclosporine A for ocular application: A stability study. *Eur J Pharm Sci*. 2005;26(1):124-129. doi:10.1016/j.ejps.2005.05.003
21. Berton P, Mishra MK, Choudhary H, Myerson AS, Rogers RD. Solubility Studies of Cyclosporine Using Ionic Liquids. *ACS Omega*. 2019;4(5):7938-7943. doi:10.1021/acsomega.9b00603
22. El Tayar N, Mark AE, Vallat P, Brunne RM, Testa B, van Gunsteren WF. Solvent-Dependent Conformation and Hydrogen-Bonding Capacity of Cyclosporin A: Evidence from Partition Coefficients and Molecular Dynamics Simulations. *J Med Chem*. 1993;36(24):3757-3764. doi:10.1021/jm00076a002
23. Lallemand F, Schmitt M, Bourges JL, Gurny R, Benita S, Garrigue JS. Cyclosporine A delivery to the eye: A comprehensive review of academic and industrial efforts. *Eur J Pharm Biopharm*. 2017;117:14-28. doi:10.1016/j.ejpb.2017.03.006
24. Lallemand F, Felt-Baeyens O, Besseghir K, Behar-Cohen F, Gurny R. Cyclosporine A delivery to the eye: A pharmaceutical challenge. *Eur J Pharm Biopharm*. 2003;56(3):307-318. doi:10.1016/S0939-6411(03)00138-3

25. Patel A, Cholkar K, Agrahari V, Mitra AK. Ocular drug delivery systems: An overview. *World J Pharmacol*. 2013;2(2):47-64. doi:10.5497/wjp.v2.i2.47
26. Pepić I, Lovrić J, Filipović-Grčić J. How do polymeric micelles cross epithelial barriers? *Eur J Pharm Sci*. 2013;50(1):42-55. doi:10.1016/j.ejps.2013.04.012
27. Ghezzi M, Ferraboschi I, Delledonne A, et al. Cyclosporine-loaded micelles for ocular delivery : Investigating the penetration mechanisms. 2022;349(July):744-755. doi: 10.1016/j.jconrel.2022.07.019
28. Guo J, Wu T, Ping Q, Chen Y, Shen J, Jiang G. Solubilization and pharmacokinetic behaviors of sodium cholate/lecithin- mixed micelles containing cyclosporine A. *Drug Deliv J Deliv Target Ther Agents*. 2005;12(1):35-39. doi:10.1080/10717540590889691
29. Luschmann C, Tessmar J, Schoeberl S, Strau O, Luschmann K, Goepferich A. Self-Assembling Colloidal System for the Ocular Administration of Cyclosporine A. *Cornea*. 2014;33(1). doi: 10.1097/ICO.0b013e3182a7f3bf
30. Yu Y, Chen D, Li Y, Yang W, Tu J, Shen Y. Improving the topical ocular pharmacokinetics of lyophilized cyclosporine A-loaded micelles: formulation, in vitro and in vivo studies. *Drug Deliv*. 2018;25(1):888-899. doi:10.1080/10717544.2018.1458923
31. Sonvico F, Colombo G, Quarta E, et al. Nasal delivery as a strategy for the prevention and treatment of COVID-19. *Expert Opin Drug Deliv*. 2023;20(8):1115-1130. doi:10.1080/17425247.2023.2263363
32. Tandon M, Wu W, Moore K, et al. SARS-CoV-2 accelerated clearance using a novel nitric oxide nasal spray (NONS) treatment: A randomized trial. *Lancet Reg Heal - Southeast Asia*. 2022;3:100036. doi:10.1016/j.lansea.2022.100036
33. Pescina S, Sonvico F, Clementino A, Padula C, Santi P, Nicoli S. Preliminary investigation on simvastatin-loaded polymeric micelles in view of the treatment of the back of the eye. *Pharmaceutics*. 2021;13(6). doi:10.3390/pharmaceutics13060855
34. Grimaudo MA, Nicoli S, Santi P, Concheiro A, Alvarez-Lorenzo C. Cyclosporine-loaded cross-linked inserts of sodium hyaluronan and hydroxypropyl-β-cyclodextrin for ocular administration. *Carbohydr Polym*. 2018;201(August):308-316. doi:10.1016/j.carbpol.2018.08.073
35. Ghezzi M, Pescina S, Padula C, et al. Polymeric micelles in drug delivery: An insight of the techniques for their characterization and assessment in biorelevant conditions. *J Control Release*. 2021;332:312-336. doi:10.1016/j.jconrel.2021.02.031
36. Eichner H, Behbehani AA, Hochstrasser K. Diagnostic value of nasal secretions, current state: normal values. *Laryngol Rhinol Otol (Stuttg)*. 1983;62(12):561-565.

37. Mahajan HS, Gattani SG. Gellan gum based microparticles of metoclopromide hydrochloride for intranasal delivery: Development and evaluation. *Chem Pharm Bull*. 2009;57(4):388-392. doi:10.1248/cpb.57.388

38. Castile J, Cheng YH, Simmons B, Perelman M, Smith A, Watts P. Development of in vitro models to demonstrate the ability of PecSys®, an in situ nasal gelling technology, to reduce nasal run-off and drip. *Drug Dev Ind Pharm*. 2013;39(5):816-824. doi:10.3109/03639045.2012.707210

39. Clementino AR, Pellegrini G, Banella S, et al. Structure and Fate of Nanoparticles Designed for the Nasal Delivery of Poorly Soluble Drugs. *Mol Pharm*. 2021;18(8):3132-3146. doi:10.1021/acs.molpharmaceut.1c00366

40. Munda R, Schroeder TJ, Pedersen SA, et al. Cyclosporine pharmacokinetics in pancreas transplant recipients. *Transplant Proc*. 1988;20(2 Suppl 2):487—490.

41. Ammerman N, Beier-Sexton M, Azad A. Growth and maintenance of Vero cell lines. *Curr Protoc Microbiol*. 2008;Appendix 4(Appendix 4E). doi:10.1002/9780471729259.mca04es11

42. Burnett L, McQueen M, Jonsson J, Torricelli F, Ethics IT on. IFCC Position Paper: Report of the IFCC Taskforce on Ethics: Introduction and framework. *Clin Chem Lab Med*. 2007;45:1098-1104. doi:10.1515/CCLM.2007.199

43. Lei C, Yang J, Hu J, Sun X. On the Calculation of TCID50 for Quantitation of Virus Infectivity. *Virol Sin*. 2020;12250. doi:10.1007/s12250-020-00230-5

44. Reed L, Muench H. A simple method of estimating fifty per cent endpoints. *Am J Epidemiol*. 1938;27(3):493-497. doi:10.1093/oxfordjournals.aje.a118408

45. Kundoor V, Dalby RN. Effect of formulation- and administration-related variables on deposition pattern of nasal spray pumps evaluated using a nasal cast. *Pharm Res*. 2011;28(8):1895-1904. doi:10.1007/s11095-011-0417-6

46. Puig-Rigall J, Grillo I, Dreiss CA, González-Gaitano G. Structural and Spectroscopic Characterization of TPGS Micelles: Disruptive Role of Cyclodextrins and Kinetic Pathways. *Langmuir*. 2017;33(19):4737-4747. doi:10.1021/acs.langmuir.7b00701

47. Di Cola E, Cantu' L, Brocca P, et al. Novel O/W nanoemulsions for nasal administration: Structural hints in the selection of performing vehicles with enhanced mucopenetration. *Colloids Surfaces B Biointerfaces*. 2019;183:110439. doi:10.1016/j.colsurfb.2019.110439

48. Stetefeld J, McKenna SA, Patel TR. Dynamic light scattering: a practical guide and applications in biomedical sciences. *Biophys Rev*. 2016;8(4):409-427. doi:10.1007/s12551-016-0218-6

49. Pescina S, Grolli Lucca L, Govoni P, et al. Ex Vivo Conjunctival Retention and Transconjunctival Transport of Poorly Soluble Drugs Using Polymeric Micelles.

Pharmaceutics. 2019;11(9). doi:10.3390/pharmaceutics11090476

50. Larhed AW, Artursson P, Gråsjö J, Björk E. Diffusion of Drugs in Native and Purified Gastrointestinal Mucus. *J Pharm Sci*. 1997;86(6):660-665. doi:10.1021/js960503w
51. Xu Q, Ensign LM, Boylan NJ, et al. Impact of Surface Polyethylene Glycol (PEG) Density on Biodegradable Nanoparticle Transport in Mucus ex Vivo and Distribution in Vivo. *ACS Nano*. 2015;9(9):9217-9227. doi:10.1021/acsnano.5b03876
52. Suk JS, Xu Q, Kim N, Hanes J, Ensign LM. PEGylation as a strategy for improving nanoparticle-based drug and gene delivery. *Adv Drug Deliv Rev*. 2016;99:28-51. doi:10.1016/j.addr.2015.09.012
53. Wang Y-Y, Lai SK, Suk JS, Pace A, Cone R, Hanes J. Addressing the PEG Mucoadhesivity Paradox to Engineer Nanoparticles that "Slip" through the Human Mucus Barrier. *Angew Chemie*. 2008;120(50):9872-9875. doi:10.1002/ange.200803526
54. Lai SK, O'Hanlon DE, Harrold S, et al. Rapid transport of large polymeric nanoparticles in fresh undiluted human mucus. *Proc Natl Acad Sci*. 2007;104(5):1482-1487. doi:10.1073/pnas.0608611104
55. Tang BC, Dawson M, Lai SK, et al. Biodegradable polymer nanoparticles that rapidly penetrate the human mucus barrier. *Proc Natl Acad Sci U S A*. 2009;106(46):19268-19273. doi:10.1073/pnas.0905998106
56. Lai SK, Wang Y-Y, Wirtz D, Hanes J. Micro- and macrorheology of mucus. *Adv Drug Deliv Rev*. 2009;61(2):86-100. doi:10.1016/j.addr.2008.09.012
57. Bansil R, Stanley E, Lamont JT. Mucin Biophysics. *Annu Rev Physiol*. 1995;57(1):635-657. doi:10.1146/annurev.ph.57.030195.003223
58. Ostacolo C, Caruso C, Tronino D, et al. Enhancement of corneal permeation of riboflavin-5'-phosphate through vitamin E TPGS: A promising approach in corneal trans-epithelial cross linking treatment. *Int J Pharm*. 2013;440(2):148-153. doi:10.1016/j.ijpharm.2012.09.051
59. Shahab MS, Rizwanullah M, Sarim Imam S. Formulation, optimization and evaluation of vitamin E TPGS emulsified dorzolamide solid lipid nanoparticles. *J Drug Deliv Sci Technol*. 2022;68:103062. doi:10.1016/j.jddst.2021.103062
60. H.T. Pacl, J.L. Tipper, R.R. Sevalkar, A. Crouse, C. Crowder, UAB Precision Medicine Institute, S. Ahmad, A. Ahmad, G.D. Holder, C. J. Kuhlman, K. C. Chinta, S. Nadeem, T. J. Green, C. M. Petit, A. J. C. Steyn, M. Might KSH. Water-soluble tocopherol derivatives inhibit SARS-CoV-2 RNA-dependent RNA polymerase. *(Preprint)*. Published online 2021.
61. Ma-Lauer Y, Zheng Y, Malešević M, von Brunn B, Fischer G, von Brunn A. Influences of cyclosporin A and non-immunosuppressive derivatives on cellular cyclophilins and viral nucleocapsid protein during human coronavirus 229E replication. *Antiviral Res*.

2020;173(July 2019):104620. doi:10.1016/j.antiviral.2019.104620

62. Angelini MM, Akhlaghpour M, Neuman BW, Buchmeier MJ. Severe Acute Respiratory Syndrome Coronavirus Nonstructural Proteins 3, 4, and 6 Induce Double-Membrane Vesicles. *MBio*. 2013;4(4):e00524-13. doi:10.1128/mBio.00524-13

63. Oudshoorn D, Rijs K, Limpens RWAL, et al. Expression and Cleavage of Middle East Respiratory Syndrome Coronavirus nsp3-4 Polyprotein Induce the Formation of Double-Membrane Vesicles That Mimic Those Associated with Coronaviral RNA Replication. *MBio*. 2017;8(6):e01658-17. doi:10.1128/mBio.01658-17

64. Lundin A, Dijkman R, Bergström T, et al. Targeting Membrane-Bound Viral RNA Synthesis Reveals Potent Inhibition of Diverse Coronaviruses Including the Middle East Respiratory Syndrome Virus. *PLOS Pathog*. 2014;10(5):1-15. doi:10.1371/journal.ppat.1004166

65. Collnot E-M, Baldes C, Schaefer UF, Edgar KJ, Wempe MF, Lehr C-M. Vitamin E TPGS P-Glycoprotein Inhibition Mechanism: Influence on Conformational Flexibility, Intracellular ATP Levels, and Role of Time and Site of Access. *Mol Pharm*. 2010;7(3):642-651. doi:10.1021/mp900191s

66. Augustijns PF, Bradshaw TP, Gan LSL, Hendren RW, Thakker DR. Evidence for a Polarized Efflux System in Caco-2 Cells Capable of Modulating Cyclosporine A Transport. *Biochem Biophys Res Commun*. 1993;197(2):360-365. doi:10.1006/bbrc.1993.2487

67. Grimaudo MA, Pescina S, Padula C, et al. Poloxamer 407/TPGS Mixed Micelles as Promising Carriers for Cyclosporine Ocular Delivery. *Mol Pharm*. 2018;15(2):571-584. doi:10.1021/acs.molpharmaceut.7b00939

SUPPLEMENTARY MATERIAL

METHODS

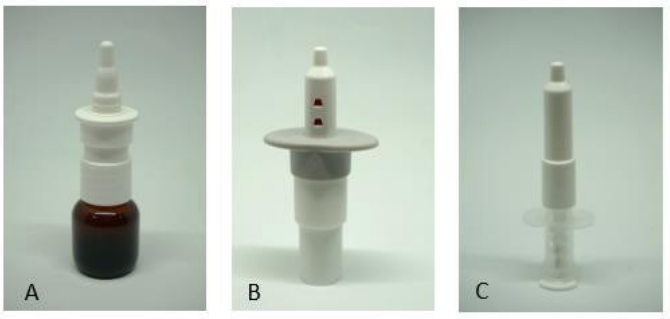

Figure 1 *- The three devices used for the deposition experiment in a nasal cast: glass vial equipped with CPS spray pump (A), a Bidose system BDSI V3 device (B) and a BiVax system atomized (C) assembled using a standard kit BDSI (references 2457_010 et 2457_140).*

Table 1 *– Automated actuation parameters for DSD, SP and PG assessment.*

Parameter	Device		
	CPS spray pump	**Bidose system**	**BiVax system**
Stroke force (kg)	7	8	8
Velocity (mm/s)	70	70	22
Acceleration (mm/s^2)	3000	5000	5000
Hold time (ms)	300	300	300
Symmetric Profile	Yes	Yes	Yes

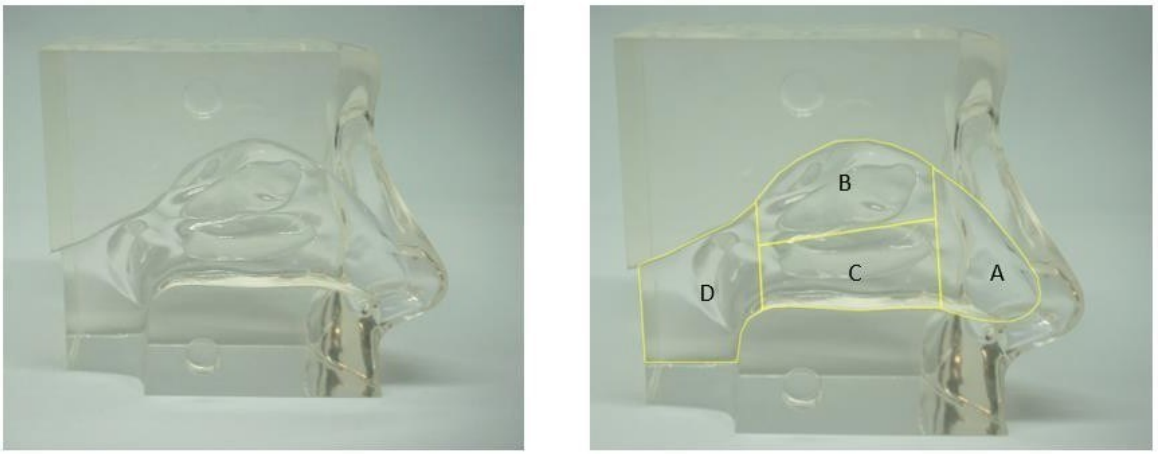

Figure 2 *- The Koken ® cavity model of a nose (left) and the partition of the nasal cavity (right) in vestibule (A), middle-upper turbinate (B), lower turbinate (C) and throat (D).*

RESULTS

Stability of the blank and CSA-loaded micelles over 7 months

All the developed micelles showed good stability over 7 months at 25°C (**Table 2**). The particle size of the micelles remained unchanged over time, except for the ML micelles, for which a statistically significant increase from about 11 nm to about 18 nm was noted (*p=0.0049*), accompanied by a significant increase in terms of PDI. An increase in the PDI value was still observed for the HL micelles, but in this case the particle size has not undergone any statistically significant change. During 7 months of storage at 25°C, both the zeta potential remained unchanged over time and the encapsulation efficiency remained stable. The statistical analysis indeed, did not pointed out any significant alteration in terms of drug loading; however, this could be related to the relatively high standard deviation found for the collected data.

Table 2 - *characterization of the blank and CSA-loaded micelles at time 0 and after 3 months and 7 months stored at 25°C (n=3)*

	Month 3				Month 7			
	Size [nm]	PDI	Zeta potential [mV]	CSA EE%	Size [nm]	PDI	Zeta potential [mV]	CSA EE%
Blank	11.61 ± 0.98	0.11	-1.48 ± 0.27	--	13.94 ± 1.42	0.28	-0.76 ± 1.60	--
LL Micelles (0.1 mg/mL CSA)	14.63 ± 5.06	0.22	-3.41 ± 2.18	88.43 ± 13.58	18.35 ± 5.77	0.33	-4.14 ± 3.99	83.60 ± 11.18
ML Micelles (0.25 mg/mL CSA)	11.35 ± 0.35	0.11	-2.32 ± 1.91	96.35 ± 4.55	17.64 ± 3.22*	0.43	-3.00 ± 2.23	89.91 ± 8.81
HL Micelles (0.5 mg/mL CSA)	11.45 ± 0.65	0.13	-1.12 ± 0.81	96.72 ± 4.79	17.27 ± 5.81	0.38	-1.97 ± 2.94	95.97 ± 3.28

** = value significatively different for that obtained at time 0, according to ANOVA statistic test*

Dynamic viscosity calculated at both 25°C and 37°C

Figure 3 illustrates the dynamic viscosity, η, calculated by the rheometer both at 25°C and at 37°C for all the developed micelles. The addition of the drug at increasing concentrations didn't seem to have an impact on the viscosity of the formulation, as confirmed by the statistical analysis. Moreover, not even the increase in temperature (37°C) led to a significant change in the viscosity of the formulations, confirming that the nasal environment should not alter the viscosity of the system.

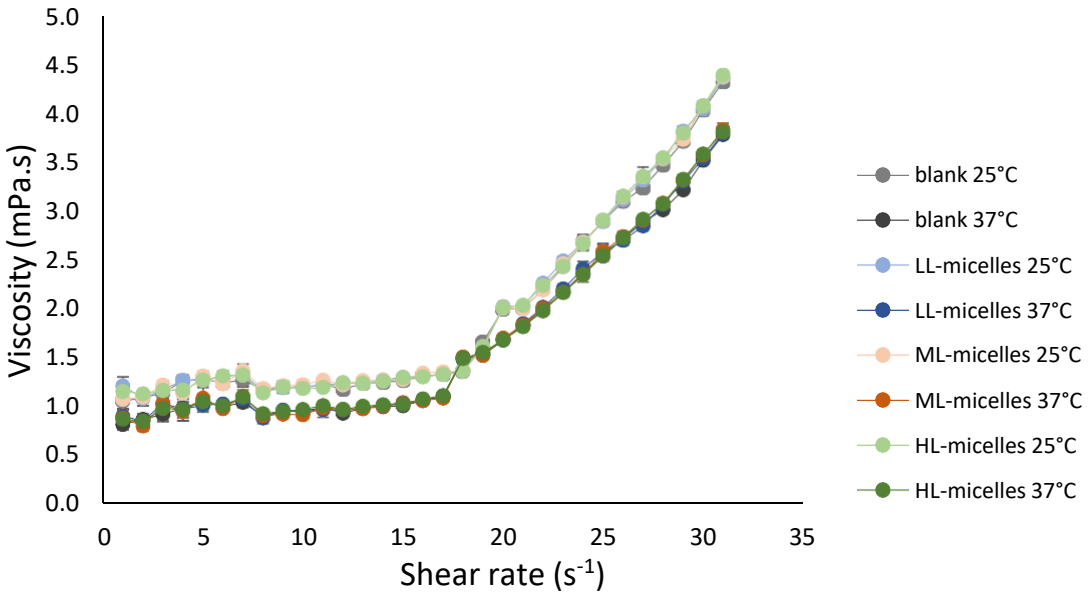

Figure 3 – *The comparison of the dynamic viscosity of the blank, LL, ML and HL micelles calculated both at 25°C and at 37°C*

Fitting parameters for SANS data

Table 3 – *fitting parameter for SANS data*

	Core radius	Shell thickness	Particle radius	sld core	sld shell	sld solvent
	[nm]	*[nm]*	*[nm]*	*[10^{-6}/Å^2]*	*[10^{-6}/Å^2]*	*[10^{-6}/Å^2]*
TPGS	**3.50**	**2.9**	**6.40**	**0.55**	**5.68**	**6.35**
TPGS+0.5 CSA	**3.45**	**2.9**	**6.35**	**0.55**	**5.68**	**6.35**
TPGS+2.5 CSA	**3.21**	**2.9**	**6.11**	**0.55**	**5.68**	**6.35**

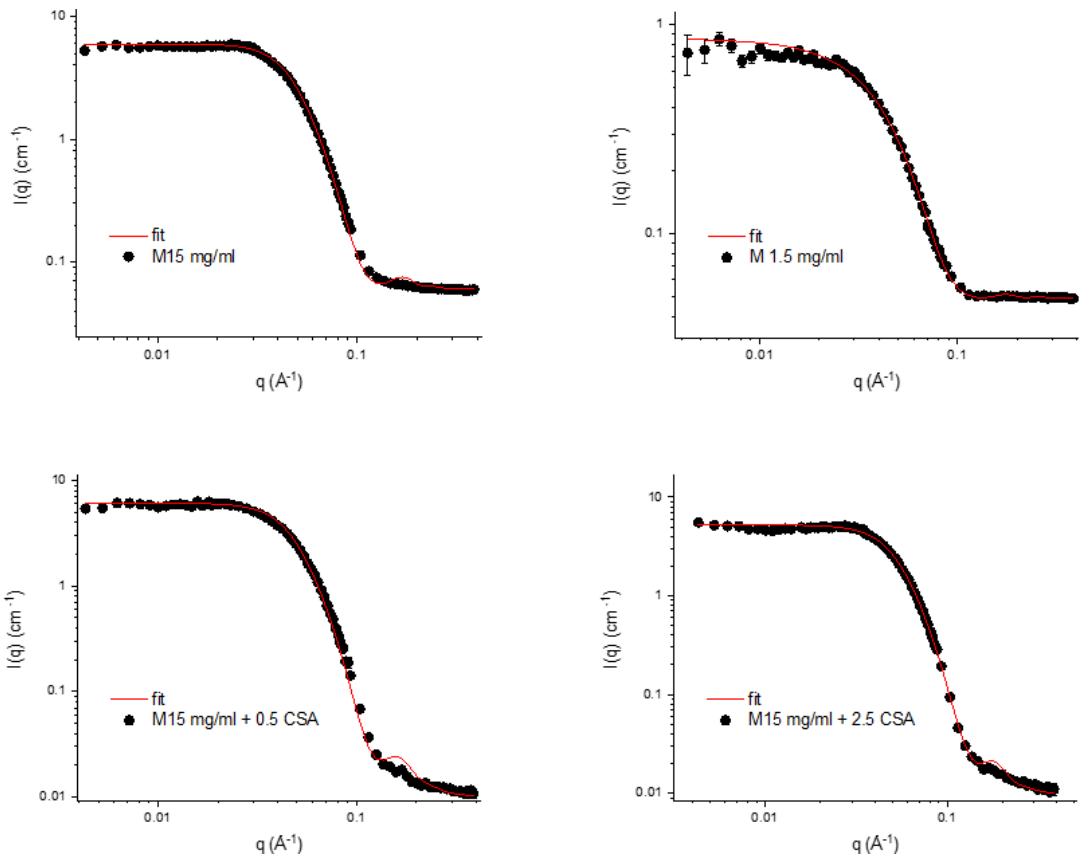

Figure 4 – *Fitting of SANS spectra for micelles at 15 mg/mL and 1.5 mg/mL with CSA at 0.5 mg/mL and 2.5 mg/mL. SANS data analysis was performed using SasView 5.0.5 software. The scattering curves from the micelles were fitted to a core–shell sphere (CSS) model for the P(q) combined with a hard-sphere (HS) structure factor for the S(q). In the data analysis, the scattering length density (sld) of the core and shell were left free. Results are reported in Table 2.*

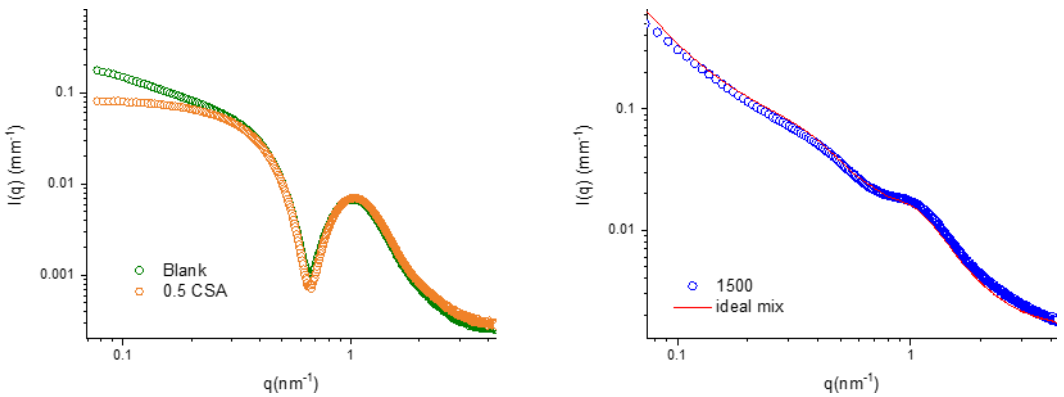

Figure 5 *–left) SAXS spectra of micelles (30 mg/mL) with and without CSA 0.5 mg/mL. Right) reconstruction of the equilibrium mixed mucin-micelle spectrum by adding the experimental spectra of mucin and micelles appropriately weighted according to the concentration of the two components in the mixed sample.*

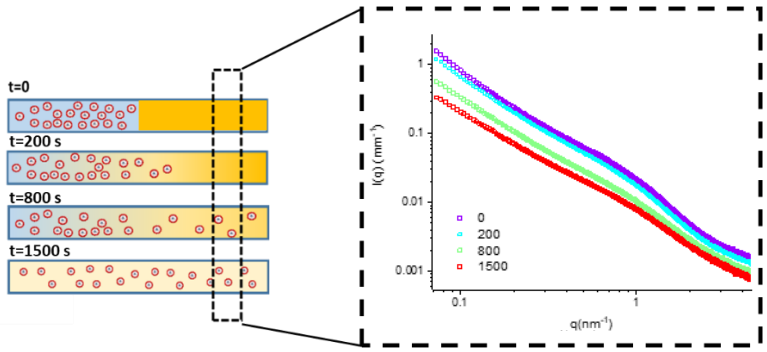

Figure 6 - *Sketch of the experimental set up and time evolution of the SAXS spectra acquired at 2.4 mm distance from the mucin/SNES contact interface (as indicated by the dotted square) over time (from t=0 to t=1500 s).*

Antiviral activity of the developed micelles against SARS-CoV-2 tested at 0.0005 m.o.i The results obtained by treating the VERO E6 cells infected with the viral amount of 0.0005 confirmed the data obtained by using the higher viral amount (0.005 m.o.i). All the drug-loaded micelles indeed turned out to perform significatively better at inhibiting the viral replication than both the pure CSA and the blank micelles. However, as expected, the absolute efficiency of the drug-loaded micelles turned out to be higher when 0.0005 m.o.i was used as viral titer. We observed that regardless of the viral amount, the behavior of the HL and ML micelles turned out tobe comparable, while that of the LL micelles was slightly different. When the infected cells were pre-treated (one hour treatment before the infection, **Figure 7A**) using the HL, ML and LL micelles the antiviral activity turned out to be never lower than 70% and was significatively better if compared to both CSA alone and blank micelles. It was observed a certain antiviral action also applying the blank micelles, proving that also blank micelles were able to inhibit the viral replicationby about 50-60%, values however significantly lower than those obtained with the corresponding loaded micelles. The CSA controls, in which the drug suspension was used, turned out to be ineffective against SARS-CoV-2 at all the concentrations tested.

When a treatment contextual to the infection was used (one hour treatment in presence of the virus, **Figure 7B**), in all the cases the loaded micelles turned out to perform significatively better than the CSA alone and the blank micelles controls. As already observed when a higher viral amount was exploited to infect cells, all the drug-loaded formulations showed a similar trend, consisting in an increasing antiviral activity with increasing CSA concentrations, leading to values above 90% of viral inhibition for HL, ML, and LL starting from 8, 4 and 2 µM, respectively.

CSA solution used at concentration between 2 and 16 µM turned out to be significantly less effective if compared to the loaded micelles. CSA raw material showed a certain antiviral activity

which increased linearly with the concentration, however never exceeding 70%. It must be underlined that this antiviral activity is the highest among all the results obtained applying the various approaches to treat the infected cells. The blank micelles used as reference, although showing an appreciable effect (48-93%), often even higher than CSA raw material, remained in all cases significantly less effective than the corresponding drug-loaded micelles.

When applied post-infection (one hour treatment two hours after the infection, **Figure 7C**), all the drug-loaded micelles turned out to be significatively more effective at hindering viral replication if compared to both the blank micelles and the CSA raw material, as already observed when cells were treated with a higher viral amount.

HL and ML micelles showed a similar behavior, demonstrating to be more effective at the lowest CSA concentration tested, 2 µM. More precisely, the HL micelles exhibited a 113% viral inhibition, while the ML micelles exhibited a 121% viral inhibition. The LL micelles effectiveness was proportional to the CSA concentration, with a peak in correspondence of the 8 µM drug concentration (111%). When applied two hours after the infection, CSA raw material turned out to be able to inhibit the viral replication of only up to 48% when used at the highest concentration tested of 32 µM. A certain antiviral activity was also registered at a drug concentration of 16 µM, at which the viral replication was inhibited by 25%. Under this concentration, no antiviral effect was observed for the raw peptide.

Blank micelles highlighted a certain antiviral activity (44-88%) significantly lower to the drug-loaded micelles. When a delayed treatment protocol (one hour treatment six hours after the infection, **Figure 7D**) was used to treat cells infected with 0.0005 m.o.i, the results confirmed those obtained by working against an higher viral amount. In this case indeed, the lowest percentages of viral inhibition for all the three different developed micellar formulations were obtained (86% at 32 µM, 81% at 16 µM, 76% at 8 µM for HL, ML and LL micelles, respectively).

The not-formulated CSA demonstrated a 37% viral inhibition at 32 µM, and a 30% viral inhibition at 16 µM. Its effectiveness dramatically decreased with lower concentrations becoming totally ineffective for concentrations below 8 µM. Nevertheless, in all the cases the drug-loaded micelles performed significatively better than the CSA material. In most cases the ML and LL micelles performed significatively better than the blank micelles, while the activity of the HL micelles turned out to be in most cases superposable to that observed for the blank micelles.

When the treatment was applied twice, *i.e.* pre- and post-infection (one hour treatment before the infection and one treatment two hours after the infection, **Figure 7E**), all the developed CSA-loaded micellar formulations showed significatively improved values of viral inhibition if compared to both the raw peptide and the blank micelles at all the CSA concentrations tested.

The HL and ML micelles showed a similar trend consisting of very high antiviral activity, never going

under 93%. More precisely, the highest values were found at 2 µM, and were 128% for HL and of 135% for ML micelles. As already observed, the behavior showed by the LL micelles was slightly different, *i.e.* consisted in a peak of activity (119%) at 8 µM followed by lower values at decreasing CSA concentrations, however never going under 97% inhibition. The CSA showed a maximum of 43% of antiviral activity when tested at the highest concentration (32 µM) followed by a linear decreasing activity with decreasing concentrations. For all the blank formulation controls was evidenced a higher antiviral activity compared to the one obtained by using the peptide solution, however, the inhibition never exceeded the value of 89%. In the case of repeated post-treatments (one hour treatment repeated two, four and six hours after the infection, **Figure 7F**) the developed CSA-loaded micellar formulations provided an overall performance quite similar to the previous condition. The HL and ML micelles showed high antiviral activity in all conditions tested, never going below 78%. More precisely, the highest values were recorded at 2 µM, and were 135% for HL and of 103% for ML micelles. As already observed, the results obtained using the LL micelles were slightly different, showing the highest activity (110%) at 8 µM but lower values at decreasing CSA concentrations, however never going under 101% inhibition.

Again, the antiviral activity of CSA raw material and blank micelles was significatively lower than that of the drug-loaded formulations. CSA indeed demonstrated to be able to inhibit the SARS-CoV-2 replication by up to 39%, while the activity of the blank micelles has not exceeded 88%.

Finally, when a pre-treatment was associated with repeated post-treatments (one hour treatment before infection and repeated treatments two, four and six hours after the infection, **Figure 7G**) confirmed the two previous conditions data (**Figure 7E** and **7F**), as observed working against a higher viral amount. Indeed, all the drug-loaded micelles turned out to perform significatively better than the pure drug and the control blank formulation. The antiviral activity observed using the HL and ML micelles was again very high (always above 96%) with the highest value (124% for the HL and 155% for the ML micelles) recorded at 2 µM CSA concentration. LL micelles peak of antiviral activity (122%) was observed at the highest CSA concentration tested (8 µM). CSA raw material and blank micelles antiviral activity (max. 38% for CSA raw material and 90% for blank micelles controls) was lower than the one obtained for the corresponding drug-loaded micelles at all the concentrations tested.

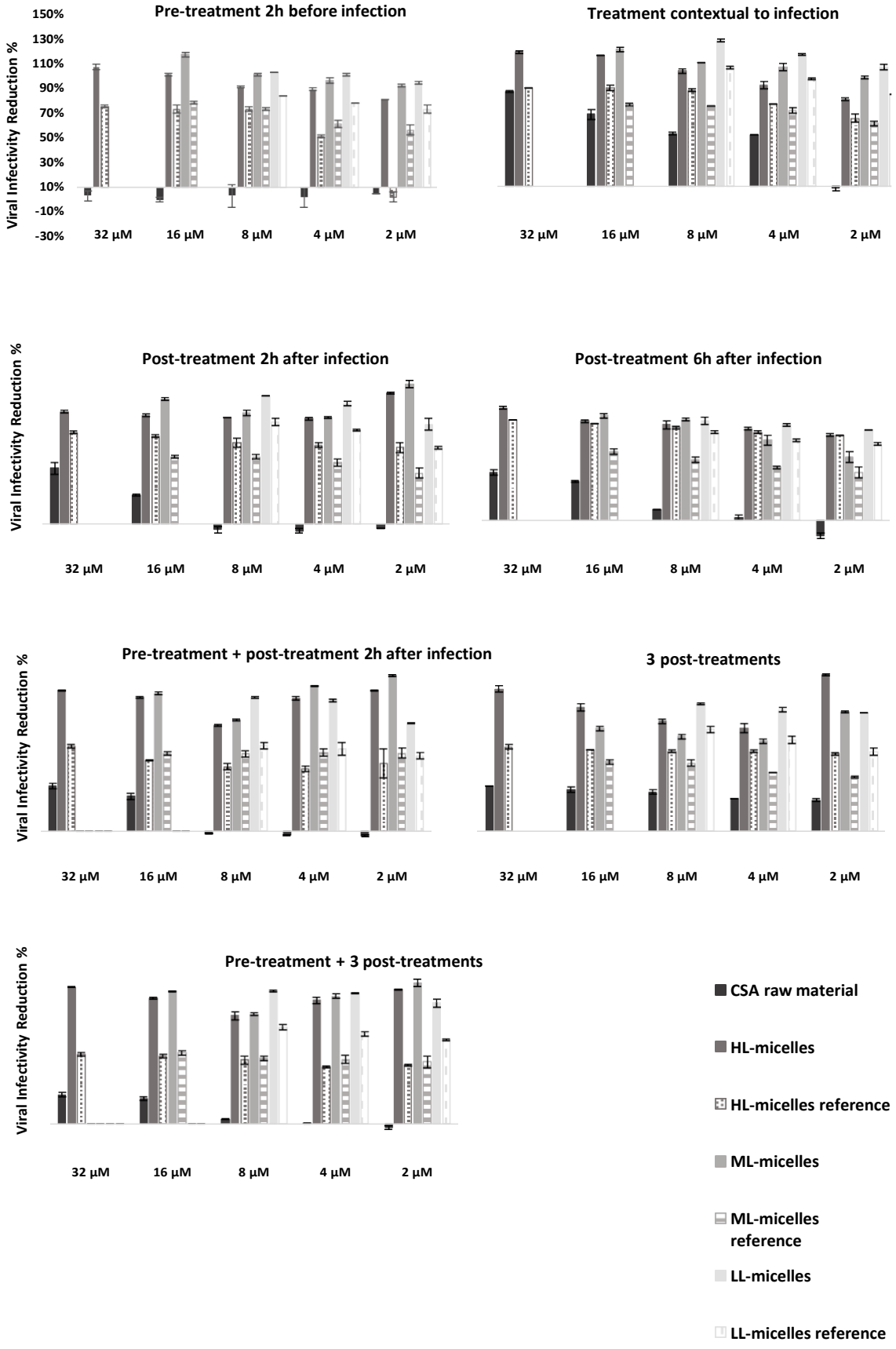
Pre-treatment 2h before infection
Treatment contextual to infection
Post-treatment 2h after infection
Post-treatment 6h after infection
Pre-treatment + post-treatment 2h after infection
3 post-treatments
Pre-treatment + 3 post-treatments
Viral Infectivity Reduction %
150%
130%
110%
90%
70%
50%
30%
10%
-10%
-30%
32 µM
16 µM
8 µM
4 µM
2 µM
CSA raw material
HL-micelles
HL-micelles reference
ML-micelles
ML-micelles reference
LL-micelles
LL-micelles reference

Figure 7 *- Antiviral activity of the HL micelles, ML micelles and LL micelles compared to the raw CSA and the blank formulations, against 0.0005 m.o.i as viral amount. Each graph represents the results obtained by treating the infected cells with one of the seven different protocols tested: treatment 1h before infection (protocol A), treatment contextual to the infection (protocol B), post-treatment 2h after the infection (protocol C), post-treatment 6h after the infection (protocol C6), pre-treatment 1h before the infection followed by a post-treatment 2h after the infection (protocol D), 3 post-treatments spaced 1h apart (protocol E), pre-treatment 1h before the infection followed by 3 post-treatments spaced 1h apart (protocol F).*

p values obtained by the statistical analysis

Table 4 – *p values obtained from the one-way ANOVA and Tukey HSD Post Hoc test for the antiviral activity of the HL, ML and LL micelles compared to the pure CSA and the blank micelles. Results refer to the situation in which the loaded micelles, the blank micelles and the CSA solution have been used to pre-treat cells 1 hour before being infected with 0.005 m.o.i. as viral amount. The table only shows the data referring to the concentration at which the drug-loaded micelles exhibited the highest antiviral efficacy.*

Pre-treatment 0.005 moi	**HL-micelles 32 µM**	**ML-micelles 16 µM**	**LL-micelles 8 µM**	**Blank micelles (reference of HL 32 µM)**	**Blank micelles (reference of ML 16 µM)**	**Blank micelles (reference of LL 8 µM)**	**CSA 32 µM**	**CSA 16 µM**	**CSA 8 µM**
HL-micelles 32 µM	-	1	1	<0.0001	<0.0001	1	<0.0001	<0.0001	<0.0001
ML-micelles 16 µM	1	-	1	<0.0001	<0.0001	1	<0.0001	<0.0001	<0.0001
LL-micelles 8 µM	1	1	-	<0.0001	<0.0001	1	<0.0001	<0.0001	<0.0001
Blank micelles (reference of HL 32 µM)	<0.0001	<0.0001	<0.0001	-	1	<0.0001	<0.0001	<0.0001	<0.0001
Blank micelles (reference of ML 16 µM)	<0.0001	<0.0001	<0.0001	1	-	<0.0001	<0.0001	<0.0001	<0.0001
Blank micelles (reference of LL 8 µM)	1	1	1	<0.0001	<0.0001	-	<0.0001	<0.0001	<0.0001
CSA 32 µM	<0.0001	<0.0001	<0.0001	<0.0001	<0.0001	<0.0001	-	1	1
CSA 16 µM	<0.0001	<0.0001	<0.0001	<0.0001	<0.0001	<0.0001	1	-	1
CSA 8 µM	<0.0001	<0.0001	<0.0001	<0.0001	<0.0001	<0.0001	1	1	-

Table 5 – *p values obtained from the one-way ANOVA and Tukey HSD Post Hoc test for the antiviral activity of the HL, ML and LL micelles compared to the pure CSA and the blank micelles. Results refer to the situation in which the loaded micelles, the blank micelles and the CSA solution have been used to treat cells contextually to the infection with 0.005 m.o.i. as viral amount. The table only shows the data referring to the concentration at which the drug-loaded micelles exhibited the highest antiviral efficacy.*

Treatment contextual to infection **0.005 moi**	**HL-micelles 32 µM**	**ML-micelles 16 µM**	**LL-micelles 8 µM**	**Blank micelles (reference of HL 32 µM)**	**Blank micelles (reference of ML 16 µM)**	**Blank micelles (reference of LL 8 µM)**	**CSA 32 µM**	**CSA 16 µM**	**CSA 8 µM**
HL-micelles 32 µM	-	0.7167	<0.0001	<0.0001	<0.0001	<0.0001	<0.0001	<0.0001	<0.0001
ML-micelles 16 µM	0.7167	-	0.0001	<0.0001	<0.0001	<0.0001	0.7382	<0.0001	<0.0001
LL-micelles 8 µM	<0.0001	0.0001	-	<0.0001	<0.0001	<0.0001	0.7773	<0.0001	<0.0001
Blank micelles (reference of HL 32 µM)	<0.0001	<0.0001	<0.0001	-	0.9933	<0.0001	<0.0001	1	<0.0001
Blank micelles (reference of ML 16 µM)	<0.0001	<0.0001	<0.0001	0.9933	-	<0.0001	<0.0001	0.9987	<0.0001
Blank micelles (reference of LL 8 µM)	<0.0001	<0.0001	<0.0001	<0.0001	<0.0001	-	<0.0001	<0.0001	<0.0001
CSA 32 µM	<0.0001	0.7382	0.7773	<0.0001	<0.0001	<0.0001	-	<0.0001	<0.0001
CSA 16 µM	<0.0001	<0.0001	<0.0001	1	0.9987	<0.0001	<0.0001	-	<0.0001
CSA 8 µM	<0.0001	<0.0001	<0.0001	<0.0001	<0.0001	<0.0001	<0.0001	<0.0001	-

Table 6 – *p values obtained from the one-way ANOVA and Tukey HSD Post Hoc test for the antiviral activity of the HL, ML and LL micelles compared to the pure CSA and the blank micelles. Results refer to the situation in which the loaded micelles, the blank micelles and the CSA solution have been used to post-treat cells 2 hours after the infection with 0.005 m.o.i. as viral amount. The table only shows the data referring to the concentration at which the drug-loaded micelles exhibited the highest antiviral efficacy.*

Post-treatment 2h after infection **0.005 moi**	**HL-micelles 2 µM**	**ML-micelles 2 µM**	**LL-micelles 8 µM**	**Blank micelles (reference of HL 2 µM)**	**Blank micelles (reference of ML 2 µM)**	**Blank micelles (reference of LL 8 µM)**	**CSA 2 µM**	**CSA 8 µM**
HL-micelles 2 µM	-	0.2926	1	<0.0001	<0.0001	<0.0001	<0.0001	<0.0001
ML-micelles 2 µM	0.2926	-	0.0534	<0.0001	<0.0001	<0.0001	<0.0001	<0.0001
LL-micelles 8 µM	1	0.0534	-	<0.0001	<0.0001	<0.0001	<0.0001	<0.0001
Blank micelles (reference of HL 2 µM)	<0.0001	<0.0001	<0.0001	-	<0.0001	<0.0001	<0.0001	<0.0001
Blank micelles (reference of ML 2 µM)	<0.0001	<0.0001	<0.0001	<0.0001	-	<0.0001	<0.0001	<0.0001
Blank micelles (reference of LL 8 µM)	<0.0001	<0.0001	<0.0001	<0.0001	<0.0001	-	<0.0001	<0.0001
CSA 2 µM	<0.0001	<0.0001	<0.0001	<0.0001	<0.0001	<0.0001	-	0.9345
CSA 8 µM	<0.0001	<0.0001	<0.0001	<0.0001	<0.0001	<0.0001	0.9345	-

Table 7 – *p values obtained from the one-way ANOVA and Tukey HSD Post Hoc test for the antiviral activity of the HL, ML and LL micelles compared to the pure CSA and the blank micelles. Results refer to the situation in which the loaded micelles, the blank micelles and the CSA solution have been used to post-treat cells 6 hours after the infection with 0.005 m.o.i. as viral amount. The table only shows the data referring to the concentration at which the drug-loaded micelles exhibited the highest antiviral efficacy.*

Post-treatment 6h after infection **0.005 moi**	**HL-micelles 32 µM**	**ML-micelles 16 µM**	**LL-micelles 8 µM**	**Blank micelles (reference of HL 32 µM)**	**Blank micelles (reference of ML 16 µM)**	**Blank micelles (reference of LL 8 µM)**	**CSA 32 µM**	**CSA 16 µM**	**CSA 8 µM**
HL-micelles 32 µM	-	0.9999	1	<0.0001	<0.0001	<0.0001	<0.0001	<0.0001	<0.0001
ML-micelles 16 µM	0.9999	-	1	<0.0001	0.0156	<0.0001	<0.0001	<0.0001	<0.0001
LL-micelles 8 µM	1	1	-	<0.0001	0.0109	<0.0001	<0.0001	<0.0001	<0.0001
Blank micelles (reference of HL 32 µM)	<0.0001	<0.0001	<0.0001	-	0.1145	1	0.0015	<0.0001	<0.0001
Blank micelles (reference of ML 16 µM)	<0.0001	0.0156	0.0109	0.1145	-	0.8902	<0.0001	<0.0001	<0.0001
Blank micelles (reference of LL 8 µM)	<0.0001	<0.0001	<0.0001	1	0.8902	-	<0.0001	<0.0001	<0.0001
CSA 32 µM	<0.0001	<0.0001	<0.0001	0.0015	<0.0001	<0.0001	-	<0.0001	<0.0001
CSA 16 µM	<0.0001	<0.0001	<0.0001	<0.0001	<0.0001	<0.0001	<0.0001	-	<0.0001
CSA 8 µM	<0.0001	<0.0001	<0.0001	<0.0001	<0.0001	<0.0001	<0.0001	<0.0001	-

Table 8 – *p values obtained from the one-way ANOVA and Tukey HSD Post Hoc test for the antiviral activity of the HL, ML and LL micelles compared to the pure CSA and the blank micelles. Results refer to the situation in which the loaded micelles, the blank micelles and the CSA solution have been used to pre-treat (1 hour before the infection) and post-treat (2 hours after the infection) cells infected with 0.005 m.o.i. as viral amount. The table only shows the data referring to the concentration at which the drug-loaded micelles exhibited the highest antiviral efficacy.*

Pre- treatment + post-treatment 2h after infection **0.005 moi**	**HL-micelles 2 µM**	**ML-micelles 2 µM**	**LL-micelles 8 µM**	**Blank micelles (reference of HL 2 µM)**	**Blank micelles (reference of ML 2 µM)**	**Blank micelles (reference of LL 8 µM)**	**CSA 2 µM**	**CSA 8 µM**
HL-micelles 2 µM	-	0.0009	0.9894	<0.0001	<0.0001	<0.0001	<0.0001	<0.0001
ML-micelles 2 µM	0.0009	-	<0.0001	<0.0001	<0.0001	<0.0001	<0.0001	<0.0001
LL-micelles 8 µM	0.9894	<0.0001	-	<0.0001	<0.0001	<0.0001	<0.0001	<0.0001
Blank micelles (reference of HL 2 µM)	<0.0001	<0.0001	<0.0001	-	0.2313	<0.0001	<0.0001	<0.0001
Blank micelles (reference of ML 2 µM)	<0.0001	<0.0001	<0.0001	0.2313	-	0.9156	<0.0001	<0.0001
Blank micelles (reference of LL 8 µM)	<0.0001	<0.0001	<0.0001	<0.0001	0.9156	-	<0.0001	<0.0001
CSA 2 µM	<0.0001	<0.0001	<0.0001	<0.0001	<0.0001	<0.0001	-	1
CSA 8 µM	<0.0001	<0.0001	<0.0001	<0.0001	<0.0001	<0.0001	1	-

Table 9 – *p values obtained from the one-way ANOVA and Tukey HSD Post Hoc test for the antiviral activity of the HL, ML and LL micelles compared to the pure CSA and the blank micelles. Results refer to the situation in which the loaded micelles, the blank micelles and the CSA solution have been used as repeated post-treatment on cells infected with 0.005 m.o.i. as viral amount. The table only shows the data referring to the concentration at which the drug-loaded micelles exhibited the highest antiviral efficacy.*

3 post-treatments **0.005 moi**	**HL-micelles 2 µM**	**ML-micelles 2 µM**	**LL-micelles 8 µM**	**Blank micelles (reference of HL 2 µM)**	**Blank micelles (reference of ML 2 µM)**	**Blank micelles (reference of LL 8 µM)**	**CSA 2 µM**	**CSA 8 µM**
HL-micelles 2 µM	-	0.0008	0.1348	<0.0001	<0.0001	<0.0001	<0.0001	<0.0001
ML-micelles 2 µM	0.0008	-	1	<0.0001	<0.0001	<0.0001	<0.0001	<0.0001
LL-micelles 8 µM	0.1348	1	-	<0.0001	<0.0001	<0.0001	<0.0001	<0.0001
Blank micelles (reference of HL 2 µM)	<0.0001	<0.0001	<0.0001	-	<0.0001	<0.0001	<0.0001	<0.0001
Blank micelles (reference of ML 2 µM)	<0.0001	<0.0001	<0.0001	<0.0001	-	<0.0001	<0.0001	<0.0001
Blank micelles (reference of LL 8 µM)	<0.0001	<0.0001	<0.0001	<0.0001	<0.0001	-	<0.0001	<0.0001
CSA 2 µM	<0.0001	<0.0001	<0.0001	<0.0001	<0.0001	<0.0001	-	0.0023
CSA 8 µM	<0.0001	<0.0001	<0.0001	<0.0001	<0.0001	<0.0001	0.0023	-

Table 10 – *p values obtained from the one-way ANOVA and Tukey HSD Post Hoc test for the antiviral activity of the HL, ML and LL micelles compared to the pure CSA and the blank micelles. Results refer to the situation in which the loaded micelles, the blank micelles and the CSA solution have been used as a pre-treatment (1 hour before infection) and repeated post-treatment on cells infected with 0.005 m.o.i. as viral amount. The table only shows the data referring to the concentration at which the drug-loaded micelles exhibited the highest antiviral efficacy.*

Pre-treatment + 3 post-treatments **0.005 moi**	**HL-micelles 2 µM**	**ML-micelles 2 µM**	**LL-micelles 8 µM**	**Blank micelles (reference of HL 2 µM)**	**Blank micelles (reference of ML 2 µM)**	**Blank micelles (reference of LL 8 µM)**	**CSA 2 µM**	**CSA 8 µM**
HL-micelles 2 µM	-	0.6669	1	<0.0001	<0.0001	<0.0001	<0.0001	<0.0001
ML-micelles 2 µM	0.6669	-	0.0715	<0.0001	<0.0001	<0.0001	<0.0001	<0.0001
LL-micelles 8 µM	1	0.0715	-	<0.0001	<0.0001	<0.0001	<0.0001	<0.0001
Blank micelles (reference of HL 2 µM)	<0.0001	<0.0001	<0.0001	-	1	<0.0001	<0.0001	<0.0001
Blank micelles (reference of ML 2 µM)	<0.0001	<0.0001	<0.0001	1	-	<0.0001	<0.0001	<0.0001
Blank micelles (reference of LL 8 µM)	<0.0001	<0.0001	<0.0001	<0.0001	<0.0001	-	<0.0001	<0.0001
CSA 2 µM	<0.0001	<0.0001	<0.0001	<0.0001	<0.0001	<0.0001	-	0.0481
CSA 8 µM	<0.0001	<0.0001	<0.0001	<0.0001	<0.0001	<0.0001	0.0481	-

Table 11 – *p values obtained from the one-way ANOVA and Tukey HSD Post Hoc test for the antiviral activity of the HL, ML and LL micelles compared to the pure CSA and the blank micelles. Results refer to the situation in which the loaded micelles, the blank micelles and the CSA solution have been used to pre-treat cells 1 hour before being infected with 0.0005 m.o.i. as viral amount. The table only shows the data referring to the concentration at which the drug-loaded micelles exhibited the highest antiviral efficacy.*

Pre-treatment 0.0005 moi	**HL-micelles 32 µM**	**ML-micelles 16 µM**	**LL-micelles 8 µM**	**Blank micelles (reference of HL 32 µM)**	**Blank micelles (reference of ML 16 µM)**	**Blank micelles (reference of LL 8 µM)**	**CSA 32 µM**	**CSA 16 µM**	**CSA 8 µM**
HL-micelles 32 µM	-	0.5237	1	<0.0001	<0.0001	<0.0001	<0.0001	<0.0001	<0.0001
ML-micelles 16 µM	0.5237	-	0.0305	<0.0001	<0.0001	<0.0001	<0.0001	<0.0001	<0.0001
LL-micelles 8 µM	1	0.0305	-	<0.0001	<0.0001	0.0002	<0.0001	<0.0001	<0.0001
Blank micelles (reference of HL 32 µM)	<0.0001	<0.0001	<0.0001	-	1	0.7304	<0.0001	<0.0001	<0.0001
Blank micelles (reference of ML 16 µM)	<0.0001	<0.0001	<0.0001	1	-	0.404	<0.0001	<0.0001	<0.0001
Blank micelles (reference of LL 8 µM)	<0.0001	<0.0001	0.0002	0.7304	0.404	-	<0.0001	<0.0001	<0.0001
CSA 32 µM	<0.0001	<0.0001	<0.0001	<0.0001	<0.0001	<0.0001	-	1	1
CSA 16 µM	<0.0001	<0.0001	<0.0001	<0.0001	<0.0001	<0.0001	1	-	1
CSA 8 µM	<0.0001	<0.0001	<0.0001	<0.0001	<0.0001	<0.0001	1	1	-

Table 12 – *p values obtained from the one-way ANOVA and Tukey HSD Post Hoc test for the antiviral activity of the HL, ML and LL micelles compared to the pure CSA and the blank micelles. Results refer to the situation in which the loaded micelles, the blank micelles and the CSA solution have been used to treat cells contextually to the infection with 0.0005 m.o.i. as viral amount. The table only shows the data referring to the concentration at which the drug-loaded micelles exhibited the highest antiviral efficacy.*

Treatment contextual to infection 0.0005 moi	**HL-micelles 32 µM**	**ML-micelles 16 µM**	**LL-micelles 8 µM**	**Blank micelles (reference of HL 32 µM)**	**Blank micelles (reference of ML 16 µM)**	**Blank micelles (reference of LL 8 µM)**	**CSA 32 µM**	**CSA 16 µM**	**CSA 8 µM**
HL-micelles 32 µM	-	1	0.0061	<0.0001	<0.0001	<0.0001	<0.0001	<0.0001	<0.0001
ML-micelles 16 µM	1	-	0.1811	<0.0001	<0.0001	<0.0001	<0.0001	<0.0001	<0.0001
LL-micelles 8 µM	0.0061	0.1811	-	<0.0001	<0.0001	<0.0001	<0.0001	<0.0001	<0.0001
Blank micelles (reference of HL 32 µM)	<0.0001	<0.0001	<0.0001	-	<0.0001	<0.0001	1	<0.0001	<0.0001
Blank micelles (reference of ML 16 µM)	<0.0001	<0.0001	<0.0001	<0.0001	-	<0.0001	0.0008	0.0191	<0.0001
Blank micelles (reference of LL 8 µM)	<0.0001	<0.0001	<0.0001	<0.0001	<0.0001	-	<0.0001	<0.0001	<0.0001
CSA 32 µM	<0.0001	<0.0001	<0.0001	1	0.0008	<0.0001	-	<0.0001	<0.0001

CSA 16 µM	<0.0001	<0.0001	<0.0001	<0.0001	0.0191	<0.0001	<0.0001	-	<0.0001
CSA 8 µM	<0.0001	<0.0001	<0.0001	<0.0001	<0.0001	<0.0001	<0.0001	<0.0001	-

Table 13 – *p values obtained from the one-way ANOVA and Tukey HSD Post Hoc test for the antiviral activity of the HL, ML and LL micelles compared to the pure CSA and the blank micelles. Results refer to the situation in which the loaded micelles, the blank micelles and the CSA solution have been used to post-treat cells 2 hours after the infection with 0.0005 m.o.i. as viral amount. The table only shows the data referring to the concentration at which the drug-loaded micelles exhibited the highest antiviral efficacy.*

Post-treatment 2h after infection **0.0005 moi**	**HL-micelles 2 µM**	**ML-micelles 2 µM**	**LL-micelles 8 µM**	**Blank micelles (reference of HL 2 µM)**	**Blank micelles (reference of ML 2 µM)**	**Blank micelles (reference of LL 8 µM)**	**CSA 2 µM**	**CSA 8 µM**
HL-micelles 2 µM	-	0.2485	1	<0.0001	<0.0001	<0.0001	<0.0001	<0.0001
ML-micelles 2 µM	0.2485	-	0.0328	<0.0001	<0.0001	<0.0001	<0.0001	<0.0001
LL-micelles 8 µM	1	0.0328	-	<0.0001	<0.0001	<0.0001	<0.0001	<0.0001
Blank micelles (reference of HL 2 µM)	<0.0001	<0.0001	<0.0001	-	<0.0001	<0.0001	<0.0001	<0.0001
Blank micelles (reference of ML 2 µM)	<0.0001	<0.0001	<0.0001	<0.0001	-	<0.0001	<0.0001	<0.0001
Blank micelles (reference of LL 8 µM)	<0.0001	<0.0001	<0.0001	<0.0001	<0.0001	-	<0.0001	<0.0001
CSA 2 µM	<0.0001	<0.0001	<0.0001	<0.0001	<0.0001	<0.0001	-	1
CSA 8 µM	<0.0001	<0.0001	<0.0001	<0.0001	<0.0001	<0.0001	1	-

Table 14 – *p values obtained from the one-way ANOVA and Tukey HSD Post Hoc test for the antiviral activity of the HL, ML and LL micelles compared to the pure CSA and the blank micelles. Results refer to the situation in which the loaded micelles, the blank micelles and the CSA solution have been used to post-treat cells 6 hours after the infection with 0.0005 m.o.i. as viral amount. The table only shows the data referring to the concentration at which the drug-loaded micelles exhibited the highest antiviral efficacy.*

Post-treatment 6h after infection **0.0005 moi**	**HL-micelles 32 µM**	**ML-micelles 16 µM**	**LL-micelles 8 µM**	**Blank micelles (reference of HL 32 µM)**	**Blank micelles (reference of ML 16 µM)**	**Blank micelles (reference of LL 8 µM)**	**CSA 32 µM**	**CSA 16 µM**	**CSA 8 µM**
HL-micelles 32 µM	-	0.9123	0.017	0.1992	<0.0001	<0.0001	<0.0001	<0.0001	<0.0001
ML-micelles 16 µM	0.9123	-	0.9998	1	<0.0001	0.0003	<0.0001	<0.0001	<0.0001
LL-micelles 8 µM	0.017	0.9998	-	1	<0.0001	0.2014	<0.0001	<0.0001	<0.0001
Blank micelles (reference of HL 32 µM)	0.1992	1	1	-	<0.0001	0.0173	<0.0001	<0.0001	<0.0001
Blank micelles (reference of ML 16 µM)	<0.0001	<0.0001	<0.0001	<0.0001	-	<0.0001	<0.0001	<0.0001	<0.0001

Blank micelles (reference of LL 8 µM)	<0.0001	0.0003	0.2014	0.0173	<0.0001	-	<0.0001	<0.0001	<0.0001
CSA 32 µM	<0.0001	<0.0001	<0.0001	<0.0001	<0.0001	<0.0001	-	0.8135	<0.0001
CSA 16 µM	<0.0001	<0.0001	<0.0001	<0.0001	<0.0001	<0.0001	0.8135	-	<0.0001
CSA 8 µM	<0.0001	<0.0001	<0.0001	<0.0001	<0.0001	<0.0001	<0.0001	<0.0001	-

Table 15 – *p values obtained from the one-way ANOVA and Tukey HSD Post Hoc test for the antiviral activity of the HL, ML and LL micelles compared to the pure CSA and the blank micelles. Results refer to the situation in which the loaded micelles, the blank micelles and the CSA solution have been used to pre-treat (1 hour before the infection) and post-treat (2 hours after the infection) cells infected with 0.0005 m.o.i. as viral amount. The table only shows the data referring to the concentration at which the drug-loaded micelles exhibited the highest antiviral efficacy.*

Pre- treatment + post- treatment 2h after infection **0.0005 moi**	**HL-micelles 2 µM**	**ML-micelles 2 µM**	**LL-micelles 8 µM**	**Blank micelles (reference of HL 2 µM)**	**Blank micelles (reference of ML 2 µM)**	**Blank micelles (reference of LL 8 µM)**	**CSA 2 µM**	**CSA 8 µM**
HL-micelles 2 µM	-	0.5866	0.2504	<0.0001	<0.0001	<0.0001	<0.0001	<0.0001
ML-micelles 2 µM	0.5866	-	<0.0001	<0.0001	<0.0001	<0.0001	<0.0001	<0.0001
LL-micelles 8 µM	0.2504	<0.0001	-	<0.0001	<0.0001	<0.0001	<0.0001	<0.0001
Blank micelles (reference of HL 2 µM)	<0.0001	<0.0001	<0.0001	-	<0.0001	<0.0001	<0.0001	<0.0001
Blank micelles (reference of ML 2 µM)	<0.0001	<0.0001	<0.0001	<0.0001	-	<0.0001	<0.0001	<0.0001
Blank micelles (reference of LL 8 µM)	<0.0001	<0.0001	<0.0001	<0.0001	<0.0001	-	<0.0001	<0.0001
CSA 2 µM	<0.0001	<0.0001	<0.0001	<0.0001	<0.0001	<0.0001	-	<0.0001
CSA 8 µM	<0.0001	<0.0001	<0.0001	<0.0001	<0.0001	<0.0001	<0.0001	-

Table 16 – *p values obtained from the one-way ANOVA and Tukey HSD Post Hoc test for the antiviral activity of the HL, ML and LL micelles compared to the pure CSA and the blank micelles. Results refer to the situation in which the loaded micelles, the blank micelles and the CSA solution have been used as repeated post-treatment on cells infected with 0.0005 m.o.i. as viral amount. The table only shows the data referring to the concentration at which the drug-loaded micelles exhibited the highest antiviral efficacy.*

3 post-treatments **0.0005 moi**	**HL-micelles 2 µM**	**ML-micelles 2 µM**	**LL-micelles 8 µM**	**Blank micelles (reference of HL 2 µM)**	**Blank micelles (reference of ML 2 µM)**	**Blank micelles (reference of LL 8 µM)**	**CSA 2 µM**	**CSA 8 µM**
HL-micelles 2 µM	-	<0.0001	<0.0001	<0.0001	<0.0001	<0.0001	<0.0001	<0.0001
ML-micelles 2 µM	<0.0001	-	0.175	<0.0001	<0.0001	<0.0001	<0.0001	<0.0001
LL-micelles 8 µM	<0.0001	0.175	-	<0.0001	<0.0001	<0.0001	<0.0001	<0.0001
Blank micelles (reference of HL 2 µM)	<0.0001	<0.0001	<0.0001	-	<0.0001	<0.0001	<0.0001	<0.0001
Blank micelles (reference of ML 2 µM)	<0.0001	<0.0001	<0.0001	<0.0001	-	<0.0001	<0.0001	<0.0001
Blank micelles (reference of LL 8 µM)	<0.0001	<0.0001	<0.0001	<0.0001	<0.0001	-	<0.0001	<0.0001
CSA 2 µM	<0.0001	<0.0001	<0.0001	<0.0001	<0.0001	<0.0001	-	0.464
CSA 8 µM	<0.0001	<0.0001	<0.0001	<0.0001	<0.0001	<0.0001	0.464	-

Table 17 – *p values obtained from the one-way ANOVA and Tukey HSD Post Hoc test for the antiviral activity of the HL, ML and LL micelles compared to the pure CSA and the blank micelles. Results refer to the situation in which the loaded micelles, the blank micelles and the CSA solution have been used as a pre-treatment (1 hour before infection) and repeated post-treatment on cells infected with 0.0005 m.o.i. as viral amount. The table only shows the data referring to the concentration at which the drug-loaded micelles exhibited the highest antiviral efficacy.*

Pre- treatment + 3 post-treatments **0.0005 moi**	**HL-micelles 2 µM**	**ML-micelles 2 µM**	**LL-micelles 8 µM**	**Blank micelles (reference of HL 2 µM)**	**Blank micelles (reference of ML 2 µM)**	**Blank micelles (reference of LL 8 µM)**	**CSA 2 µM**	**CSA 8 µM**
HL-micelles 2 µM	-	<0.0001	1	<0.0001	<0.0001	<0.0001	<0.0001	<0.0001
ML-micelles 2 µM	<0.0001	-	<0.0001	<0.0001	<0.0001	<0.0001	<0.0001	<0.0001
LL-micelles 8 µM	1	<0.0001	-	<0.0001	<0.0001	<0.0001	<0.0001	<0.0001
Blank micelles (reference of HL 2 µM)	<0.0001	<0.0001	<0.0001	-	<0.0001	<0.0001	<0.0001	<0.0001
Blank micelles (reference of ML 2 µM)	<0.0001	<0.0001	<0.0001	<0.0001	-	0.0004	<0.0001	<0.0001
Blank micelles (reference of LL 8 µM)	<0.0001	<0.0001	<0.0001	<0.0001	0.0004	-	<0.0001	<0.0001
CSA 2 µM	<0.0001	<0.0001	<0.0001	<0.0001	<0.0001	<0.0001	-	<0.0001
CSA 8 µM	<0.0001	<0.0001	<0.0001	<0.0001	<0.0001	<0.0001	<0.0001	-

CHAPTER 2

THERAPEUTIC EFFECT OF CYCLOSPORINE A-LOADING TPGS MICELLES ON A MOUSE MODEL OF LPS-INDUCED NEUROINFLAMMATION

Therapeutic effect of cyclosporine A-loading TPGS micelles on a mouse model of LPS-induced neuroinflammation

Fabiola Guareschi [a], Carla Fonseca [b,c,d,e], Soraia Silva [b,c], Silvia Pescina [a], Sara Nicoli [a], Francesca Buttini [a,f], Fabio Sonvico [a,f], Ana Fortuna [b,c*]*

[a] *Advanced Drug Delivery Research Laboratory, Department of Food and Drug Science, University of Parma, Parma, Italy*

[b] *Laboratory of Pharmacology, Department of Pharmacy, University of Coimbra, Coimbra, Portugal*

[c] *CIBIT/ICNAS - Coimbra Institute for Biomedical Imaging and Translational Research, University of Coimbra, Coimbra, Portugal*

[d] *Department of Pharmacology, Toxicology and Therapeutic Chemistry, Faculty of Pharmacy and Food Science, Universitat de Barcelona, Barcelona, Spain*

[e] *Institute of Neurosciences, Universitat de Barcelona, Barcelona, Spain*

[f] *University Research Centre for the Innovation of Health Products, Biopharmanet-TEC, University of Parma, Parma, Italy*

*Corresponding author at: Laboratory of Pharmacology, Faculty of Pharmacy, University of Coimbra, Pólo das Ciências da Saúde, Azinhaga de Santa Comba, 3000-548 Coimbra, Portugal.
E-mail address: anacfortuna@gmail.com (A. Fortuna)

*Corresponding author at: Advanced Drug Delivery Research Laboratory, Department of Food and Drug Science, University of Parma, Parco Area delle Scienze 27/A, 43124 Parma, Italy.
E-mail address: fabio.sonvico@unipr.it (F. Sonvico)

Published in December 2024, ***European Journal of Pharmaceutical Sciences***

ABSTRACT

Neuroinflammation is an undoubtedly hallmark of neurodegenerative diseases characterized by memory impairment, loss of coordination and muscle strength such as Alzheimer's disease, Parkinson disease and Multiple Sclerosis as well as depressive disorders. Cyclosporine A (CSA) has already been identified as a promising neuroprotective peptide, due to its well-known anti-inflammatory properties. Herein, CSA was incapsulated into α-tocopheryl polyethylene glycol 1000 succinate (TPGS) micelles and intranasally administered at 40 mg/kg dose to an LPS-induced mouse model of neuroinflammation. After the treatment, mice were subjected to behavioral tests to assess cognitive and motor skills, while the biodistribution of CSA in plasma and olfactory bulb was studied by a new HPLC method validated for precision and accuracy. The results highlighted that in comparison to the classic oral CSA suspension, the intranasal (IN) administration showed significatively better safety and efficiency profiles.

Noteworthy, IN administration of CSA micelles showed relevant antidepressive effects and a certain ability to revert LPS-induced motor impairment.

This work pointed out that the innovative and noninvasive IN administration of TPGS micelles could represent a safe and effective alternative to the classic oral route to deliver CSA at the Central Nervous System level, where its beneficial activity against neuroinflammation can be exploited.

1. INTRODUCTION

Neuroinflammation has been indicated as a key factor in neuronal impairment leading to the development of neurodegenerative disorders including Alzheimer's, Parkinson's and Huntington's diseases [1,2] as well as of psychiatric diseases such as depressive disorders [3,4].

As already reported by others, cyclosporine A (CSA) can reduce neuroinflammation [5] potentially preventing the related disorders. CSA is a lipophilic undecapeptide (logP = 2.92, 1202 kDa) characterized by immunosuppressive activity, and for this reason this natural compound is mainly indicated for treatment and/or prevention of organ rejection in transplants [6]. In addition to this, considering its ability to inhibit cyclo-oxygenase-2 (COX-2) and the release of interleukin-1 (IL-1), interleukin-2 (IL-2), and tumor necrosis factor-alpha (TNF-α) in neural cells [7,8], CSA has been suggested to provide neuroprotective action in neurodegenerative diseases [9]. However, to effectively target the brain and actively inhibit neuroinflammation, a drug must be able to cross the Blood-Brain-Barrier (BBB) which is a physical and metabolic barrier consisting of cells, capillaries, pericytes, astrocytes and neurons that prevent the access to the brain to the large majority of xenobiotics [10]. It is known that peptides, such as CSA, have a very low ability to cross the BBB particularly owing to the expression of efflux transporters such as P-glycoprotein (P-gp) [11]. P-gp mediates the active efflux of CSA, as already demonstrated in *in vivo* studies [11], thus preventing the drug access into the target site. In addition to this, the molecular weight of the peptide is approximately 2-3 times higher than the size threshold that allows a molecule to cross the BBB as such [12]. These findings highlight that new strategies are needed to avoid the BBB for the administration of therapeutic peptides such as CSA [13]. Several strategies have already been tested to reach this objective, including the direct administration of therapeutic agents into the damaged region of the brain via Extracellular Space (ECS) using a catheter, or the intraventricular administration using a reservoir implanted into one of the ventricles, and the intrathecal delivery exploiting external pumps [10]. However, these approaches are very invasive and risky since require surgery, and present a number of side effects and potential clinical complications; moreover, they bring pain to the patient [10].

Over the last decades, the intranasal (IN) route of administration has gained value as a potential noninvasive strategy to directly deliver drugs into the brain [14,15] through the olfactory region of the nasal mucosa, which represents the unique natural and direct connection between the environment and the brain [16]. More precisely, after being intranasally administered, the drug can be internalized into the neurons and transported along axons to the olfactory bulb; transported through paracellular pathway exploiting the spaces between cells or across the channels next to the nerves; transported through transcellular pathway across the basal epithelial cells [17–21].

However, concerning peptides such as CSA, it is necessary to guarantee their stabilization, enhance their residence time on nasal mucosa and improve the penetration across the mucosal tissue [22]. Nano-sized drug delivery systems, including micelles, nanoparticles and liposomes, can be exploited as vehicles to reach these objectives and effectively promote nose-to-brain direct delivery through a noninvasive route [10]. Our group has previously developed and characterized α-tocopheryl polyethylene glycol 1000 succinate (TPGS) micelles loaded with CSA for the local nasal treatment of viral infections [23] but in this research, we aimed at deliver the peptide into the brain through nasal instillation. These drug delivery systems were characterized by a particle size of around 15 nm with more than 90% drug encapsulation efficiency and their ability to penetrate across the nasal mucosa has already been confirmed *in vitro* and *ex vivo* [23] (shown in **Supplementary Material**). Moreover, in recent years TPGS has been recognized by Food and Drug Administration (FDA) as pharmaceutically safe adjuvant [24], making the micellar formulation highly biocompatible.

Thus, the present study was carried out to investigate whether CSA, formulated as intranasally administered TPGS micelles, prevents depressive-like behavior and cognitive impairment as well as to assess the advantages that the IN treatment can bring in terms of safety compared to the classic oral route.

For this purpose, CSA loading TPGS micelles were administered to CD-1 male mice previously injected with lipopolysaccharide (LPS) O55:B5 produced by *Escherichia coli*. This is a well-known animal model of neuroinflammation [3,4] associated to cognitive impairment [25,26] as well as behavioral alterations such as anxiety, depression and decreased locomotion [3,4]. Indeed, LPS is a cell-wall compound produced by gram-negative bacteria and it actively stimulates the immune system leading to the activation of inflammatory processes [27]. In this work, the potential neuroprotective effects of CSA loading TPGS micelles were evaluated for the first time *in vivo* in a mouse model of neuroinflammation exploiting several behavioral tests to investigate cognitive and motor skills. In addition, the distribution profile of CSA was evaluated in plasma and olfactory bulb, employing a new validated bioassay for CSA using High Performance Liquid Chromatography (HPLC) with diode array detection (DAD).

2. MATERIALS AND METHODS

2.1 Chemicals and Reagents

Cyclosporine A (CSA, MW 1202.61 g/mol) was obtained from Metapharmaceutical (Barcelona, Spain); celecoxib (CXB, MW 381.37 g/mol), used as internal standard (IS), was obtained from Shandong Zhishang Chem Co., Ltd. (Zhangqiu, China); α-tocopheryl polyethylene glycole 1000 succinate (TPGS, MW 1513 g/mol) was from PMC ISOCHEM (Gennevilliers, France). LPS, *E.coli* O55:B5 was purchased from Santa Cruz Biotechnology, Inc. (Dallas, TX, USA). Isoflurane was from HiFarmaX (Lisbon, Portugal). Diethyl ether was from Honeywell (Muskegon, MI, USA); n-hexane was from Fisher Chemical (Loughborough, UK) while trifluoroacetic acid (TFA) was from Merck Life Science (Algés, Portugal). Gradient grade acetonitrile was acquired from Thermo Fisher Scientific (Loughborough, UK), and ultrapure water (HPLC grade; 18.2 MΩ·cm) was obtained using a Milli-Q water purification apparatus, Sartoriusarium® pro from Sartorius (Goettingen, Germany).

2.2 Quantification of cyclosporine A in plasma and olfactory bulb

2.2.1 Stock solutions and standard preparation

The stock solutions of CSA and CXB were prepared both at a concentration of 1 mg/mL by dissolving the powder in acetonitrile. Each stock solution was vortexed until the complete dissolution of the compound and stored at 4°C in an amber glass flask with screw cap until used. The CSA stock solution was further diluted in acetonitrile to obtain a 200 µg/mL work solution, used to prepare six calibration standards. The calibration standards were prepared in acetonitrile at the following drug concentrations: 5, 10, 16, 20, 30 and 50 µg/mL. Four quality control (QC) samples were then prepared by diluting the CSA work solution in acetonitrile, following the international guidelines [28–30]. Specifically, the QC sample at the lower limit of quantification (QC_{LLOQ}) had the same CSA concentration of the lowest calibration standard; the QC sample at low concentration (QC_1) was prepared at the concentration of 14 µg/mL, which is less than three times the concentration of LLOQ; the QC sample at medium concentration (QC_2) was prepared at the concentration of 25 µg/mL, which is within the 30-50% of the range of the calibration curve; the QC sample at high concentrations (QC_3) had the concentration of 40 µg/mL, which is higher than 75% of the upper limit of quantification. The work solution of CXB was prepared in acetonitrile at a concentration of 50 µg/mL by diluting the stock solution.

2.2.2 HPLC apparatus

The quantitative analysis of CSA was performed exploiting a Shimadzu Prominence HPLC system (Shimadzu Corporation, Kyoto, Japan), consisting of a solvent delivery unit LC-20A, a DGU-20A5

degasser system, a SIL-20AHT autosampler, a CTO-10ASVP column oven, an SPD-M20A diode-array detection (DAD) and an RF-20AXS fluorescence detector. The data were acquired and elaborated using LCsolution software (Shimadzu Corporation, Kyoto, Japan). The stationary phase consisted in a Phoroshell 120 EC-C18 column (2.7 µm particle size, 4.6 × 150 mm) purchased from Agilent (Santa Clara, CA, USA). The column was equipped with an EC-C18 guard column (2.7 µm particle size, 4.6 × 5 mm) from Agilent, Santa Clara, United States.

The optimized conditions for the detection of CSA and the IS consisted in the use of a mixture of acetonitrile with 0.1% trifluoroacetic acid (TFA) (mobile phase A) and ultrapure water with 0.1% TFA (mobile phase B) exploiting a gradient elution as described in **Table 1**. The oven temperature was kept at 60°C, the total flow rate was 1.2 mL/min and the run time was 18 minutes. The injection volume was 25 µL for the analysis of plasma samples, while 40 µL for the analysis of olfactory bulb samples. The selected wavelengths for the detection of the compounds were 222 nm and 250 nm for CSA and CXB, respectively.

Table 1 *– High-performance liquid chromatography gradient program*

Time (min)	***Mobile phase A : Mobile phase B***
0	60 : 40
3.5	60 : 40
7	95 : 5
12	80 : 20
14	60 : 40
18	60 : 40

2.2.3 Plasma and olfactory bulb sample preparation

Blood samples were collected into heparin-lithium tubes (Aquisel, Barcelona, Spain) and centrifugated at 1,250 × g for 10 minutes at 4°C. Plasma was finally collected and frozen at -20°C until being used. Immediately before starting the analysis, the samples were thawed at room temperature.

The olfactory bulb was isolated from the whole brain and placed into a plastic Eppendorf; then, according to the protocol published by Serralheiro *et al*. [31], the tissue was homogenized with 500 µL of saline regardless of the weight of the tissue, using a high-shear mixing Ultra-Turrax (Ystral GmbH, Dottingen, Germany) at 24,000 rpm for 2 minutes. Then, the homogenate was centrifugated at 4,100 x g for 15 minutes at 4°C using an Eppendorf Centrifuge model 5430 R (Eppendorf AG, Hamburg, Germany). The supernatant was collected and frozen at -20°C until being used.

To prepare the calibration curve, 100 µL of mice plasma or olfactory bulb homogenates were spiked

with 10 µL of each CSA spiking solution and 10 µL of the IS spiking solution (50 µg/mL) in ice. Diethyl Ether (1.5 mL) was added, and the mixture was vortexed for 5 minutes; the samples were left to stand for 1 minute at room temperature and then centrifugated at 12,045 g for 5 minutes at room temperature using a MiniSpin centrifuge (Eppendorf AG, Hamburg, Germany). The supernatant was quantitatively transferred to a glass tube and evaporated to dryness under a gentle stream of nitrogen at 60°C using a Stuart Sample Concentrator SBH130D/3. The dried residue was reconstituted with 100 µL of a mixture composed of 65% acetonitrile with 0.1% TFA and 35% Milli-Q water with 0.1% TFA. The solution was vortexed for 1 minute, transferred to a plastic Eppendorf and washed trice using n-Hexane. Each washing was performed with 400 µL of n-Hexane, then vortexing for 2 minutes the sample and centrifugating it at 12,045 g for 2 minutes at room temperature using a MiniSpin centrifuge. The amount of n-Hexane used to wash the sample was removed with a micropipette [32] and the washed phase was collected with a micropipette and injected into the HPLC.

2.2.4 Method validation

The validation of the method was realized by exploiting five independent calibration curves prepared in CD-1 mice plasma and three independent calibration curves prepared in olfactory bulb. Each calibration curve was set in a CSA concentration range between the LLOQ and the highest calibration standard (*i.e.*, 0.5 – 5 µg/mL).

To check the linearity, the ratio between the peak area of CSA and IS was plotted versus the concentration and the correlation coefficient was calculated; several weighting factors ($1/x^2$, $1/y^2$, $1/x$, $1/y$, $1/\sqrt{x}$, $1/\sqrt{y}$) were considered in order to identify the one allowing to obtain the lowest percentage of relative error (RE%) [33], and $1/x^2$ was selected as the most suitable and applied during all the validation process.

Accuracy and precision were evaluated both within and between days (intra-day and inter-day, respectively), by preparing and analyzing five (for plasma samples) or three (for olfactory bulb samples) times both the LLOQ and all the QCs in the same day and over different days.

Accuracy indicates the difference between the experimentally determined value and the nominal one and it is expressed as bias percentage (Bias %) as indicated in **Equation 1** below. It was obtained by comparing the experimental values of QC_{LLOQ}, QC_1, QC_2 and QC_3 to their nominal concentration. According to the guidelines [29,30], the accuracy of the experimentally determined values of each QC should not exceed ± 15 % of the nominal value, while for the QC_{LLOQ} the determined values should be within ± 20 % of the nominal value.

$$Bias\% = \frac{C_{determined-}\ C_{nominal}}{C_{nominal}}\ x\ 100 \quad \textbf{(1)}$$

Precision indicates how far the results differ from each other, and it is calculated as coefficient of variation (CV%) as indicated in **Equation 2**. It was calculated by analyzing the standard deviation and the average of the experimental values of QC_{LLOQ}, QC_1, QC_2 and QC_3. According to the guidelines [29,30], the precision of the experimentally determined values of each QC should not exceed ± 15 % of the nominal value, while for the QC_{LLOQ} the values should be within ± 20 %.

$$CV\% = \frac{Standard\ Deviation}{Mean}\ x\ 100 \quad \textbf{(2)}$$

The recovery of the extraction method described above was calculated from the comparison between the results obtained by spiking the biological samples then subjecting them to the extraction method and the results obtained by analyzing the non-extracted analyte solutions at the same nominal concentrations (**Equation 3**). The relative recovery was calculated at the following concentrations: 1.4 µg/mL (QC_1), 2.5 µg/mL (QC_2) and 4 µg/mL (QC_3).

$$Recovery\% = \frac{extracted\ spiked\ biological\ sample}{non-extracted\ sample\ solution}\ x\ 100 \quad \textbf{(3)}$$

2.3 CSA-loading micellar formulation: adaptation and characterization

Considering the low amount of CSA found in plasma and olfactory bulb during the preliminary studies performed in mice intranasally administered with a 5 mg/mL CSA-loading TPGS micellar formulation as well as the relatively high LLOQ of the HPLC analytical method, the micellar formulation needed to be adapted to allow the detection of the active compound in biological samples collected during the pharmacokinetic studies. For this reason, the amount of TPGS was increased ten times compared to the previously developed and optimized TPGS micellar formulation [23], to improve the solubility of the drug. In this condition, 30 mg/mL of CSA could be solubilized into the micellar mixture.

The adapted CSA-loading TPGS micellar formulation (30 mg/mL) was prepared by dissolving TPGS in saline at a concentration of 30% (w/v). The mixture was stirred at room temperature and protected from light until the complete dissolution of TPGS. Then, CSA powder was weighed and directly added to the previously prepared blank micellar formulation, in order to reach a drug concentration of 30 mg/mL. The formulation was stirred initially at 700 rpm (Hot Plate stirrer 11-

300-49SHP, Hampton, New Hampshire, USA) to ensure that the entire amount of powder was incorporated into the liquid, then it was sonicated in ice for two minutes to allow the disintegration of the powder's agglomerate and improve the interaction with the liquid leading to the dissolution of the drug. The formulation was then stirred overnight at room temperature at 300 rpm and finally centrifugated at 9,500 × g for 10 minutes at 20°C using an Eppendorf Centrifuge model 5430 R (Eppendorf AG, Hamburg, Germany). The supernatant was collected and stored at 4°C protected from light until further use.

The characterization of the adapted drug-loading micelles was realized after equilibrating the formulation at room temperature until the gel was completely liquefied, since at 4°C it became solid due to the high amount of TPGS. The formulation was characterized for size, PDI, viscosity and drug encapsulation efficiency.

2.3.1 Particle size, Polydispersity Index and surface Zeta potential

Size and Polydispersity Index (PDI) were analyzed by Dynamic Light Scattering (DLS) exploiting a Malvern Zetasizer Nano ZS (range 0.3 nm - 10 µm, Malvern Instruments Ltd., Malvern, UK) using 1 mL of the formulation without dilution into a disposable polystyrene cuvette. Measurements were performed at the temperature of 25°C and at a scattering angle of 173°. The refractive index and the viscosity of the dispersant were 1.33 and 0.8872 mPa·s, respectively. The refractive index of the material was set at the value of 1.00 while the absorption was 0.010. Analyses were repeated three times for each sample, with 15 sub-runs for measurement to increase data and correlation and reported as cumulative unimodal/multimodal fitting (sample dependent) and Z-average mean particle size.

2.3.2 Viscosity

The dynamic viscosity of the 30 mg/mL CSA-loading micellar formulation was measured by a Discovery HR20 Rheometer (Waters TA instruments, New Castle, USA) and data were analyzed using TRIOSTM software version 5.7.0.56. All the measurements were done at 25°C without diluting the sample, which was analyzed using a stainless-steel Peltier parallel plate geometry (diameter 40 mm, 1 mm gap). The duration of the measurements was 60 seconds, and the shear rate was 1.67 1/s. The analysis was done in triplicate.

2.3.3 Drug Loading Encapsulation Efficiency (EE%)

The drug loading encapsulation efficiency (EE%) was determined by HPLC. For this purpose, a CSA calibration curve was built in the concentration range of 100-500 µg/mL by diluting the stock

solution (1 mg/mL) in acetonitrile. The analytical method condition as well as the instrumentation used were the same as described in **Section 2.2.2**, with the only difference represented by the injection volume, that in this case was 10 µL.

2.4 *In vivo* studies in CD-1 mice

2.4.1 Animals and Ethics

CD-1 male mice weighing approximately 30-35 g were purchased from Charles River Laboratories (France), and maintained in a 12 h light/dark cycle, at 20 ± 2 °C and a relative humidity of 55 ± 5%, with *ad libitum* access to a standard diet (4RF21, Mucedola, Italy) and tap water. All the procedures carried out on the animals and their care were done following the international regulations of the European Directive (2010) regarding the protection of laboratory animals used for scientific purposes (2010/63/EU) (European Parliament, Council of the European Union, 2010) and the Portuguese law on animal welfare (Decreto-Lei 113/2013).

2.4.2 *In vivo* intranasal repeated dose efficacy study on LPS-induced neuroinflammation mouse model

To investigate if multiple IN dosing of CSA micelles could have any preventive effect against cognitive function and depressive-like behavior while maintaining the safety profile of oral formulations, CD-1 male mice were divided into four groups (n=10): the control group that did not receive LPS or CSA, and three other groups that were injected with LPS. These 3 groups varied according to their treatment: one was intranasally administered with the blank 30%-TPGS micellar formulation (IN-bnk_{mic}), another group received CSA-loading 30%-TPGS micellar formulation by IN route (30 mg/mL, IN-CSA_{mic}), while the third group was administered orally with a 15 mg/mL CSA suspension prepared in saline (O-CSA_{susp}). The dose of CSA administered was the same (40 mg/kg). The administration was done every 12 hours (at 8 a.m and at 8 p.m) for three consecutive days. Mice intranasally administered received 25 µL of micellar formulation per nostril. The IN administration was performed exploiting the Fine Mist Sprayer (Aptar, IL, USA), that was carefully filled with the formulation to avoid bubbles, then the dead volume was eliminated according to the indications provided by the supplier. The device was weighed before and after each administration to confirm the accurate delivered volume. Animals treated with O-CSA_{susp} received 100 µL of treatment by oral gavage. LPS was used to induce depressive-like behavior and compromise memory function as described in [4]. It was intraperitoneally administered at the dose of 1 mg/kg [34,35], 30 minutes after the last administration of the treatment. The LPS solution was previously prepared by dissolving the weighted powder in saline to have a stock solution at a concentration of 1 mg/mL, that was further

diluted to obtain a work solution having a concentration of 0.1 mg/mL. On the day after LPS injection, the animals were subjected to the behavioral tests reported in **Section 2.4.4**. A timeline showing the management of both the therapy and LPS administration is reported in **Supplementary Material.**

2.4.3 CSA concentrations in plasma and olfactory bulb after single intranasal and oral administration

The *in vivo* administration of the CSA formulated as IN micelles or oral suspension was performed with the aim of comparing the different distribution profiles of CSA in plasma and olfactory bulb. The animals were divided in two groups: the first group was intranasally administered with the 30 mg/mL CSA-loading 30%-TPGS micellar formulation (IN-CSA_{mic}), while the second group was orally administered with the 15 mg/mL CSA suspension in saline (O-CSA_{susp}). Both groups received the dose of 40 mg/kg. The IN group received 25 µL of formulation in each nostril while the oral group received 100 µL of formulation. Each group, composed of twelve animals, was randomly divided into three subgroups (n=4) that were sacrificed at 15 minutes, 30 minutes and 1 hour post administration. Blood and olfactory bulb were immediately collected and processed as described in **Section 2.2.3**.

2.4.4 Behavioral tests

To assess the neuroprotective properties of multiple IN doses of the CSA micellar formulation and investigate whether the side effects exploiting the IN route of administration could be decreased comparatively to the classic oral route, the animals were subjected to Novel Object Recognition Test (NORT) and Tail Suspension Test (TST). These behavioral tests allow to assess the cognitive function and the depressive-like behavior of the animals, respectively. Coordination was assessed by Wire Hanging Test (WHT) as well as locomotor activity was evaluated by Open Field Test (OFT). Moreover, olfactive function was determined by Buried Food Test (BFT) to foresee eventual side effects. All these tests were performed the day after the intraperitoneal administration of LPS at a dose of 1 mg/kg [34,35]. The behavior of mice during OFT and NORT was analyzed using SMART video system (version 3.0; Panlab S.L., Spain) software.

NOVEL OBJECT RECOGNITION TEST (NORT)

NORT was performed to investigate the effect that the CSA IN micelles have on the cognitive function, particularly on the memory processes [36]. NORT was divided into four sessions, each one made on a different day. In the first two days animals were subjected to habituation, consisting in the 5 minutes-lasting free exploration of the empty open-field box described below in section

"**Open Field Test (OFT)**". On the third day, the animals were subjected to training, consisting in a 10 minutes-lasting exploration of the open field box in which two new and identical objects have been placed in the center area. Mice that did not explore the object for at least 8 seconds were excluded from the test. On the last day of the test, mice were put again in the open field box with two objects, of which one was identical to the ones used for training (familiar object), while the other was different (new object). Before testing each animal, the cage and the objects were cleaned with 70% ethanol to remove any odor belonging to the previously tested animal. Just the situations in which mice directly touched the object with their nose or when they faced with the object at a distance not higher than 2 cm were considered as exploration-like behaviors [4]. The Preference Index (PI) was calculated to express the tendency of the animal to explore more the new object than the familiar one and it was calculated according to the **Equation 4**, where T_{new} is the time spent in the exploration of the new object and T_{tot} is the sum of the time spent in the exploration of the new object and the familiar object.

$$PI = \frac{T_{new}}{T_{tot}} \quad \textbf{(4)}$$

In addition, the Discrimination Index (DI) was also calculated as in the following **Equation 5**, where T_{fam} is the time spent exploring the familiar object.

$$DI = \frac{T_{new} - T_{fam}}{T_{tot}} \quad \textbf{(5)}$$

PI and DI were exploited as indicators of the tendency of the animals to explore more the novel object than the familiar one, assuming that mice with intact cognitive function spend longer time exploring the novel object [36]. Recognition memory was evaluated considering the time spent by the animals in investigating the new object [36].

TAIL SUSPENSION TEST (TST)

TST is widely used to assess the depressive state of rodents; specifically, it has been used to demonstrate the depressive-like behavior effect induced by LPS [37]. The test is based on the premise that when the mouse is subjected to the stress of being suspended from the tail without the possibility of escaping, it develops the tendency to assume an immobile posture. Thus, if a therapeutic treatment has any anti-depressive effect, the immobility is reversed and the treated animal develops an escape-oriented behavior [38].

The test was done by suspending the animal from the tail using tape into a suspension box in a position that does not allow the mouse to escape, for example by holding the surface of the box used for the test. The duration of the test was 6 minutes, during which the behavior of the mice was recorded, and the time spent by the mice trying to escape was registered. Only the situation in which the animal vigorously moved its body trying to reach the walls or the bar from which it hanged

was considered as an escape-related behavior. On the other hand, when the movement of the body was confined to the front legs and the hind ones were not involved or when the animal just swung, it was not considered as an escape-oriented behavior.

BURIED FOOD TEST (BFT)

BFT was performed to study the impact that the IN administration of the drug-loading and blank micellar formulation could have on the olfactory function of mice. This test measures how quickly a mouse kept without food overnight is able to find a piece of palatable food consisting in this case in a cookie. During the three days before the test, the animals were weighed and the food was restricted to 90% of the body weight, and at the same time in each cage many pieces of cookie were put [39]. The cage was refilled with cookies every time it was necessary. The day before the test, all the food was removed to induce starvation. At least 30 minutes before starting the test, the animals were subjected to habituation, consisting in staying in a clean cage filled with 3 cm of bedding without any food. The test was then performed after burying a piece of cookie under the 3cm-bedding, in a position that was not visible from the animal. The test lasted 5 minutes, but the timer was stopped if the animal could find and eat the cookie within 5 minutes.

OPEN FIELD TEST (OFT)

The animals were singularly placed in the central area of an open field box, characterized by the following dimensions: 40 cm length × 40 cm width × 30 cm height. The floor of the box was divided into 16 equal squares, of which 4 constitute the central area (20 × 20 cm) while the other 12 constitute the peripheral region. The behavior of the mice and their movements were recorded for 5 minutes at standard room-lighting conditions, and before testing each animal the cage was cleaned with 70% ethanol to remove any odor belonging to the previously tested animal. To evaluate anxiety-related behavior and locomotor activity, for each group of animals, the following parameters were registered and compared: the time spent in the center squares; the number of entries in the central squares; the overall velocity, calculated as the ratio between the total squared crossed and the time spent in both the peripheral and the central region [40,41].

WIRE HANGING TEST (WHT)

WHT was exploited to analyze the effect that the chronic treatment with CSA could have on the coordination and muscle condition. It is based on the fact that healthy mice are able to stay hanging on a wire until they are exhausted [42]. The test was performed by handling the animal from the tail and bringing it near the metallic wire positioned at around 40 cm from the floor on which soft cloths had been placed to cushion any falls. Then, the mouse was let grasp the wire just with the front legs

[43]. The test lasted 1 minute, during which the time between the beginning of the experiment and the first fall was registered as well as the number of falls. Every time that the animal fell, it was manually brought back to the wire. If the mouse, instead of falling due to lack of grip on the wire, just slipped on the vertical supports lateral to the wire itself, this condition was not considered as a fall and the animal was simply repositioned on the wire.

2.5 Statistical Analysis

All the data obtained by the *in vivo* test were processed using GraphPad Prism® 8.3.0.53 (San Diego, CA, USA). One-way analysis of variance (ANOVA) associated with Multiple Comparison Test were exploited to determine if the differences between experimental data were significant. Differences were considered statistically different when $p < 0.05$ (*).

3. RESULTS

3.1 HPLC method validation for the quantification of CSA in biological samples

3.1.1 Accuracy, Precision and Recovery in olfactory bulb and plasma

Table 2 summarizes the inter- and intra-day accuracy and precision of the HPLC method used to quantify CSA in mice plasma and olfactory bulb homogenate.

In mice plasma, the inter-day accuracy varied from -2.02 % to 3.92 % considering all the quality control levels, while the overall intra-day accuracy in plasma was between -11.79 % and -3.69 %. Regarding the precision, in plasma samples this parameter turned out to be between 8.55 % and 19.42 % considering the inter-day data, while it was between 2.24 % and 11.23 % considering the intra-day ones. Finally, the HPLC technique revealed linearity over a defined concentration range (0.5 – 5 µg/mL) attested by a determination coefficient (r^2) of 0.9935.

On the other hand, in olfactory bulb samples, the inter-day accuracy was between -1.99 % and 6.90 % while the intra-day accuracy was between -12.84 % and 5.63 % considering all the quality control levels. The inter-day precision turned out to be in the range of 1.41 % and 12.06 %, while the same parameter calculated intra-day was between 5.61 % and 9.45 %. In this case linearity was confirmed as well in the concentration range 0.5 – 5 µg/mL, and the r^2 turned out to be 0.9922.

Table 2 *- Inter- and Intra- day accuracy and precision data of cyclosporine A (CSA) obtained by applying the optimized HPLC technique to analyze plasma and olfactory bulb samples.*

		QC_{LLOQ}	QC_1	QC_2	QC_3
C_{nom} (µg/mL)		0.5	1.4	2.5	4
C_{exp} (µg/mL) (Mean ± SD)	Plasma (*n=5*)	0.515 ± 0.185	1.372 ± 0.230	2.598 ± 0.333	3.964 ± 0.377
	Olfactory bulb (*n=3*)	0.490 ± 0.062	1.497 ± 0.218	2.496 ± 0.039	3.956 ± 0.074
Inter-day Accuracy (Bias %)	Plasma (*n=5*)	2.99	-2.02	3.92	-0.90
	Olfactory bulb (*n=3*)	-1.99	6.90	-0.15	-1.11
Intra-day Accuracy (Bias %)	Plasma (*n=5*)	-11.79	-3.69	-4.66	-4.78
	Olfactory bulb (*n=3*)	-12.84	-1.71	-6.31	5.63
Inter-day Precision (CV%)	Plasma (*n=5*)	19.42	12.71	10.96	8.55
	Olfactory bulb (*n=3*)	7.72	12.06	1.41	1.74
Intra-day Precision (CV%)	Plasma (*n=5*)	6.20	8.46	11.23	2.24
	Olfactory bulb (*n=3*)	5.61	9.45	8.52	8.47

C_{nom}, nominal concentration; C_{exp}, experimental concentration estimated employing the correspondent mean calibration equation; CV, coefficient of variation; QC, quality control; SD, Standard Deviation

The average recovery of CSA obtained by applying the extraction procedure described in **Section 2.2.3** and analyzing the samples by HPLC was 87.8 % ± 9.38 in plasma, with a CV% of 10.69 %. In olfactory bulb samples, the average recovery was 92.5 % ± 8.68, with a CV% of 9.38 %.

3.2 Characterization of the CSA-loading micellar formulation

The adapted micellar formulation was characterized for particle size, PDI and surface potential by Dynamic Light Scattering, while viscosity was determined by rheometer measurements. The drug entrapment into the micellar structure was calculated by liquid chromatography.

The average particle size calculated for the CSA-loading micellar formulation was 82.26 ± 2.23 nm, while the PDI was 0.362. Micelles showed an overall neutral surface, attested by the Zeta-potential value that was -0.552 ± 0.001 mV.

The dynamic viscosity of the micelles at room temperature turned out to be 0.06 ± 0.01 Pa·s. The CSA loading encapsulation efficiency (EE%) calculated by HPLC was 81.97 ± 12.57 %.

3.3 Behavioral tests

NOVEL OBJECT RECOGNITION TEST

No differences were observed between the control and IN-bnk_{mic} groups regarding the number of time that the animals explored the new object (**Figure 1A**). However, the tendency to explore more the new object than the familiar one (expressed by both PI and DI parameters) was higher in IN-bnk_{mic} group, with statistically significant differences relatively to the control group ($p<0.05$) (**Figure 1B** and **1C**). When previously administered with IN CSA micelles, the animals exhibited similar values to those observed in the IN-bnk_{mic} group ($p>0.05$, **Figure 1**), suggesting that the treatment did not ameliorate or compromise mouse memory. Importantly, the number of times that the animals explored the new object, the PI and the DI were statistically higher after IN-CSA_{mic} treatment than O-CSA_{susp} treatment ($p<0.05$, **Figure 1**). Moreover, the O-CSA_{susp} presented a lower number of explorations than the control group and IN-bnk_{mic} ($p<0.05$, **Figure 1A**), indicating that the oral treatment is not able to preserve the cognitive function of the animals.

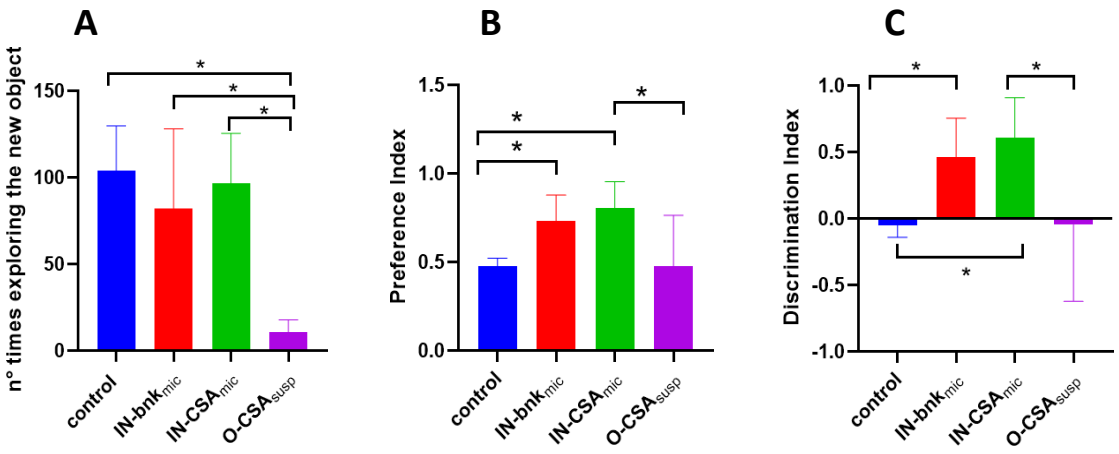

Figure 1 *- Number of times in which mice explored the novel object (A), Preference Index (B) and Discrimination Index (C), during the Novel Object Recognition Test. The graphs show the comparison between the control group (blue), the groups treated intranasally with blank micellar formulation (IN-bnk$_{mic}$, n=10) or the cyclosporine A (CSA) micellar formulation (IN-CSAmic, n=10) and the group treated orally with the CSA suspension (O-CSA$_{susp}$, n=5). * p < 0.05*

TAIL SUSPENSION TEST

The depressive-like behavior caused by the LPS-induced neuroinflammation was assessed resorting to the TST. The control group spent most of the time (209.20 ± 52.97 seconds) in escape-oriented behavior, while IN-bnk$_{mic}$ and O-CSA$_{susp}$ showed significantly lower time values than the control and IN-CSA$_{mic}$ groups ($p<0.05$, **Figure 2**). More precisely, O-CSA$_{susp}$ just showed escape-oriented behavior for 111.89 ± 22.47 seconds, while IN-bnk$_{mic}$ showed it for 129.30 ± 25.43 seconds and IN-CSA$_{mic}$ mice group for 181.30 ± 49.04 seconds. Moreover, no statistical differences were found between the IN-CSA$_{mic}$ and control groups (**Figure 2**).

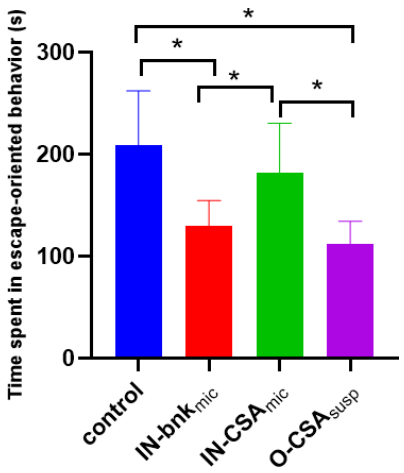

Figure 2 *- Time spent by the mice in escape-oriented behavior during the Tail Suspension Test. The graph shows the comparison between the control group (blue), the groups treated intranasally with blank micellar formulation (IN-bnk$_{mic}$, n=10) or the cyclosporine A (CSA) micellar formulation (IN-CSAmic, n=10) and the group treated orally with the CSA suspension (O-CSA$_{susp}$, n=9). * p < 0.05*

BURIED FOOD TEST

The BFT pointed out that LPS reduced the odors' perception of the animals. Specifically, while 70% of the control animals found and ate the cookie within 5 minutes, only 20% of the IN-bnk$_{mic}$ mice could find and eat the cookie. However, the treatment with CSA, regardless the route of administration, did not revert this effect as none of the IN-CSA$_{mic}$ or the O-CSA$_{susp}$ animals could find and eat the cookie.

OPEN FIELD TEST

The time spent by the mice in the center squares of the Open Field arena is shown in **Figure 3**. Accordingly, it is noteworthy that the animals injected with LPS and that did not receive CSA (IN-bnk$_{mic}$ group) exhibited a shorter time in the center squares comparatively to the control group that did not receive LPS ($p<0.05$). These findings suggest the anxiogenic effect of acute LPS administration. Additionally, IN treatment with CSA did not reveal statistically significant differences with IN-bnk$_{mic}$ group, indicating no anxiolytic effect at the dose of 40 mg/kg. However, the same dose administered by oral gavage revealed that the animals spent the shortest time in the center squares (6 s *versus* 24 s and 23 s obtained with IN-CSA$_{mic}$ group and IN-bnk$_{mic}$ group, respectively), with statistically significant differences in relation to the other three animal groups ($p<0.05$, **Figure 3A**). These results suggest that oral CSA treatment increases the anxiety-like behavior of the animals.

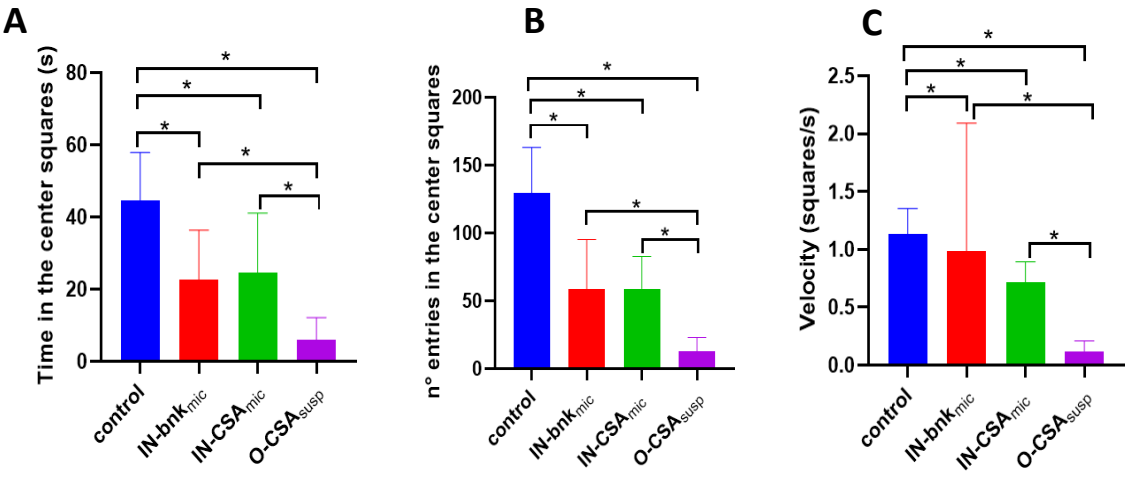

Figure 3 *- Time spent by mice in the center squares of the Open Field arena (A), number of entries in the center squares of the Open Field arena (B) and overall velocity calculated for mice in the Open Field arena(C). The graphs show the comparison between the control group (blue), the groups treated intranasally with blank micellar formulation (IN-bnk$_{mic}$, n=10) or the cyclosporine A (CSA) micellar formulation (IN-CSAmic, n=10) and the group treated orally with the CSA suspension (O-CSA$_{susp}$, n=5). * p < 0.05*

The aforementioned results were corroborated with those observed by analyzing the number of entries in the center squares of the Open Field arena. As shown in **Figure 3B**, LPS injection reduces the number of entries in central squares, with the three groups presenting statistical differences comparatively to the control group not injected with LPS ($p<0.05$). No statistical differences were observed between IN-CSA_{mic} and IN-bnk_{mic} groups, suggesting that the IN CSA formulation does not compromise the anxiety-behavior of the animals. In opposition, the animals treated orally with the CSA suspension showed a dramatically lower ($p<0.05$) number of entries in the center squares compared to all the other groups, indicating that oral CSA may have more adverse effects and possibly even aggravate the anxiogenic state of the animals.

The overall velocity of the animals during the test is summarized in **Figure 3C** and it gives information regarding the locomotor activity of each animal group. Accordingly, LPS reduced the locomotor velocity comparatively to control group ($p<0.05$). The group treated with IN CSA micelles did not show statistical differences comparatively to the IN-bnk_{mic} group while oral CSA treatment decreased the locomotor velocity of the animals, highlighting the significant differences between O-CSA_{susp} and the other three groups.

WIRE HANGING TEST

To investigate if repeated treatments with CSA could impair strength and coordination, mice were subjected to the WHT. The total number of falls within one minute and the latency time to the first fall are represented in **Figure 4**. Accordingly, the number of falls of the animals treated intranasally with micelles (drug loaded and blank) was comparable to the one of the controls. Moreover, the latency time to the first fall was significantly lower in IN-$bnk_{mic,}$ and O-CSA_{susp} groups compared to the control, suggesting that oral CSA treatment did not improve the strength and coordination of the animals. In opposition, no differences were observed between the latency times of IN-CSA_{mic} and the control, suggesting IN CSA treatment can reverse the impact of LPS in animal strength and coordination.

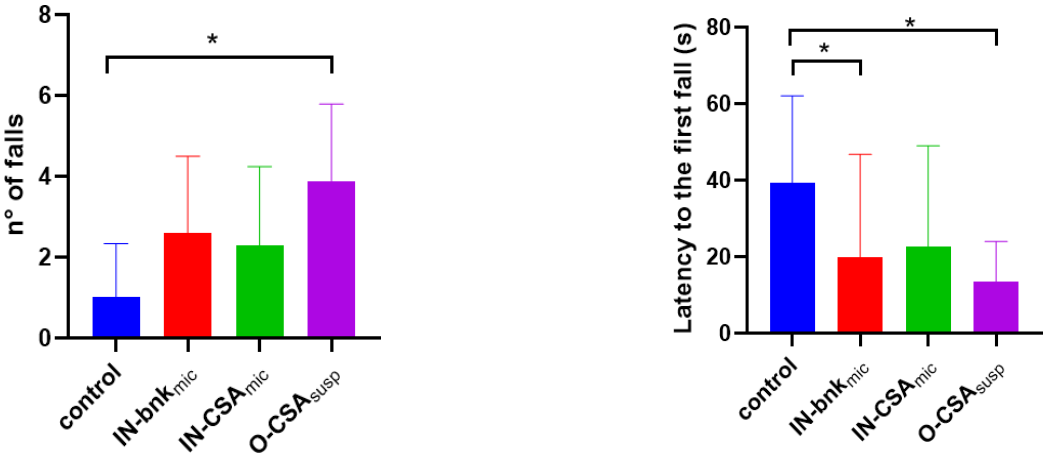

Figure 4 *- Number of times in which the mice fell (left) and the latency to the first fall (right) during the Wire Hanging Test. The graphs show the comparison between the control group (blue), the groups treated intranasally with blank micellar formulation (IN-bnk$_{mic}$, n=10) or the cyclosporine A (CSA) micellar formulation (IN-CSAmic, n=10) and the group treated orally with the CSA suspension (O-CSA$_{susp}$, n=9). * p < 0.05*

3.4 CSA concentrations in plasma and olfactory bulb after single intranasal and oral administration

At the end of the behavioral tests, mice were administered with CSA by IN instillation or oral gavage and sacrificed at 15, 30 and 60 minutes to determine the concentration of CSA in plasma and olfactory bulb by HPLC-DAD. The plasma concentrations *versus* time profiles are represented in **Figure 5**. Accordingly, no statistical differences were found between IN and oral formulations at 15 minutes and 30 minutes post-administration. However, 1h post-administration, plasma concentrations were significantly lower after the IN administration.

In olfactory bulb, CSA was not detected, or, as happened in several samples but only after nasal administration, it was detected but was below the LLOQ of the analytical technique.

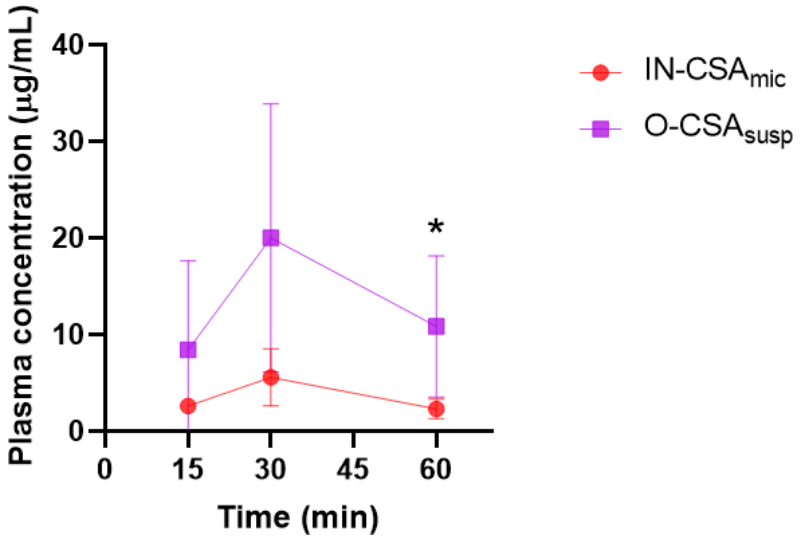

Figure 5 *- Concentration-time profile of cyclosporine A (CSA) in mice plasma after a single dose (40 mg/kg) of CSA- loading micelles administered intranasally (IN-CSA$_{mic}$, n=4 per time point) or CSA suspension administered orally (O- CSA$_{susp}$, n=4 per time point). * p<0.05*

4. DISCUSSION

To understand if the IN administration of CSA micelles formulation can prevent cognitive impairment and depressive-like behaviors, a suitable animal model of neuroinflammation consisting of LPS-injected CD-1 mouse was exploited. The findings corroborate previous studies [4,44] showing that LPS induces depression [45–47], anxiety-related behavior [48] and motor impairment [49,50].

Indeed, the LPS-injected mice that did not receive CSA showed dramatically longer periods of immobility during the TST compared to the controls, suggesting a depressive-like behavior induced by LPS. Interestingly, the IN administration of CSA reversed this effect, since the IN-CSA$_{mic}$ group exhibited an escape-related behavior comparable to the one of the controls (**Figure 2**). The antidepressive effect of CSA has already been shown in literature [51], but herein we demonstrated that it strongly depends on both the drug formulation and the route of administration, since the antidepressive effect was not observed for the CSA suspension administrated by oral gavage.

Surprisingly, LPS injection did not decrease the PI and DI as it has been reported in literature to other mice strains [52], probably owing to the fact that CD-1 mice have been rarely exploited as LPS-induced neuroinflammation model [45]. Nevertheless, the PI and DI values observed here are within those reported by other research groups [4]. It is important to note that the values of PI and DI observed for the IN-CSA$_{mic}$ were not different from those reported for IN-bnk$_{mic}$, suggesting that the IN treatment does not compromise the cognitive function of the LPS mice. In opposition, oral administration of CSA significantly reduced PI and DI in relation to the other animals, indicating that oral administration is not able to preserve animal memory.

Moreover, the results from the Buried Food Test pointed out that LPS can negatively affect odor perception. Although the IN, as well as the oral treatment with CSA, were not able to revert this effect, the animals receiving the treatment intranasally showed a more proactive behavior during the test compared to the oral group.

This observation agrees with the findings obtained in the OFT. Indeed, the anxiogenic effect of LPS was highlighted by the fact that LPS-injected mice that did not receive CSA spent significatively less time in the central zone of the Open Field arena (**Figure 3A**), showing an overall lower velocity than the controls. However, the animals receiving the CSA treatment by IN administration (IN-CSA_{mic}) showed a tendency to explore the central area of the Open Field arena that was lower compared to the controls and similar compared to IN-bnk_{mic}. Anyway, both the velocity and the time spent in the center area were extremely higher for all the IN groups than for the oral one, demonstrating that the oral suspension cannot be exploited as a treatment to prevent anxiety.

Complementarily, the negative effect of LPS on motor coordination and muscle strength was demonstrated in the WHT. CSA micelles intranasally administered prevented this condition, since the latency to the first fall and the number of falls observed for IN-CSA_{mic} group were comparable to the ones of the controls (**Figure 4**). This probably means that the IN therapy with CSA micelles could prevent the alteration in strength and coordination induced by LPS, allowing to the LPS-injected animals to maintain the same muscle strength and coordination characterizing the control animals. Once again, the oral drug suspension was unable to act as the IN CSA micellar formulation, since the latency time to the first fall was significantly shortened comparatively to the controls.

All together, these observations highlight that CSA oral gavage is accompanied by adverse effects (anxiogenic effects and locomotor, strength and coordination impairment) that were not reported when the treatment was intranasally administered, highlighting that the IN administration of CSA micelles formulations is associated to a better safety profile than the oral one.

The confirmation of this aspect was given by the analysis of blood samples collected at predetermined timepoints, that highlighted a clear higher systemic exposure when CSA was orally administered in comparison with the IN administration. In addition to this, CSA was detected in a few cases in olfactory bulb samples collected from the IN-CSA_{mic} group even if the concentration was not quantifiable, being lower than the LLOQ (data not shown). Probably, the low concentration of drug found in the olfactory bulb could be explained by an insufficient protective action of the TPGS micellar structure against drug's enzymatic degradation into the nasal cavity. It is reported indeed, that TPGS is characterized by a melting point temperature of ~ 37–41 °C [53] that is the same characterizing the nostril environment. Therefore, once in contact with the nasal mucosa, the micellar structure may become less rigid, thus exposing the drug to degradation by enzymes such as esterases, transferases and Cytochrome P-450 [18,54–57].

On the other hand, CSA could not be detected at the olfactory bulb level when CSA was administered orally, formulated as a suspension. In this case, the drug was just found in blood compartments, probably as a consequence of the fact that TPGS can inhibit P-gp also at the intestinal level, enhancing the oral bioavailability of CSA as already seen in previous studies [58–61].
Importantly, the overall results of the pharmacokinetic study contribute to demonstrating that CSA, formulated as a micellar formulation and intranasally administered, can be absorbed by the olfactory epithelium and delivered to the brain bypassing the BBB. This is possible since TPGS is a well-known absorption enhancer, owing to the fact that it is one of the most efficient specific inhibitors of P-gp expressed at the BBB level [62–64].
TPGS micelles indeed, have already demonstrated a certain ability to interact with the nasal mucosa and penetrate across the mucus layer [23], allowing the absorption of CSA by the olfactory epithelium. Hence, once reached the central nervous system, the peptide drug can mediate a protective effect against neuroinflammation induced by LPS, while systemic exposure is reduced in comparison to oral administration, thus lowering the risk of side effects due to the interaction between the drug and unspecific targets.
Finally, the results of the behavioral tests highlighted that, interestingly, the blank micelles as well exhibited a certain therapeutic effect, especially against memory impairment, anxiety and muscular weakness.
This activity could be due to the antioxidant properties of the vitamin E-derivative TPGS, present at high concentration in the micellar formulation. The *in vivo* hydrolysis of this compound indeed, leads to the release of vitamin E [65], that can act as antioxidant [66,67] neutralizing the toxic effects of the reactive oxygen species (ROS) largely produced as a result of the neuroinflammation process [68], that is known to contribute to the progression of neurodegenerative diseases.

5. CONCLUSIONS

The 30% w/v TPGS micellar formulation encapsulating CSA at a concentration of 30 mg/mL administered to LPS-injected CD-1 mouse model of neuroinflammation showed relevant antidepressant properties and a better safety profile comparatively to the oral classic treatment. The therapeutic effects are strongly dependent on the route of administration and the pharmaceutical formulation of the drug. Indeed, the effects were just registered when the treatment was administered intranasally as a micellar formulation. Moreover, the safety profile of the IN CSA micelles was demonstrated to be better than that shown by the oral suspension.

DECLARATION OF COMPETING INTEREST

The authors report no declaration of interest.

ACKNOWLEDGEMENTS

The graphical abstract was created by BioRender.com.

This research did not receive any specific grant from funding agencies in the public, commercial, or not-for-profit sectors.

REFERENCES

1. Allison DJ, Ditor DS. The common inflammatory etiology of depression and cognitive impairment: a therapeutic target. *J Neuroinflammation*. 2014;11(1):151. doi:10.1186/s12974-014-0151-1
2. Nguyen MD, Julien J-P, Rivest S. Innate immunity: the missing link in neuroprotection and neurodegeneration? *Nat Rev Neurosci*. 2002;3(3):216-227. doi:10.1038/nrn752
3. Zhao J, Bi W, Xiao S, et al. Neuroinflammation induced by lipopolysaccharide causes cognitive impairment in mice. *Sci Rep*. 2019;9(1):1-12. doi:10.1038/s41598-019-42286-8
4. Gouveia F, Fonseca C, Silva A, et al. Intranasal irbesartan reverts cognitive decline and activates the PI3K/AKT pathway in an LPS-induced neuroinflammation mice model. *Int Immunopharmacol*. 2024;128(December 2023). doi:10.1016/j.intimp.2023.111471
5. Partoazar A, Nasoohi S, Rezayat SM, et al. Nanoliposome containing cyclosporine A reduced neuroinflammation responses and improved neurological activities in cerebral ischemia/reperfusion in rat. *Fundam Clin Pharmacol*. 2017;31(2):185-193. doi:10.1111/fcp.12244
6. Borlongan C V, Stahl CE, Keep MF, Elmér E, Watanabe S. Cyclosporine-A enhances choline acetyltransferase immunoreactivity in the septal region of adult rats. *Neurosci Lett*. 2000;279(2):73-76. doi:10.1016/S0304-3940(99)00962-3
7. Choi HB, Khoo C, Ryu JK, Van Breemen E, Kim SU, McLarnon JG. Inhibition of lipopolysaccharide-induced cyclooxygenase-2, tumor necrosis factor-α and [Ca2+]i responses in human microglia by the peripheral benzodiazepine receptor ligand PK11195. *J Neurochem*. 2002;83(3):546-555. doi:10.1046/j.1471-4159.2002.01122.x
8. Gabryel B, Łabuzek K, Małecki A, Herman ZS. Immunophilin ligands decrease release of pro-inflammatory cytokines IL-1beta, TNF-alpha and IL-2 in rat astrocyte cultures exposed to simulated ischemia in vitro. *Pol J Pharmacol*. 2004;56(1):129—136.
9. Hailer NP. Immunosuppression after traumatic or ischemic CNS damage: It is neuroprotective and illuminates the role of microglial cells. *Prog Neurobiol*. 2008;84(3):211-233. doi:10.1016/j.pneurobio.2007.12.001
10. Gu Z, Chen H, Zhao H, et al. New insight into brain disease therapy: nanomedicines-crossing blood–brain barrier and extracellular space for drug delivery. *Expert Opin Drug Deliv*. 2022;19(12):1618-1635. doi:10.1080/17425247.2022.2139369
11. Sakata A, Tamai I, Kawazu K, et al. In vivo evidence for ATP-dependent and P-glycoprotein-mediated transport of cyclosporin A at the blood-brain barrier. *Biochem Pharmacol*. 1994;48(10):1989-1992. doi:10.1016/0006-2952(94)90601-7

12. Pardridge WM. The blood-brain barrier: Bottleneck in brain drug development. *NeuroRx*. 2005;2(1):3-14. doi:10.1602/neurorx.2.1.3
13. Samaridou E, Alonso MJ. Nose-to-brain peptide delivery – The potential of nanotechnology. *Bioorganic Med Chem*. 2018;26(10):2888-2905. doi:10.1016/j.bmc.2017.11.001
14. Illum L. Transport of drugs from the nasal cavity to the central nervous system. *Eur J Pharm Sci*. 2000;11(1):1-18. doi:10.1016/S0928-0987(00)00087-7
15. Thorne RG, Emory CR, Ala TA, Frey WH. Quantitative analysis of the olfactory pathway for drug delivery to the brain. *Brain Res*. 1995;692(1):278-282. doi:10.1016/0006-8993(95)00637-6
16. Samaridou E, Alonso MJ. Nose-to-brain peptide delivery – The potential of nanotechnology. *Bioorganic Med Chem*. 2018;26(10):2888-2905. doi:10.1016/j.bmc.2017.11.001
17. Djupesland PG, Messina JC, Mahmoud RA. The nasal approach to delivering treatment for brain diseases: An anatomic, physiologic, and delivery technology overview. *Ther Deliv*. 2014;5(6):709-733. doi:10.4155/tde.14.41
18. Hongbing Wu KH, Jiang X. From nose to brain: understanding transport capacity and transport rate of drugs. *Expert Opin Drug Deliv*. 2008;5(10):1159-1168. doi:10.1517/17425247.5.10.1159
19. Mistry A, Stolnik S, Illum L. Nanoparticles for direct nose-to-brain delivery of drugs. *Int J Pharm*. 2009;379(1):146-157. doi:10.1016/j.ijpharm.2009.06.019
20. Hanson LR, Frey WH. Intranasal delivery bypasses the blood-brain barrier to target therapeutic agents to the central nervous system and treat neurodegenerative disease. *BMC Neurosci*. 2008;9(3):S5. doi:10.1186/1471-2202-9-S3-S5
21. Pardeshi CV, Belgamwar VS. Direct nose to brain drug delivery via integrated nerve pathways bypassing the blood–brain barrier: an excellent platform for brain targeting. *Expert Opin Drug Deliv*. 2013;10(7):957-972. doi:10.1517/17425247.2013.790887
22. Vyas, Tushar, Sandip B. Tiwari and MMA. Formulation and physiological factors influencing CNS delivery upon intranasal administration. *Crit Rev Ther Drug Carr Syst*. 2006;23.4. doi:10.1615/CritRevTherDrugCarrierSyst.v23.i4.20
23. Guareschi F, Del Favero E, Ricci C, et al. Cyclosporine A micellar nasal spray characterization and antiviral action against SARS-CoV-2. *Eur J Pharm Sci*. 2024;193:106673. doi:10.1016/j.ejps.2023.106673
24. Guo Y, Luo J, Tan S, Otieno BO, Zhang Z. The applications of Vitamin e TPGS in drug delivery. *Eur J Pharm Sci*. 2013;49(2):175-186. doi:10.1016/j.ejps.2013.02.006
25. Choi D-Y, Lee JW, Lin G, et al. Obovatol attenuates LPS-induced memory impairments in mice via inhibition of NF-κB signaling pathway. *Neurochem Int*. 2012;60(1):68-77.

doi:10.1016/j.neuint.2011.11.005

26. Shaw KN, Commins S, O'Mara SM. Lipopolysaccharide causes deficits in spatial learning in the watermaze but not in BDNF expression in the rat dentate gyrus. *Behav Brain Res*. 2001;124(1):47-54. doi:10.1016/S0166-4328(01)00232-7
27. Zakaria R, Wan Yaacob WMH, Othman Z, Long I, Ahmad AH, Al-Rahbi B. Lipopolysaccharide-induced memory impairment in rats: A model of Alzheimer's disease. *Physiol Res*. 2017;66(4):553-565. doi:10.33549/physiolres.933480
28. ICH-International Council for Harmonisation of Technical Requirements for Pharmaceuticals for Human Use, Bioanalytical Method Validation, 2019.
29. EMA-European Medicines Agency, Guideline on Bioanalytical Method Validation, 44, 2012, pp. 1–23.
30. FDA - Food and Drug Administration, Bioanalytical Method Validation Guidance for Industry, 2018 (accessed 13 July 2020) https://www.fda.gov/downloads/drugs/guidances/ucm070107.Pdf.
31. Serralheiro A, Alves G, Fortuna A, Falcão A. Direct nose-to-brain delivery of lamotrigine following intranasal administration to mice. *Int J Pharm*. 2015;490(1-2):39-46. doi:10.1016/j.ijpharm.2015.05.021
32. Zaghloul AA, Hussain A, Khan MA, Ahsan F. Development of a HPLC method for the determination of cyclosporin-A in rat blood and plasma using naproxen as an internal standard. *J Pharm Biomed Anal*. 2003;31(6):1101-1107. doi:10.1016/S0731-7085(03)00018-9
33. Almeida AM, Castel-Branco MM, Falcão AC. Linear regression for calibration lines revisited: Weighting schemes for bioanalytical methods. *J Chromatogr B Anal Technol Biomed Life Sci*. 2002;774(2):215-222. doi:10.1016/S1570-0232(02)00244-1
34. Yayama K, Hiyoshi H, Sugiyama K, Okamoto H. The lipopolysaccharide-induced up-regulation of bradykinin B 2-receptor in the mouse heart is mediated by tumor necrosis factor-α and angiotensin II. *Biol Pharm Bull*. 2006;29(6):1143-1147. doi:10.1248/bpb.29.1143
35. Zolfaghari SI, Rabbani Khorasgani M, Noorbakhshnia M. The effects of lactobacilli (L. rhamnosus, L. reuteri, L. Plantarum) on LPS-induced memory impairment and changes in CaMKII-α and TNF-α genes expression in the hippocampus of rat. *Physiol Behav*. 2021;229(October 2020). doi:10.1016/j.physbeh.2020.113224
36. Leger M, Quiedeville A, Bouet V, et al. Object recognition test in mice. *Nat Protoc*. 2013;8(12):2531-2537. doi:10.1038/nprot.2013.155
37. Can A, Dao DT, Terrillion CE, Piantadosi SC, Bhat S, Gould TD. The tail suspension test. *J Vis*

Exp. 2011;(58):3-7. doi:10.3791/3769

38. Cryan JF, Mombereau C, Vassout A. The tail suspension test as a model for assessing antidepressant activity: Review of pharmacological and genetic studies in mice. *Neurosci Biobehav Rev*. 2005;29(4-5):571-625. doi:10.1016/j.neubiorev.2005.03.009
39. Lehmkuhl AM, Dirr ER, Fleming SM. Olfactory assays for mouse models of neurodegenerative disease. *J Vis Exp*. 2014;(90):3-8. doi:10.3791/51804
40. Darcet F, Mendez-David I, Tritschler L, Gardier AM, Guilloux JP, David DJ. Learning and memory impairments in a neuroendocrine mouse model of anxiety/depression. *Front Behav Neurosci*. 2014;8(MAY):1-13. doi:10.3389/fnbeh.2014.00136
41. Seibenhener, M. L., Wooten MC. Use of the Open Field Maze to Measure Locomotor and Anxiety-like Behavior in Mice. J. Vis. Exp. (96), e52434, (2015). doi:10.3791/52434.
42. Rafael JA, Nitta Y, Peters J, Davies KE. Testing of SHIRPA, a mouse phenotypic assessment protocol, on Dmdmdxand Dmdmdx3cvdystrophin-deficient mice. *Mamm Genome*. 2000;11(9):725-728. doi:10.1007/s003350010149
43. Aartsma-Rus A, van Putten M. Assessing functional performance in the Mdx mouse model. *J Vis Exp*. 2014;(85):1-11. doi:10.3791/51303
44. Sulakhiya K, Keshavlal GP, Bezbaruah BB, et al. Lipopolysaccharide induced anxiety- and depressive-like behaviour in mice are prevented by chronic pre-treatment of esculetin. *Neurosci Lett*. 2016;611:106-111. doi:10.1016/j.neulet.2015.11.031
45. Yin R, Zhang K, Li Y, et al. Lipopolysaccharide-induced depression-like model in mice: meta-analysis and systematic evaluation. *Front Immunol*. 2023;14(June):1-15. doi:10.3389/fimmu.2023.1181973
46. O'Connor JC, Lawson MA, André C, et al. Lipopolysaccharide-induced depressive-like behavior is mediated by indoleamine 2,3-dioxygenase activation in mice. *Mol Psychiatry*. 2009;14(5):511-522. doi:10.1038/sj.mp.4002148
47. Yu X, Yao H, Zhang X, Liu L, Liu S, Dong Y. Comparison of LPS and MS-induced depressive mouse model: behavior, inflammation and biochemical changes. *BMC Psychiatry*. 2022;22(1):590. doi:10.1186/s12888-022-04233-2
48. Lacosta S, Merali Z, Anisman H. Behavioral and neurochemical consequences of lipopolysaccharide in mice: Anxiogenic-like effects. *Brain Res*. 1999;818(2):291-303. doi:10.1016/S0006-8993(98)01288-8
49. A.J. Dunn, Y. Chapman MA. Endotoxin-induced behavioral changes of mice in the multicompartment chamber are distinct from those of interleukin-1, Neurosci. Res *Commun*. 1992;10(63-69).
50. Yirmiya R. Endotoxin produces a depressive-like episode in rats. *Brain Res*.

1996;711(1):163-174. doi:10.1016/0006-8993(95)01415-2

51. Fujisaki C, Utsuyama M, Kuroda Y, et al. An immnosuppressive drug, cyclosporine-A acts like anti-depressant for rats under unpredictable chronic stress. *J Med Dent Sci*. 2003;50(1):93-100. doi:10.11480/jmds.500113
52. Alzahrani NA, Bahaidrah KA, Mansouri RA, Alsufiani HM, Alghamdi BS. Investigation of the optimal dose for experimental lipopolysaccharide-induced recognition memory impairment: behavioral and histological studies. *J Integr Neurosci*. 2022;21(2). doi:10.31083/j.jin2102049
53. Wu, SH-W. and WKH. Characteristics of d-α-tocopheryl PEG 1000 succinate for applications as an absorption enhancer in drug delivery systems. Pharmaceutical technology. *Pharm Technol*. 1999;23(10):52-68.
54. Cuschieri A. Enzyme histochemistry of the olfactory mucosa and vomeronasal organ in the mouse. *J Anat*. 1974;118(Pt 3):477-489.
55. Thiebaud N, Veloso Da Silva S, Jakob I, et al. Odorant Metabolism Catalyzed by Olfactory Mucosal Enzymes Influences Peripheral Olfactory Responses in Rats. *PLoS One*. 2013;8(3):1-13. doi:10.1371/journal.pone.0059547
56. Hu J, Sheng L, Li L, et al. Essential Role of the Cytochrome P450 Enzyme CYP2A5 in Olfactory Mucosal Toxicity of Naphthalene. *Drug Metab Dispos*. 2014;42(1):23-27. doi:10.1124/dmd.113.054429
57. Ding X, Xie F. Olfactory Mucosa: Composition, Enzymatic Localization, and Metabolism. In: *Handbook of Olfaction and Gustation*. John Wiley & Sons, Ltd; 2015:63-92. doi:10.1002/9781118971758.ch3
58. Bogman K, Zysset Y, Degen L, et al. P-Glycoprotein and Surfactants: Effect on Intestinal Talinolol Absorption. *Clin Pharmacol \& Ther*. 2005;77(1):24-32. doi:10.1016/j.clpt.2004.09.001
59. Boudreaux, J. P., Hayes, D. H., Mizrahi, S., Maggiore, P., Blazek, J., & Dick D. Use of water-soluble liquid vitamin E to enhance cyclosporine absorption in children after liver transplant. *Transplant Proc*. 1993;25(2):1875.
60. Prasad YVR, Puthli SP, Eaimtrakarn S, et al. Enhanced intestinal absorption of vancomycin with Labrasol and d-α-tocopheryl PEG 1000 succinate in rats. *Int J Pharm*. 2003;250(1):181-190. doi:10.1016/S0378-5173(02)00544-6
61. Sokol RJ, Narkewicz MR, Smith D, Karrer FM, Kam I, Johnson KE. Improvement of cyclosporin absorption in children after liver transplantation by means of water-soluble vitamin E. *Lancet*. 1991;338(8761):212-215. doi:10.1016/0140-6736(91)90349-T
62. Bogman K, Erne-Brand F, Alsenz J, Drewe J. The Role of Surfactants in the Reversal of

Active Transport Mediated by Multidrug Resistance Proteins. *J Pharm Sci*. 2003;92(6):1250-1261. doi:10.1002/jps.10395

63. Hugger ED, Novak BL, Burton PS, Audus KL, Borchardt RT. A comparison of commonly used polyethoxylated pharmaceutical excipients on their ability to inhibit P-glycoprotein activity in vitro. *J Pharm Sci*. 2002;91(9):1991-2002. doi:10.1002/jps.10176
64. Johnson BM, Charman WN, Porter CJH. An in vitro examination of the impact of polyethylene glycol 400, pluronic P85, and vitamin E d-a-tocopheryl polyethylene glycol 1000 succinate on P-glycoprotein eflux and enterocyte-based metabolism in excised rat intestine. *AAPS PharmSci*. 2002;4(4):40. doi:10.1208/ps040440
65. Grimaudo MA, Pescina S, Padula C, et al. Poloxamer 407/TPGS Mixed Micelles as Promising Carriers for Cyclosporine Ocular Delivery. *Mol Pharm*. 2018;15(2):571-584. doi:10.1021/acs.molpharmaceut.7b00939
66. Ghezzi M, Ferraboschi I, Delledonne A, et al. Cyclosporine-loaded micelles for ocular delivery : Investigating the penetration mechanisms. 2022;349(July):744-755. doi: 10.1016/j.jconrel.2022.07.019
67. Niki E, Noguchi N. Dynamics of Antioxidant Action of Vitamin E. *Acc Chem Res*. 2004;37(1):45-51. doi:10.1021/ar030069m
68. Simpson DSA, Oliver PL. Ros generation in microglia: Understanding oxidative stress and inflammation in neurodegenerative disease. *Antioxidants*. 2020;9(8):1-27. doi:10.3390/antiox9080743

SUPPLEMENTARY MATERIAL

This Supplementary section provides additional information about the mucopenetration profile characterizing the CSA-loading TPGS micelles exploited in this work and tested *in vivo* to assess neuroprotection after being intranasally administered. However, before proceeding with the definitive *in vivo* study following an optimized protocol, previous studies have been done to optimize all the parameters. More precisely, optimal dose to be administered was defined in order to achieve penetration across the nasal mucosa, thus reaching the brain; accordingly, the concentration of CSA into the micellar formulation was then adjusted. Importantly, the drug dose and concentration were of paramount importance, since they would have affected the ability to detect the drug by HPLC into the samples withdrawn from the animal at the end of treatment. On the other hand, the dose would not have had an impact on the interaction with the nasal tissue. For this reason, the preliminary mucopenetration assessment was done exploiting the 5 mg/mL CSA-loading micellar formulation, considering that the mucoadhesive/mucopenetrating properties are not influenced by the cargo, that is encapsulated into the micelle, but depends only on the surface properties of the drug delivery system.

1. METHODS

1.1 *Ex vivo* evaluation of mucopenetration profile of CSA-loading TPGS micelles across rabbit's olfactory nasal mucosa

The permeation profile of CSA across the olfactory nasal mucosa was evaluated exploiting Franz-type vertical diffusion cells consisting in a 4.5 mL acceptor compartment and a diffusional area of 60 mm^2.

The penetration of the drug across the tissue was assessed by comparing the micellar formulation encapsulating 5 mg/mL of CSA and a CSA water suspension having a concentration of 5 mg/mL.

The olfactory region of the rabbit's nasal mucosa was exploited for the experiment, and the underlying collagen septum was removed from the tissue [1]. The *ex vivo* mucopenetration profile was evaluated following a protocol already described [2] and slightly modified. Indeed, the mucosal layer was put between the donor and the acceptor chamber of the vertical diffusion cell, and the acceptor was filled with the medium consisting of Simulated Nasal Electrolyte Solution (SNES) pH 6.5 with 0.2% SDS. Then, 35 µL of either the CSA micellar formulation or the suspension were put in the donor compartment.

Franz cells were kept at 37°C under stirring during the whole experiment. At predetermined timepoints (5, 15, 30, 60, 90, 120, 180, 240, 300 and 360 minutes) 500 µL of medium were withdrawn from the acceptor compartment and immediately replaced with fresh medium kept at

37°C using a water bath. The withdrawn sample was mixed with 200 µL of acetonitrile and then centrifugated at 9500 rpm at 25°C for 10 minutes using a NEYA-16R centrifuge (Remi elektrotechnik, Vasai, India). The supernatant was collected and analyzed by HPLC.

At the end of the experiment, the olfactory mucosa was immersed in 1 mL of acetonitrile overnight and sonicated for 5 minutes in an ultrasound bath (USC 300-T, VWR International, Radnor, PA, USA). Then, the sample was kept under constant agitation at 300 rpm for 1 hour using an orbital shaker (Shuttler MTS 4, IKA Werke GmbH & Co. KG, Germany) and finally centrifugated at 9500 rpm at 25°C for 10 minutes; the supernatant was collected and analyzed by HPLC.

To analyze the samples, two different calibration curves were exploited in the ranges of 0.15 – 10 µg/mL and 1 – 50 µg/mL.

1.2 Management of the administration of therapy and LPS in mice

Table 1 below shows the timeline followed to manage the administration of the oral or intranasal therapies and LPS to induce neuroinflammation, as well as all the behavioral tests performed on mice.

***T*able 1** – *Experimental procedures for chronic administration of CSA micellar formulation or suspension intranasally and/or orally.*

	Day 1	Day 2	Day 3	Day 4
	Weigh mice			Buried Food Test
8:00 a.m	Administration (oral or IN)	Administration (oral or IN)	Administration (oral or IN)	Hanging Wire Test
	Open Field	Open Field	Novel Object Recognition training	Novel Object Recognition Test
	Food restriction	Food restriction	Food restriction	Tail Suspension Test
8:00 p.m	Administration (oral or IN)	Administration (oral or IN)	Administration (oral or IN)	
			LPS i.p. administration	Weigh mice and food

2. RESULTS

2.1 *Ex vivo* evaluation of mucopenetration profile of CSA-loading TPGS micelles across rabbit's olfactory nasal mucosa

The *ex vivo* permeation profiles of CSA across the rabbit's olfactory mucosa exploiting the micellar formulation or the water suspension are shown in **Figure 1**. As can be seen, the micellar formulation significantly improved the permeation of the drug across the tissue if compared to the drug water suspension. Indeed, when the micellar formulation was exploited as a vehicle for the drug, almost the entire amount of CSA put on the mucosa turned out to be able to penetrate across the tissue already after 15 minutes, then reaching a plateau. On the other hand, only 6% of the drug was able to penetrate the tissue in the first 15 minutes when the suspension was used, and the amount of drug penetrated across the tissue over 6 hours never exceeded 31%. The differences between the amount of drug permeated applying the micelles or the suspension on the olfactory mucosa turned out to be significant at all the timepoints, except for the first one (5 minutes).

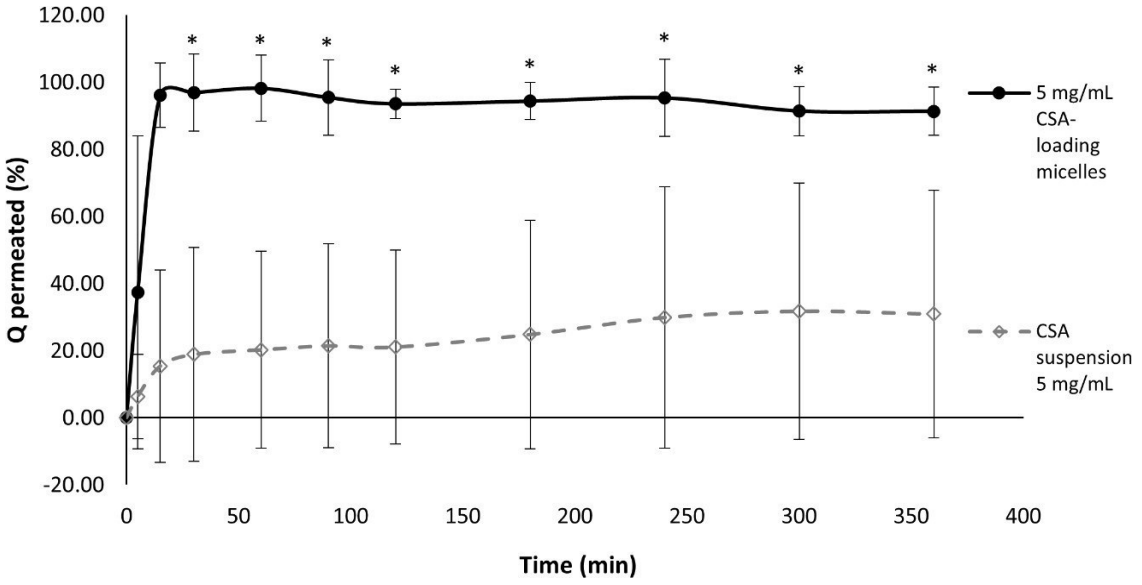

Figure 1 *- Ex vivo Cyclosporine A permeation across rabbit's olfactory mucosa up to 6 hours at 37°C using simulated nasal electrolyte solution (SNES) pH 6.5 with 0.2% Sodium Dodecyl Sulfate (SDS) as medium. Comparison between the permeation profile of the drug formulated as 5mg/mL CSA-loading TPGS micelles (black line) and the corresponding water suspension (dashed gray line). (n=4), *p<0.05*

3. DISCUSSION

The *ex vivo* permeation study performed exploiting the olfactory region of rabbit's nasal mucosa pointed out that the drug was able to penetrate relatively quickly (about 15 minutes) across the nasal mucosa layer when the TPGS micellar formulation was used as vehicle. This was probably due to the already known ability of the PEG-ylated structure of TPGS to reduce the adhesion with the surface protein of the tissue [3–6], thus favoring the permeation across it.

This result agrees with what was previously observed in the *ex vivo* mucoadhesion study performed by our group [7] in which the micellar formulation turned out to be significatively less mucoadhesive than the suspension used as reference. Thus, together the mucoadhesion and the mucopenetration experiments contribute to demonstrate that CSA formulated as TPGS micelles has a low tendency to be retained on the surface of the mucosa, but it rapidly crosses the surface reaching the depth of the tissue; on the other hand, the non-formulated drug exhibits considerable mucoadhesive properties that hinder the passage of the peptide across the olfactory epithelium.

4. CONCLUSIONS

TPGS micellar formulation represents an effective drug delivery system to enhance the intranasal absorption of CSA across the olfactory nasal mucosa, thus potentially improving Nose-to-Brain delivery.

The mucopenetrating properties shown by micelles can be exploited to preserve the drug from the mucociliary clearance and any possible physical and chemical degradation to which it can be exposed on the epithelial surface. Indeed, already 15 minutes after the application, the drug is carried across the tissue and so removed from the surface, where both the mucociliary clearance and the enzymatic degradation take place. On the other hand, the non-formulated CSA didn't show mucopenetrating properties; indeed, it turned out to be highly mucoadhesive and, as such, not able to penetrate across the tissue.

REFERENCES

1. Bortolotti F., Balducci A.G., Sonvico F., Russo P., Colombo G. In vitro permeation of desmopressin across rabbit nasal mucosa from liquid nasal sprays: The enhancing effect of potassium sorbate. *Eur J Pharm Sci*. 2009;37(1):36-42. doi:10.1016/j.ejps.2008.12.015
2. Bruinsmann FA, Pigana S, Aguirre T, et al. Chitosan-coated nanoparticles: Effect of chitosan molecular weight on nasal transmucosal delivery. *Pharmaceutics*. 2019;11(2). doi:10.3390/pharmaceutics11020086
3. Lai SK, O'Hanlon DE, Harrold S, et al. Rapid transport of large polymeric nanoparticles in fresh undiluted human mucus. *Proc Natl Acad Sci*. 2007;104(5):1482-1487. doi:10.1073/pnas.0608611104
4. Suk JS, Xu Q, Kim N, Hanes J, Ensign LM. PEGylation as a strategy for improving nanoparticle-based drug and gene delivery. *Adv Drug Deliv Rev*. 2016;99:28-51. doi:10.1016/j.addr.2015.09.012
5. Tang BC, Dawson M, Lai SK, et al. Biodegradable polymer nanoparticles that rapidly penetrate the human mucus barrier. *Proc Natl Acad Sci U S A*. 2009;106(46):19268-19273. doi:10.1073/pnas.0905998106
6. Wang Y-Y, Lai SK, Suk JS, Pace A, Cone R, Hanes J. Addressing the PEG Mucoadhesivity Paradox to Engineer Nanoparticles that "Slip" through the Human Mucus Barrier. *Angew Chemie*. 2008;120(50):9872-9875. doi:10.1002/ange.200803526
7. Guareschi F, Del Favero E, Ricci C, et al. Cyclosporine A micellar nasal spray characterization and antiviral action against SARS-CoV-2. *Eur J Pharm Sci*. 2024;193:106673. doi:10.1016/j.ejps.2023.106673

CHAPTER 3

APPLICATION OF RABBIT NASAL MUCOSA FOR EX VIVO MUCOPENETRATION AND MUCOADHESION STUDIES

This Chapter was partially taken from the following submitted Paper: Sanchez-Castillo LV., **Guareschi F**., Tsekoura E., Patterlini V., Delledonne A., Ferraboschi I., Sissa C., Sonvico F., Narain R. *"Formulation of siRNA Nanoparticles, Transfection and Enhanced Adhesion -Penetration in Nasal Mucosal Tissue"*
submitted in October 2024, *Journal of Controlled Release*

1. INTRODUCTION

The nasal mucosa represents a suitable target for therapies intended to both act locally or systemically [1]. The absorption of the drug can take place in different ways, depending on the deposition site into the nasal cavity. Indeed, the drug can be systemically absorbed exploiting the vessels mainly characterizing the respiratory region [2]; alternatively, the drug can be absorbed at the brain level exploiting the nerves present in the olfactory region [3]. A third option consists in the local action of the drug that in this case exhibits the therapeutic activity just on the surface of the nasal mucosa, while the absorption is, at least partially, avoided [2].

The fate of an administered drug after the deposition into the nasal cavity strongly depends on the interaction between the therapeutic agent and the specific region of the nasal mucosa. Indeed, it is known that the nasal epithelium can be divided into two areas, namely the respiratory and the olfactory region, that differ from an anatomical as well as a physiological point of view [1]. For instance, the respiratory epithelium is mainly involved in the mucociliary clearance process [4] owing to the wide expression of ciliated cells and mucus-secerning Goblet cells [5]. For this reason, a drug delivered at this level with high probability will undergo an early removal by the mucociliary system without being completely absorbed. However, the use of a suitable drug delivery system characterized by specific physico-chemical features can prevent the retention of the drug on the mucus layer, thus favoring the penetration across it, leading to the direct contact between the drug and the epithelial absorption site [6].

Another possible strategy to avoid mucociliary clearance may consist in the delivery of the drug precisely in the upper posterior part of the nasal epithelium, that is the olfactory region. In this region indeed, the cilia expressed on the surface of the cells are not motile and hence not involved in the mucociliary clearance activity [7]. Moreover, the dendritic portion of the olfactory neurons can intake the drug promoting its absorption into the olfactory bulb, where the olfactory axons terminate [8].

It is evident that the significant anatomical and functional differences between the respiratory and the olfactory region of the nasal mucosa can have a relevant impact on the fate of the administered therapies. For this reason, a thorough knowledge of the structure of the nasal mucosa is pivotal to understand the central role that both the features of the drug's carrier and the use of suitable device allowing to reach specific deposition site may have on the therapy's outcome.

Several studies [9–11] have already exploited imaging techniques to highlight the anatomical characteristics of the nasal mucosa. However, to the best of our knowledge, none of them exploited the two-photon microscope to study the tissue's structures. The two-photon excitation is characterized by some well-known advantages compared to the single-photon excitation, including significantly less phototoxicity and photobleaching compared to the single-photon excitation [12]. Moreover, at the longer infra-red wavelengths typically used for the two-photon microscopy, the absorbance of light by heme-containing proteins is minimal and allows a much lower light scattering [13]. The consequences of this aspect are that biological samples appear more optically transparent to infra-red light and the penetration of the microscope observation into the tissue can be much deeper than in the case of confocal laser scanning microscope [14].

In this work, the *ex vivo* rabbit nasal mucosa was fully characterized exploiting the two-photon microscope to visualize the main anatomical features of both the olfactory and the respiratory region; then, the tissue was used as model to assess the mucoadhesion and the mucopenetration profiles of a fluorescent-labeled drug delivery system. This latter consisted of trimethyl chitosan (TMC) nanoparticles (NP) loaded with cyanine3 (Cy3)-labeled siRNA, developed by the research group of Prof. Ravin Narain from University of Alberta (Edmonton, Canada).

The tissue imaging was performed by selectively marking specific structures belonging to the olfactory or the respiratory region using primary antibodies to bind specific antigens, and secondary antibodies labeled with fluorescent dyes to identify the primary ones.

More precisely, the characterization of the olfactory area was done by marking the Olfactory Marker Protein (OMP) and the Odorant Receptor, family 10, subfamily R, member 2 (OR10R2). Briefly, OMP is a protein selectively expressed by the olfactory receptor neurons and it is mainly involved in the transduction of the odorant signals [15]. Instead, OR10R2 is an odorant receptor involved in the processing of the olfactory sensory input [16]. On the other hand, the characterization of the respiratory region was performed by marking β IV-tubulin, a characteristic protein of cilia, such as those expressed on the surface of the respiratory epithelial cells [17].

Finally, the surface interaction between the nasal mucosa and the nanoparticle drug delivery system was assessed by analyzing the mucoadhesion and the mucopenetration profile. The mucoadhesion profile was assessed by treating the mucosal tissue with the fluorescent-labeled nanoparticle formulation under simulated physiological conditions; then, samples were quantitatively and qualitatively analyzed by, respectively, the microplate reader and the two-photon microscope. In addition to this, the penetration of the labeled siRNA loaded into the nanoparticle drug delivery system was monitored over time exploiting the two-photon microscope, thank to which the treated tissue could be analyzed in its depth to highlight the passage of the drug from the surface to the bottom of the tissue over time.

2. MATERIALS AND METHODS

2.1 Materials

Immunostaining of rabbit's nasal mucosa

Paraformaldehyde (PFA) powder was purchased from Fluorochem (Hadfield, UK); phosphate-buffered saline (PBS) 1× was from Gibco (Carlsbad, CA, USA); bovine serum albumin (BSA) was from Baxalta (Rome, Italy); polyethylene glycol tert-octylphenyl ether (Triton X-100) was purchased from Sigma Aldrich (Saint Louis, USA); sodium hydroxide (NaOH) was from Merck Life Science S.r.l. (Milan, Italy); hydrochloric acid (HCl) 37% was from VWR International S.r.l. (Milan, Italy); mouse anti-β IV tubulin monoclonal IgG (catalog #ab11315) was purchased from Abcam, Prodotti Gianni S.r.l. (Milan, Italy); rabbit anti-Olfactory Receptor, family 10, subfamily R, member 2 (OR10R2) polyclonal IgG (PA534046) was from ThermoFisher Scientific (Waltham, MA, USA); rabbit anti-Olfactory Marker Protein (OMP) monoclonal IgG (ab183948) was from Abcam, Prodotti Gianni S.r.l. (Milan, Italy); 4',6-diamidino-2-phenylindole (DAPI), Alexa Fluor™ Plus 647 donkey anti-rabbit polyclonal IgG (A32795) and Alexa Fluor™ 488 donkey anti-mouse polyclonal IgG (A21202) secondary antibodies were from ThermoFisher Scientific (Monza, Italy).

Preparation of TMC nanoparticles

Trimethyl chitosan (TMC) with a degree of quaternization of approximately 54-60% and a MW of 50-150 kDa, was kindly provided by Ovensa (Aurora, ON, Canada). Tripolyphosphate (TPP) and dextran sulfate (DS) having a MW of 500 kDa were from Sigma-Aldrich (St Louis, MO, USA); hyaluronic acid sodium salt (HA) with a MW 40-50 kDa was from Biosynth International Inc. (Gardner, MA, USA). Silencer® Cy™3 Labeled Negative control siRNA was purchased from Invitrogen (Thermo Fisher Scientific, Waltham, MA, USA).

2.2 Methods

2.2.1 Immunostaining of olfactory and respiratory rabbit's nasal mucosa

Preparation of Paraformaldehyde 4% w/v solution

The fixing solution was prepared following a published protocol [18]. Briefly, to prepare 500 mL of the PFA 4% w/v solution, 20 g of PFA powder were added to 400 mL of PBS 1× kept at 60°C under stirring under the extractor hood. NaOH 1N was then added drop by drop until the solution became completely clear. The solution was allowed to equilibrate at room temperature and the volume was adjusted to 500 mL using PBS 1×. Then, the pH was adjusted to 6.9 using HCl water solution 37% v/v. The PFA solution was finally aliquoted and frozen at -20°C until the use.

Preparation of antibody and DAPI working solutions

The anti-β IV tubulin antibody and the anti-OR10R2 antibody working solution (1 µg/mL) were prepared by diluting the respective stock solutions (1 mg/mL) 1000 times using a solution of bovine serum albumin (BSA) 5% v/v in Triton X100 0.1 % v/v, previously prepared dissolving Triton X100 in PBS 1×. The anti-OMP antibody working solution (1 µg/mL) was prepared by diluting the stock solution (0.5 mg/mL) 500 times in BSA 5% v/v.

Alexa Fluor 647 and Alexa Fluor 488 labeled antibodies working solutions were prepared by diluting the respective stock solutions (2mg/mL) 1000 times in BSA 5% v/v. All the antibodies working solutions were stored at 4°C and kept away from light until use.

The DAPI working solution (0.5 µg/mL) was prepared by diluting the DAPI stock solution (0.5 mg/mL) 1000 times in ultrapure water. The DAPI working solution was stored at 4°C and kept away from light until use.

Preparation of the tissue for immunostaining experiments

Immunostaining experiments were carried out to highlight the anatomical features characterizing the olfactory and respiratory regions of the nasal mucosa. For this purpose, the rabbit nasal mucosa was taken from the skull of the rabbit kindly provided by a local slaughterhouse (Bertoni Carni S.r.l., Busana, Reggio-Emilia, Italy), as described by Guareschi *et al.* [19]. Briefly, the fresh skull was cut in 2 halves longitudinally, exposing the nasal cavity. The entire respiratory or olfactory sections of the nasal mucosa with the underlying collagen from nasal septum were withdrawn using a scalpel and carefully washed using 50 mL of PBS 1× to eliminate the excess of blood. To do that, the respiratory and the olfactory regions of the nasal mucosa were identified and separated based on the anatomical references given by Pereira *et. al.* [9]. Briefly, after dividing the skull longitudinally, the nasal mucosa was divided in two halves by cutting the tissue immediately anteriorly to the first upper premolar teeth. The portion of the mucosa closer to the nostril was considered the respiratory region, while the other portion of the tissue was identified as the olfactory one.

The tissues were then fixed by immersion in 50 mL of PFA 4% w/v solution and the samples were stored at 4°C overnight and finally washed three times with fresh PBS 1×.

Then, 8 mm-diameter tissue discs belonging to either the olfactory or respiratory region of the nasal mucosa together with the underlying portion of nasal septum were obtained using a circular metal die. Successively, to block the non-specific binding sites, the tissue was immersed into 1 mL of blocking solution, consisting in a BSA 5% v/v solution in Triton X100 0.1% v/v in PBS 1×. The tissue was kept into the blocking solution at room temperature for 3 hours.

The excess of blocking solution was removed, and the tissue was immersed into 1 mL of the primary

antibody (*i.e.*, anti-OMP, anti-OR10R2 or anti-β IV Tubulin) working solution and incubated for 4 hours at room temperature and kept away from light.

The excess of primary antibody solution was removed, and the tissue was washed three times using approximately 15 mL of PBS 1×. After removing the excess of PBS, the tissue was incubated in 1 mL of the secondary antibody (*i.e.*, Alexa Fluor 488 or Alexa Fluor 647 labelled Abs) for 30 minutes at room temperature, away from any source of light.

After being washed three times with approximately 15 mL of PBS 1×, the tissue was incubated in 1 mL of DAPI working solution for 30 minutes at room temperature and away from light.

The excess of DAPI was washed one time with ultrapure water and the tissue stored in PBS 1× at room temperature and away from light until the analysis with the two-photons microscope.

To highlight the anatomical features between the respiratory and the olfactory region of the mucosa and compare them to show the main structural differences, each part of the nasal mucosa was treated with different primary and secondary antibodies, as illustrated in **Table 1**.

Table 1 *– Primary and secondary antibodies used in the immunostaining experiment carried out to mark the olfactory and the respiratory region of the rabbit's nasal mucosa. Anti-OMP and anti-OR10R2 antibodies were used to characterize the olfactory region, while anti-β IV Tubulin antibody was used to characterize the respiratory one. Moreover, both the regions were treated with either anti-OMP antibody or anti- β IV Tubulin to highlight the main anatomical differences between them.*

Region of the tissue	***Primary Ab***	***Secondary Ab***	***DAPI***
Olfactory	Anti-OMP	Anti-rabbit Alexa Fluor 647	Yes
Olfactory	Anti-OR10R2	Anti-rabbit Alexa Fluor 647	Yes
Respiratory	Anti-β IV Tubulin	Anti-mouse Alexa Fluor 488	Yes
Olfactory	Anti-OMP	Anti-rabbit Alexa Fluor 647	No
Respiratory	Anti-OMP	Anti-rabbit Alexa Fluor 647	No
Olfactory	Anti-β IV Tubulin	Anti-mouse Alexa Fluor 488	No
Respiratory	Anti-β IV Tubulin	Anti-mouse Alexa Fluor 488	No

2.2.2 Two-photon microscopy

The rabbit's nasal tissue was analyzed by a Two-Photon Microscope Nikon A1R MP+ Upright (Nikon, Tokio, Japan) equipped with a femtosecond pulsed laser Coherent Chameleon Discovery (~ 100 fs pulse duration with 80 MHz repetition rate, tunable excitation range 660–1320 nm). To focus the excitation beam and collect the two-photon excited fluorescence (TPEF) and the second harmonic generation (SHG) signals, a 25× water dipping objective characterized by a numerical aperture (NA) of 1.1 and 2-mm working distance was employed.

A dichroic mirror was used to direct TPEF/SHG signal to a series of three non-descanned detectors (high sensitivity GaAsP photomultiplier tubes) allowing fast image acquisition.

Optical filters have been put before the three detectors to allow the simultaneous acquisition of three separated channels: blue channel (415–485 nm), green channel (506–593 nm) and red channel (604–679 nm). A fourth additional photomultiplier GaAsP detector was connected to the microscope by an optical fiber and preceded by a dispersive element. GaAsP detector was used to record the spectral profile of the TPEF/SHG signal (wavelength range 430-650 nm, bandwidth of 10 nm). The overlay of the images from the three channels and their processing was performed by the operation software of the microscope (NIS-elements).

Microscope observations were performed by placing the samples in a dedicated plexiglass holder and PBS 1× was used to dip the objective and to avoid dehydration. A laser intensity of 3% was used for both the acquisition of the spectra and the 3D-scans. Moreover, spectra were also acquired at 5% laser intensity. Depending on the secondary antibody used to treat the tissue, different excitation wavelengths were used. More precisely, the tissues incubated with AlexaFluor 647 were excited at 820 nm, while those treated with AlexaFluor 488 were excited at 1000 nm.

2.2.3 TMC nanoparticles preparation

TMC nanoparticles loading Cy3-labeled siRNA (Cy3-siRNA) were prepared by Dr. Ravin Narain's research group from University of Alberta (Edmonton, Canada), and were exploited as model of drug delivery system to assess the mucoadhesion and mucopenetration profile across the nasal tissue and compare the results with those obtained by testing the raw Cy3-siRNA. Briefly, a TMC stock solution (3 mg/mL) was prepared by dissolving TMC powder in a mixture consisting of 80% v/v acetate buffer (0.01 M, containing 137 mM NaCl) at pH=5.6 and 20% v/v of bicarbonate buffer (0.1 M, containing 137 mM NaCl) at pH=9.3, to achieve a final pH of 9. This pH value is required to prevent the precipitation of the genetic material. DS (3 mg/mL) and TPP (1.5 mg/mL) stock solutions were prepared in PBS 1× while HA solution (1mg/mL) was prepared in UltraPure® water. The nanoparticle assembly process required the preliminary preparation of two solutions: the first

consisted of a siRNA:TMC solution having a 1:20 w/w ratio, prepared by slowly adding Cy3-siRNA solution (300 ng/ µL) to TMC solution (3 mg/mL) to allow the formation of complexes over 10 minutes at room temperature. The second solution consisted of an aqueous mixture of the helpers, formulated in a w/w ratio TMC:DS of 6:1. Briefly, helper (DS/TPP/HA) solutions were carefully mixed at room temperature to have a final DS/TPP/HA w/w ratio of 2:1:0.04, respectively. Finally, the Cy3-siRNA:TMC and helper (DS/TPP/HA) solutions were mixed using NanoAssemblr® Ignite™ (NanoAssemblr, Canada) at a flow rate of 20 mL/min, with a v/v ratio between the two solutions (Cy3-siRNA:TMC and DS/TPP/HA) of 6:1, respectively. Additionally, the Cy3-siRNA and the resulting nanoparticles were kept protected from light, as Cy3-siRNA is photosensitive.

2.2.4 Mucoadhesion study on rabbit nasal mucosa

The mucoadhesive profile of the siRNA:TMC NPs (having a 1:20 siRNA:TMC w/w ratio) was evaluated *ex vivo* on rabbit nasal mucosa and compared to the one of the raw Cy3-siRNA. Fresh nasal mucosal tissue was isolated from rabbit heads, which were stored in ice and used within four hours from animal death. To obtain the nasal mucosal tissue, the rabbit's skull was cut in two halves and the nasal septum supporting the entire nasal mucosa was isolated using a scalpel. Then, nasal mucosa discs of the desired size (8 mm diameter) were punched from the central region of the septum.

The tissue was attached on a Petri dish using a double-sided tape (Tesafix® 4934, KaiserKraft, Stuttgart, Germany) and treated with 20 µL of the siRNA:TMC NP formulation or the free Cy3-siRNA solution for 5 minutes, keeping the tissue in an horizontal position. Then, the tissue was placed on a 45° inclined plane apparatus, as proposed by Sandri *et al.* [20] allowing the continuous washing of the mucosa with ultrapure water to simulate physiological nasal conditions. To do this, a syringe pump (Harvard Apparatus, Holliston, MA, USA) equipped with a plastic syringe having an internal diameter of 19 mm and a 0.8 × 40 mm needle, was used to flow the ultrapure water on the tissue at a constant flow of 100 µL/min. The syringe pump was previously conditioned with ultrapure water for at least 15 minutes before starting the experiments. The water flowed on the tissue for over 30 minutes, and eluted samples were collected at 5 minutes intervals. At the end of the experiment, the remaining siRNA:TMC NPs or free Cy3-siRNA adhered to the mucosa was extracted using a borosilicate glass Potter-Elvehjem homogenizer (Fisherbrand™, Fisher Scientific, Pittsburgh, PA, USA) having a 1.5 cm diameter and a pestle length of 25 cm. Tissue grinding was performed adding 0.5 mL of ultrapure water. All the experiments were performed in triplicate, and the percentage of mucoadhesion was calculated by comparing the amount of Cy3 left adhered to the tissue with the amount initially put on it before starting the experiment. All the samples were quantified using a microplate reader Spark 10M (TECAN, Mannendorf, Switzerland). The excitation wavelength was set

at 547 nm, while the emission wavelength was set at 590 nm. The plate model was a 96 well flat bottom cell plate without lid (Costar®, Corning, NY, USA). The gain was set automatically at each measurement. To quantify Cy3-siRNA in the samples, a calibration curve was built in the range of 0.05 – 1.6 μg/mL, using the Cy3-siRNA solution as reference.

In addition to this, at the end of the mucoadhesion experiment, the tissue treated with either the siRNA:TMC NP formulation or the free Cy3-siRNA was observed by two-photon microscopy to monitor the fluorescence signal of the Cy3 signal in the nasal mucosal tissue, at different penetration depths, applying the same experimental set-up used for the mucopenetration studies, described in **Section 2.2.5**.

2.2.5 Nasal mucosal tissue penetration studies

The mucopenetration profile of siRNA:TMC NPs (having a 1:20 siRNA:TMC w:w ratio) and the free Cy3-siRNA used as control was evaluated treating an 8 mm diameter disc of rabbit nasal mucosa with 20 μL of each formulation. The tissue was observed over time by two-photon microscopy (**Section 2.2.2**) to qualitatively and semi-quantitatively determine the distribution of both the nanoparticles and the non-formulated Cy3-siRNA within the tissue. The same region of the sample was studied over time, monitoring the penetration of the formulation.

3. RESULTS

3.1 Immunostaining of the olfactory region

3.1.1 Olfactory region marked with anti-Olfactory Marker Protein

The presence of olfactory neurons in the olfactory section of the rabbit nasal mucosa was demonstrated by the high concentration of Alexa Fluor™ 647 visualized through the two-photon microscope on the superficial layer part of the olfactory tissue, as can be seen in **Figure 1**. The presence of Alexa Fluor 647 and therefore the olfactory neurons is highlighted by the red signal and is visibly homogeneously distributed on the surface of the olfactory tissue.

Moreover, as can be seen in the XZ (**Figure 1A**) and 3D (**Figure 1B**) overviews, it was highlighted the presence of tubular structures (indicated by yellow arrows) passing through the entire thickness of the tissue and connected to cell nuclei located in the medium-upper part of the tissue, marked by DAPI. The tubular structures appeared green because of the autofluorescence of the tissue. Probably, these structures can be identified as fibrous nerve bundles composing the lamina propria of the olfactory epithelium as illustrated in a histological study of the rabbit nasal mucosa done by Pereira *et al.*[9] (**Figure 1D**).

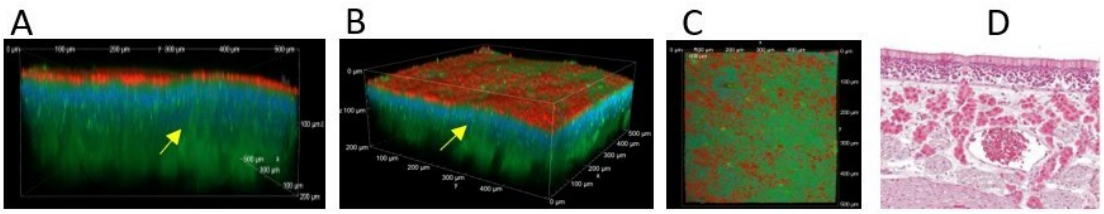

Figure 1 *- Olfactory region of rabbit's nasal mucosa marked with anti-Olfactory Marker Protein as primary antibody, Alexa Fluor™ 647 as secondary antibody (red) and DAPI (blue). A) XZ overview. B) 3D overview. C) XY overview.*
Excitation wavelength: 820 nm. The two-photon microscope analysis showed the presence of nerve bundles (yellow arrows) characterizing the lamina propria of the olfactory nasal mucosa and colored in green because of the autofluorescence of the tissue. D) Histological studies from Pereira et al. showing the structure of the olfactory nasal mucosa in which can be clearly recognized nerve bundles connecting the surface of the tissue to the lamina propria.

The presence of Alexa Fluor 647, therefore olfactory nerves, on the surface of the tissue was further unequivocally confirmed by the acquisition of the emission spectrum (**Figure 2**) at different depths in the tissue. Indeed, when the surface of the tissue is not completely flat, the two-photon microscope allows to analyze simultaneously the different levels of depth of the same slice of tissue, giving information regarding both the surface and the in-depth regions. As can be seen in **Figure 2**, the red signal of Alexa Fluor 647 was only detected on the surface of the tissue, while disappeared moving towards deeper regions that appeared blue because of the nuclei-marker DAPI. This probably happens because the primary antibody selected to bind olfactory neurons can just bind superficial parts of the nerve structure and therefore the entire structure of the nerve bundle penetrating across the tissue cannot be stained and visualized entirely.

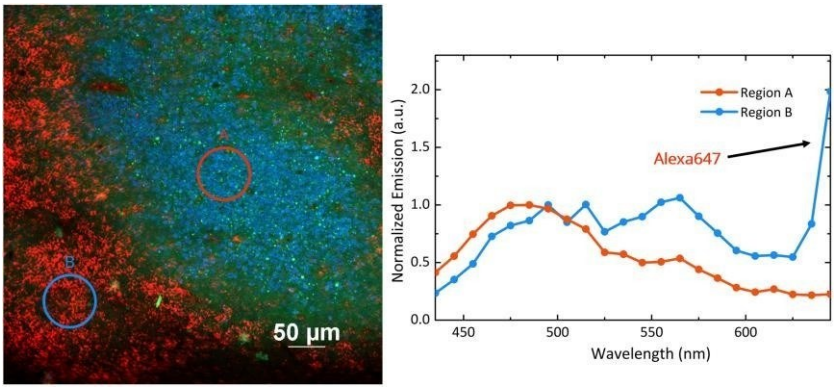

Figure 2 *- Bidimensional image of a non-flat zone of the olfactory tissue. Both the surface (red region identified by the blue circle) and the inner (blue region identified by the red circle) layer can be observed in the same image (left). A) inner region in which Alexa Fluor 647 is not detected. B) surface region in which the signal of Alexa Fluor 647 is detectable. The emission spectrum of the two regions acquired at 820 nm is also reported (right) and it was exploited to unequivocally identify the presence of the secondary antibody and therefore olfactory neurons.*

3.1.2 Olfactory region marked with anti-OR10R2

The presence of olfactory neurons in the olfactory region of the nasal mucosa was also confirmed by treating the tissue with anti-OR10R2 antibody. Also in this case, as previously observed by using the anti-OMP antibody, just the superficial part of the neuron was targeted by the primary antibody and visualize thank to the red emission of the secondary antibody, while the extension of the neuron's structure was visible along the entire thickness of the tissue through the XY and 3D overview (**Figure 3A** and **3B**, yellow arrows). As already seen, cells nuclei turned out to be localized in the middle-upper part of the mucosa highlighted by DAPI (**Figure 3**, in blue). The analysis of an XY planar overview (**Figure 3C**) of the olfactory region in which the surface of the tissue was not flat confirmed the ability of Alexa Fluor 647 to just bind the superficial part of the neuron. When this region was excited at 820 nm indeed, the surface emitted in the red region, confirming the presence of Alexa Fluor 647, while the deeper part appeared green-blue due to just the autofluorescence of the tissue (**Figure 4**).

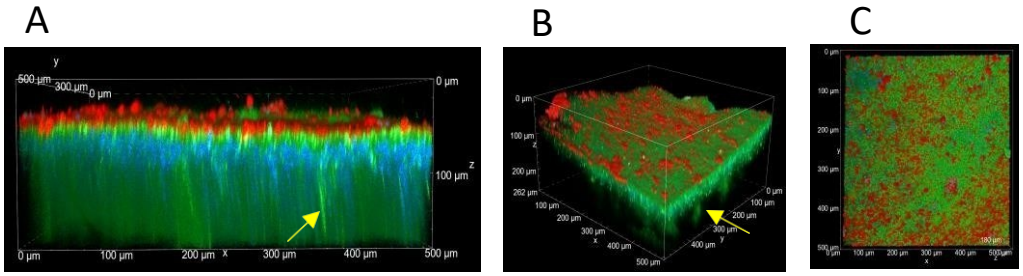

Figure 3 *- Olfactory region of rabbit's nasal mucosa marked with anti-OR10R2 as primary antibody, Alexa FluorTM 647 as secondary antibody (red) and DAPI (blue). A) XZ overview. B) 3D overview. C) XY overview. The presence of nerve bundles crossing the thickness of the tissue can be clearly identified (yellow arrows). Excitation wavelength: 820. nm.*

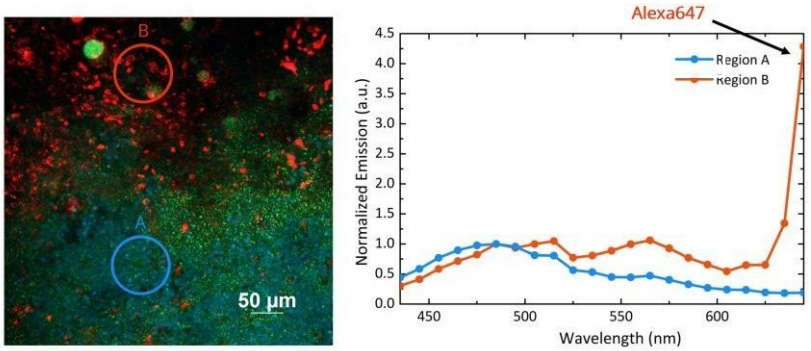

Figure 4 *- XY overview of the olfactory region of rabbit's nasal mucosa marked with anti-OR10R2 antibody, Alexa Fluor 647 and DAPI and excited at 820 nm. The non-flat region of the tissue allowed to analyze at the same time different layers of the same tissue and distinguish the area in which Alexa Fluor 647 was specifically bound to the tissue (left, region B) from the one in which it was not bound, corresponding to the deeper part of the tissue (left, region A). The presence of Alexa Fluor 647 was unequivocally determined by the acquisition of the emission spectrum (right).*

3.2 Immunostaining of the Respiratory region

3.2.1 Respiratory region marked with anti-β IV Tubulin

The images acquired by microscope confirmed the wide presence of cilia homogeneously distributed on the surface layer of the respiratory region (**Figure 5A**), bound by the primary antibody and clearly visible thank to the secondary antibody that, at the wavelength used to excite the tissue, emitted in the green region. As expected, being superficial structures, cilia disappeared when deeper layers of the tissue were analyzed, as shown in **Figure 5B**, where a non-flat area of the tissue was analyzed, allowing to observe at the same time different depth levels of the same structure.

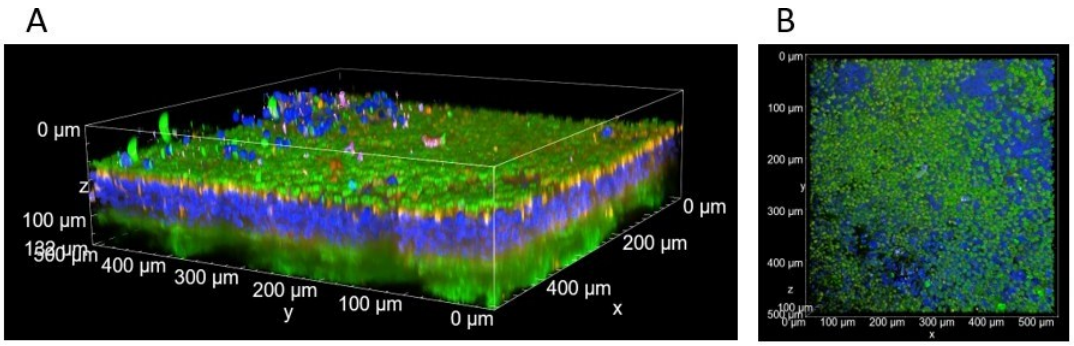

Figure 5 *- Respiratory region of rabbit's nasal mucosa marked with anti-β IV Tubulin antibody, Alexa Fluor™ 488 (bright green) and DAPI (blue). A) 3D overview. B) XY overview of a non-flat region allowing to observe at the same time different depths of the same slice of tissue. The surface of the tissue is homogeneously covered by a layer of cilia emitting in the green region due to the secondary antibody, while the nuclei of the underlying cells are in blue because they are marked with DAPI. Excitation wavelength: 1000 nm.*

Thanks to both the 3D-scan and the XY overview acquired by the two-photon microscope, the typical structure of the respiratory region could be clearly recognized. Indeed, the tissue can be ideally divided into three different sections. From the top (*i.e.,* the surface of the tissue directly in contact with the external environment) to the bottom (*i.e.,* the part of the tissue anchored to the nasal septum) it is possible to distinguish: a compact layer of cilia targeted by the primary antibody (*i.e*., anti-β IV Tubulin antibody) the not-targeted tissue with cellular nuclei marked by DAPI, and finally the presence of collagen fibers belonging to the nasal septum (**Figure 6A and 6B**). Collagen was clearly and unequivocally identified by the typical signal called "second harmonic generation" (SHD).

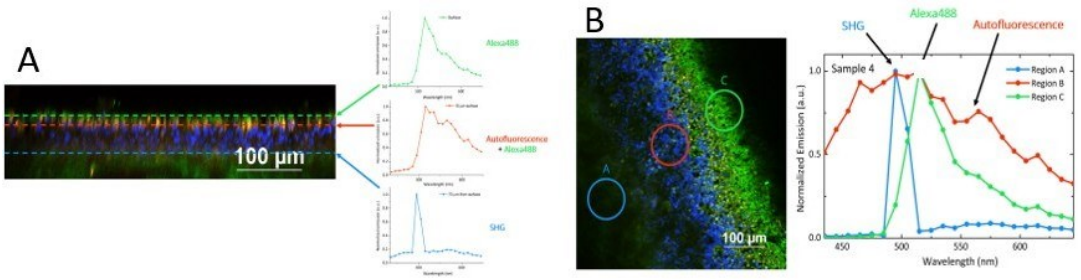

Figure 6 *- Emission spectra acquired at different depths of the respiratory region of the nasal mucosa analyzing both a 3D image (A) and an XY overview in which the surface of the tissue is not completely flat (B). From the top to the bottom of the tissue, three different sections can be individuated: the superficial ciliated layer (highlighted by the green circle), the inner part of the tissue (highlighted by the red circle) and the collagen belonging to the underlying nasal septum which supports the tissue (highlighted by the blue circle).*

3.3 Comparison between the olfactory and the respiratory region

3.3.1 Nasal mucosa marked with anti-Olfactory Marker Protein antibody

To highlight the actual anatomical differences between the olfactory and the respiratory region of the nasal mucosa and confirm a prevalence of olfactory neurons in the olfactory area compared to the respiratory one, both the respiratory and the olfactory sections were incubated with the anti-OMP, using Alexa Fluor 647 as fluorescent dye.

As shown in **Figure 7,** it is evident that most of the surface of the olfactory region is characterized by the presence of the Olfactory Marker Protein due to the high expression of olfactory neurons (**Figure 7A**). The surface, indeed, appeared almost all colored in red because of the presence of the secondary antibody.

On the other hand, in the respiratory region, the presence of neuronal structures was rarely found (**Figure 7B**). Moreover, comparing the 3D images acquired by the two-photon microscope, it seems that the fluorescent dye was not specifically bound to the surface of the respiratory region due to a specific interaction with the antigen, but probably it had just remained as a residue on the top of the tissue following incubation.

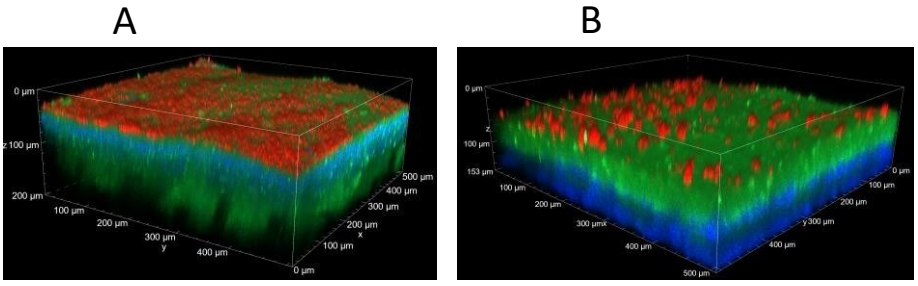

Figure 7 *- Comparison between the 3D acquisitions of the olfactory (A) and respiratory (B) region of the rabbit's nasal mucosa marked with the anti-Olfactory Marker Protein antibody using Alexa Fluor™ 647 (red) as secondary antibody. Excitation wavelength: 820 nm.*

3.3.2 Nasal mucosa marked with anti-β IV Tubulin antibody

To highlight the prevalence of ciliated cells in the respiratory region in comparison with the olfactory one, both the sections of the rabbit's nasal tissue were incubated with the anti-β IV Tubulin antibody, using Alexa Fluor 488 as fluorescent dye.

As shown in **Figure 8** below, the respiratory region is entirely covered by a thick layer of cilia, homogeneously distributed on all the surface of the tissue that appeared bright green (**Figure 8B**), while the presence of cilia is significantly less in the olfactory region (**Figure 8A**).

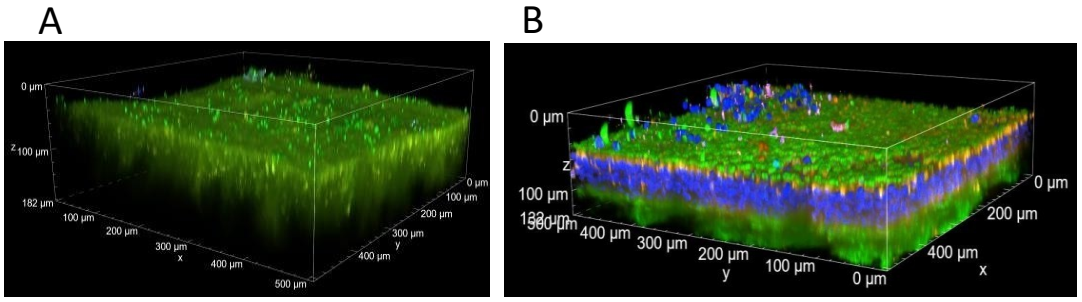

***Figure 8** - Comparison between the 3D acquisitions of the olfactory (A) and respiratory (B) region of the rabbit's nasal mucosa marked with the anti-β IV Tubulin antibody using Alexa Fluor™ 488 (bright green) as secondary antibody. Excitation wavelength: 1000 nm.*

3.4 Mucoadhesion study on rabbit nasal mucosa

After characterizing the rabbit's nasal mucosa by two-photon imaging, the tissue was exploited for mucoadhesive studies. For this purpose, the siRNA:TMC NP was used as nanocarrier model, whose mucoadhesive profile was tested and compared to the one of the raw Cy3-siRNA, exploiting a central region of the nasal mucosa. To quantify Cy3 used to label siRNA in the samples collected at predetermined timepoints during the experiment, the calibration curve shown in **Figure 9** was exploited.

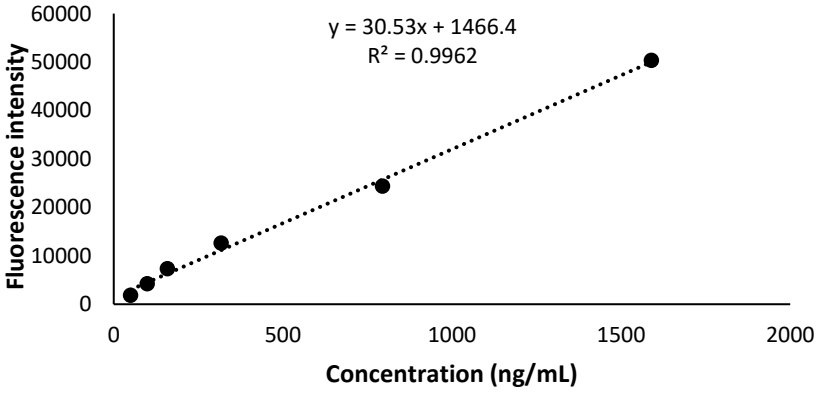

***Figure 9** – Cy3-labeled siRNA calibration curve used to quantify samples collected during the mucoadhesion experiments.*

The mucoadhesive study pointed out that, over the first 10 minutes of the experiment, the siRNA:TMC NP formulation turned out to be significantly more mucoadhesive than the non-formulated Cy3-siRNA (**Figure 10**). More precisely, around 56% of the formulation adhered to the tissue while only 30% of the free Cy3-siRNA was able to adhere to the mucosa. After 10 minutes, the raw Cy3-siRNA reached a minimum (15-20%) and the siRNA-TMC NP formulation slowly attained that minimum over 30 minutes, highlighting the formulation capacity to stick to the mucosa despite values were not significantly different mainly as a consequence of the high variability in the values obtained for the naked siRNA.

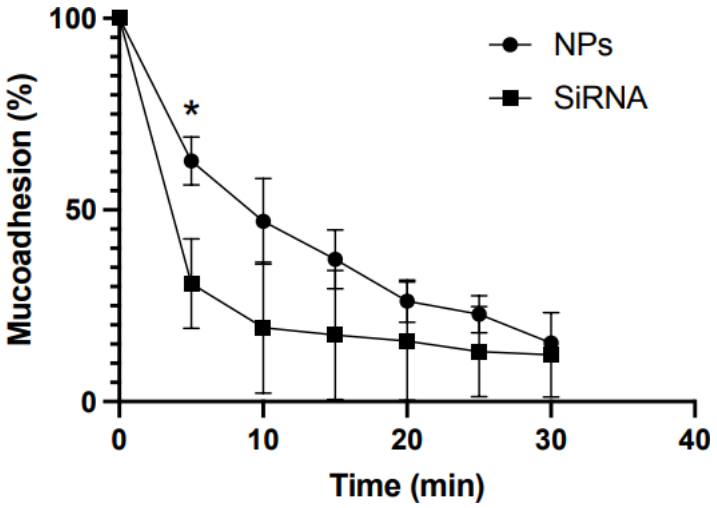

Figure 10 *- Mucoadhesion profile of siRNA:TMC NPs (1:20 siRNA:TMC w/w ratio) and free Cy3-siRNA obtained by applying the samples on* rabbit *nasal mucosa and then washing the tissue with water exploiting the inclined plane apparatus (n=6).*

Tissues treated with the Cy3 labelled NPs or free Cy3-siRNA were washed for 30 minutes and analyzed with the two-photon microscope (**Figure 11B-E**) alongside blank tissues analyzed as reference (**Figure 11A**). The surface of blank tissue was characterized by a broad emission (**Figure 12**) that fell mainly in the green channel. When exciting the sample at 1000 nm, the autofluorescence signal was overcome by the Cy3 emission. Moreover, beneath the surface in some regions of the tissue, the presence of collagen was detected thanks to the second harmonic generation signal generated by it. The results confirmed what was previously observed by the absorbance plate reader: after the washing period, the signal of Cy3 was still present on the surface of the tissues treated with free Cy3-siRNA and siRNA:TMC NP formulation. After the treatment with siRNA:TMC NPs, several aggregates were visible on the tissue, possibly because of the interaction between the NPs and the mucins present on the surface of nasal mucosal tissue (**Figure 11E**). The presence of these aggregates could be associated to an increased adhesion to the mucosa, consistent with the results obtained by using the fluorimeter.

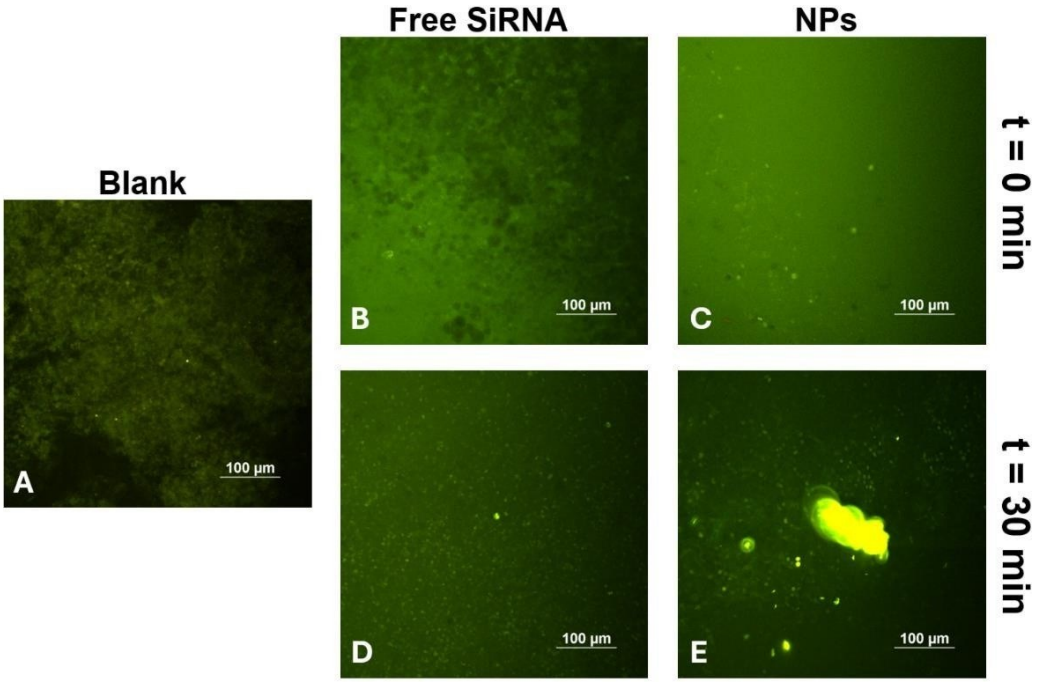

Figure 11 *– Analysis of the rabbit nasal mucosa surface by two-photon microscopy. Blank mucosa (A); mucosa treated with free Cy3-siRNA at time 0 (B) and after the 30 minutes washing period (D); mucosa treated with SiRNA:TMC NPs at time 0 (C) and after the 30 minutes washing period (E). All the images reported in the panels B-E have been acquired in the same experimental conditions (laser power and detector gain) exciting the tissues at 1000 nm.*

In order to verify the presence of Cy3 and have a semi-quantitative confirmation of what was observed from the images, we recorded emission spectra in correspondence of the focal planes of **Figure 11** images, reported in **Figure 12**. As expected, the signal of the non-treated mucosa used as control was the lowest. As regards the tissues treated with the NPs and the free Cy3-siRNA, the band shape of Cy3 was detected in all the cases, with a higher signal intensity in the former at the end of the mucoadhesion experiment (t=30 minutes, **Figure 12B**). The two-photon microscopy study confirms that the NPs have better mucoadhesive properties than the non-formulated Cy3-siRNA.

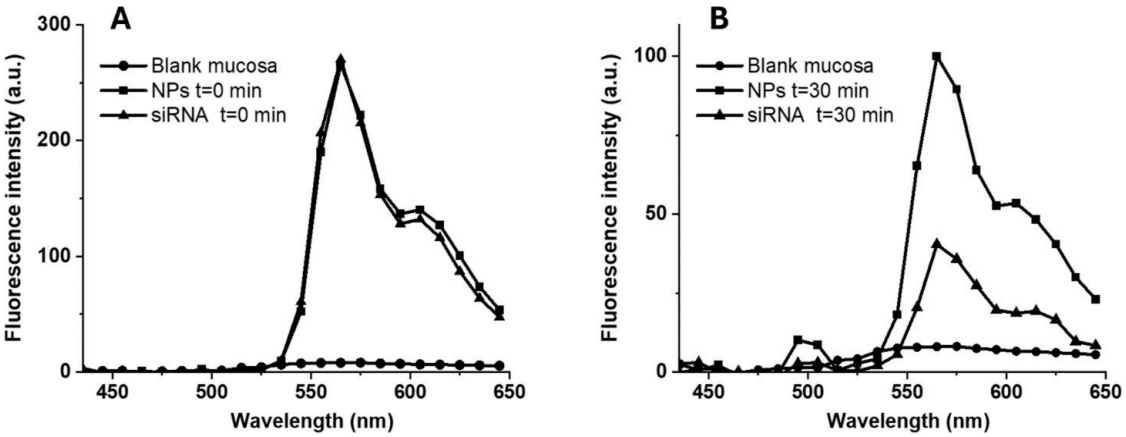

Figure 12 *- Emission spectra obtained from the rabbit nasal tissue as such (black circles) or treated with the raw Cy3-siRNA (black triangles) or SiRNA:TMC NPs (black squares) at the start (t=0 minutes, Panel A) and at the end of the mucoadhesion experiment (t=30 minutes, Panel B) in correspondence of the focal planes reported in Figure 11. All the emission spectra have been acquired in the same experimental conditions (laser power and detector gain) exciting the sample at 1000 nm.*

3.5 Mucopenetration study

The mucopenetration study performed on rabbit nasal mucosa demonstrated that the siRNA:TMC NP formulation (siRNA:TMC 1:20 w/w ratio) had a better ability to penetrate across the nasal tissue than the free Cy3-siRNA. As for mucoadhesion studies, also in this case a blank tissue was used as reference. Two nasal tissues have been analyzed by two-photon microscopy acquiring Z-stacks at different time points after the deposition on the mucosal surface of 20 µL of free Cy3-siRNA or siRNA:TMC NP formulation.

The images in **Figure 13** show the XZ view of five Z-stacks acquired at different time points of nasal tissue with the non-formulated Cy3-siRNA. In the Z-stacks, two different regions can be distinguished: a brighter one at the top, corresponding to the Cy3-siRNA solution, and a darker one at the bottom, corresponding to the mucosal tissue. The height of the Cy3-siRNA solution decreases over time, while the emission signal of the darker one does not significantly change, suggesting that the penetration of siRNA-Cy3 solution is weak or even insignificant within the mucosal tissue. The decrease of height of the Cy3-siRNA solution is attributed to the formulation spreading on the surface. This horizontal spreading occurred in approximately 45 minutes, after which the raw Cy3-siRNA seemed to have stabilized on the surface of the tissue and we no longer noticed any variation in the height of the fluorescent signal repeating the measurement after further 15 minutes (**Figure 13D-9E**).

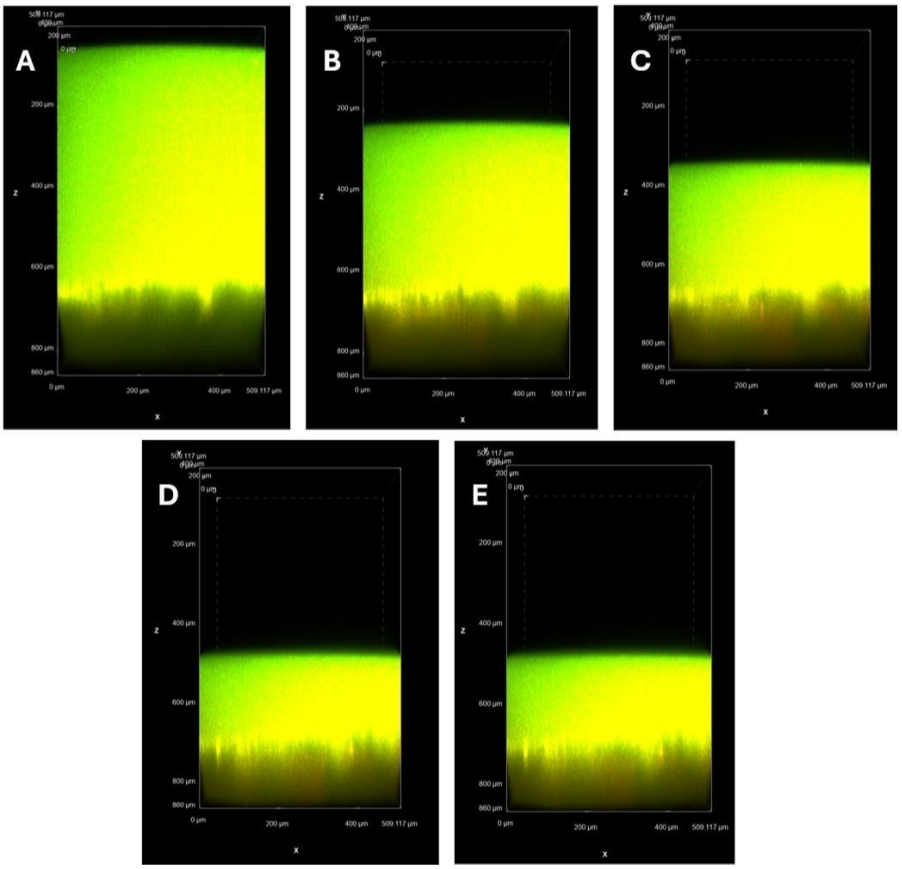

Figure 13 *– XZ views of the* 3D *renderings reconstructed from Z-stacks acquired on* the nasal tissue treated with the free Cy3-siRNA. The tissue was monitored over time *by two-photon microscopy exciting the sample at 1000 nm and* keeping the *same tissue region in* focus during the analysis. The pictures were acquired at time 0 (A), *and* after 10 minutes (B), 20 minutes (C), 35 minutes (D) and 45 minutes (E).

On the other hand, when the nasal tissue was treated with siRNA:TMC NPs (**Figure 14**), we observed a progressive penetration of the formulation across the tissue over two hours. Interestingly, as can be seen from the Z-stacks acquired with the two-photon microscope, the penetration of the NPs across the tissue seemed to take place by exploiting channels formed by the organization of the cells constituting the tissue (white arrows in **Figure 14**).

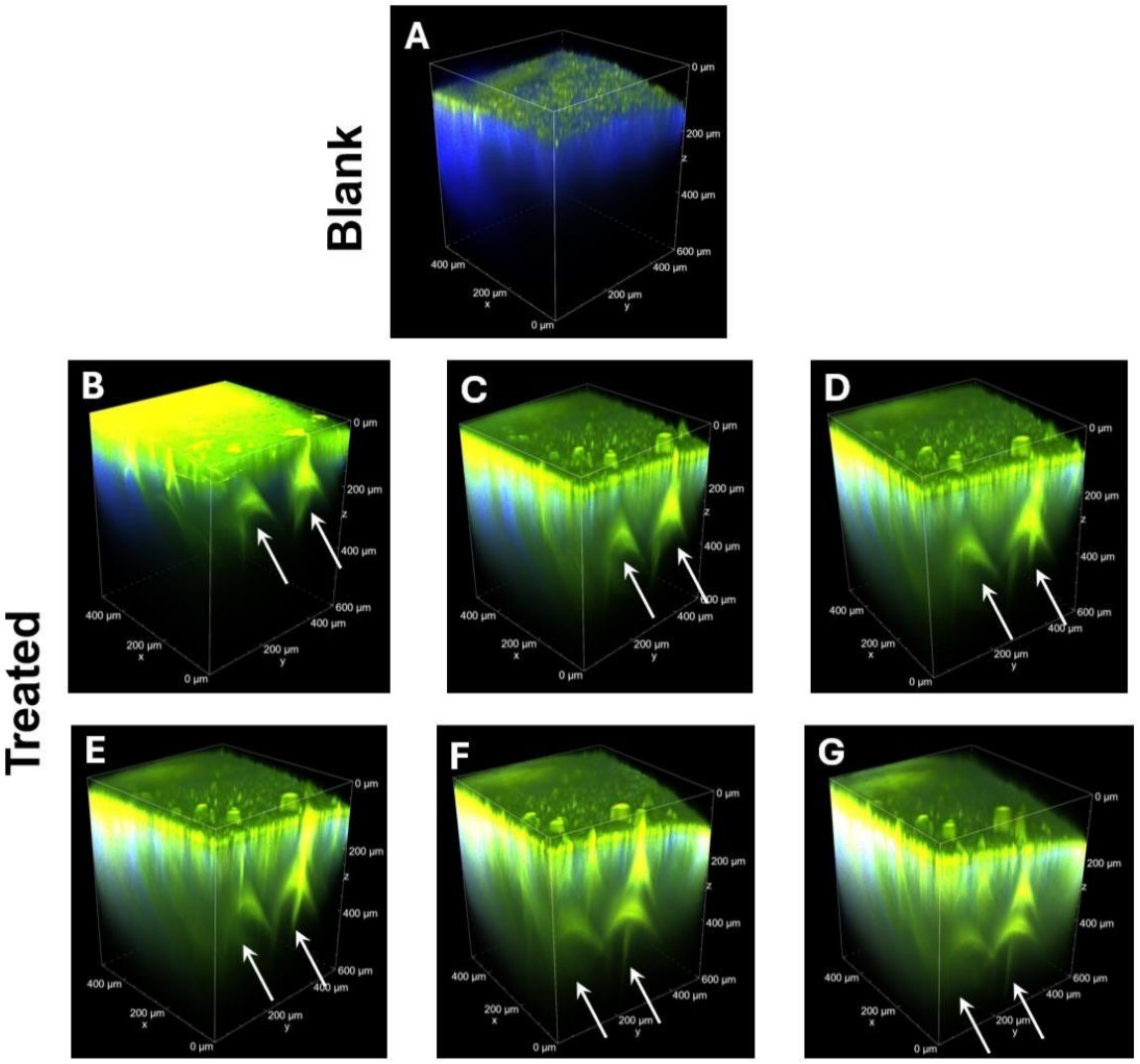

Figure 14 *– 3D images of the nasal mucosa treated with siRNA:TMC NPs (siRNA:TMC 1:20 w:w ratio) obtained with the two-photons microscope exciting the sample at λ=950 nm. The images were acquired at time 0 without treatment (A) and immediately after the treatment with siRNA:TMC NPs (B). Successively, images were acquired at 20 minutes (C), 40 minutes (D), 60 minutes (E), 90 minutes (F) and 120 minutes (G) after the treatment.*

After a permeation time of 60 minutes, we collected an emission spectrum at 300 µm of depth from the mucosal surface (**Figure 15**), to confirm the presence of Cy3. The emission of Cy3 (**Figure 15, red arrow**) as well as the SHG of collagen (**Figure 15, blue arrow**) were both clearly detectable, confirming that the NPs penetrated into the tissue. As expected, when we acquired the same emission spectrum from the blank mucosa before the NPs permeation, just the signal of collagen was detected.

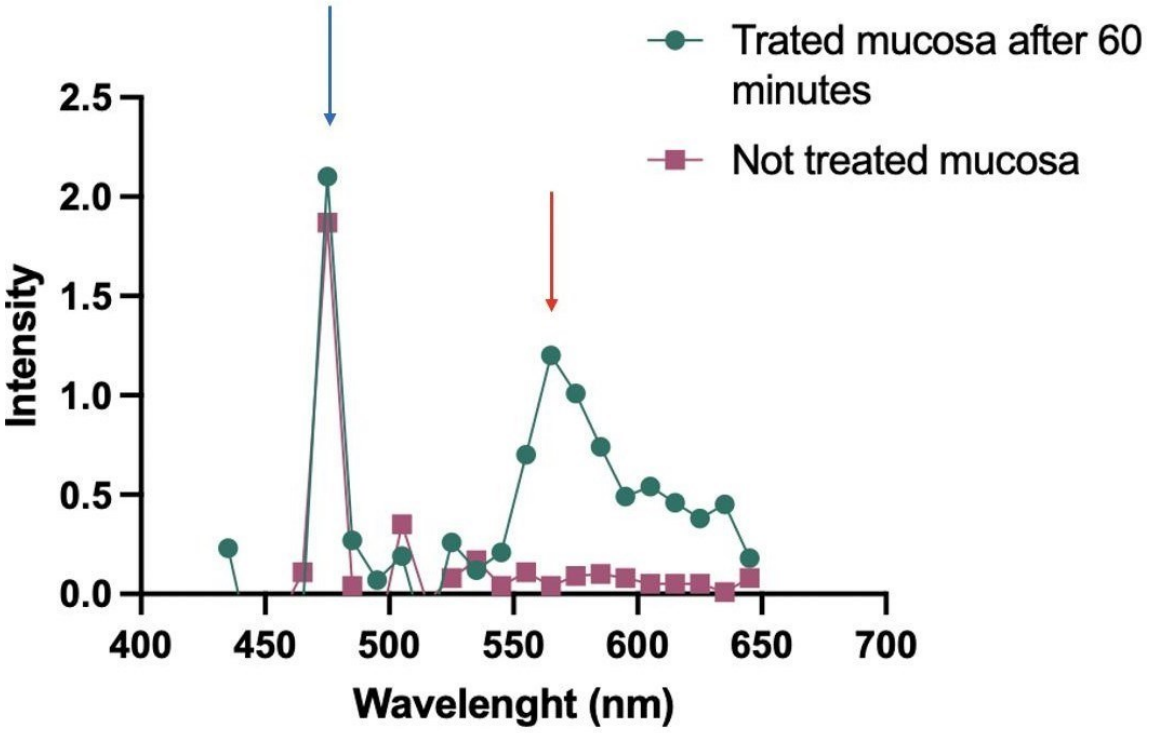

Figure 15 *– Emission spectra acquired at 300 µm of depth in the blank mucosa (before treatment) and after the permeation of siRNA:TMC NPs (siRNA:TMC 1:20 w:w ratio, 60 minutes of permeation time). The red arrow indicates the peak of Cy3 emission signal* at *565 nm recorded after the NPs permeation. The* SHG signal *(blue arrow) indicates the presence of collagen.*

Figure 16A shows the increase of Cy3 signal over time at different depths in the tissue after the permeation of the siRNA:TMC NPs. Cy3 emission resulted more intense at 200 µm of depth and progressively decreased at 400 µm and 600 µm, proving that the penetration of the formulation across the tissue was gradual. Comparing the signal variations over time following treatment with free Cy3-siRNA and the NP formulation (**Figure 16B**), the NP formulation exhibited a significantly stronger increase in Cy3 emission signal. This result clearly supports the enhanced penetration of the siRNA:TMC NPs compared to the non-formulated Cy3-siRNA. After only 20 minutes of permeation, the signal observed from the NPs at a depth of 200 µm showed an almost 3-fold increase when compared to the initial value, while the signal for the free Cy3-siRNA remained practically constant throughout the experiment.

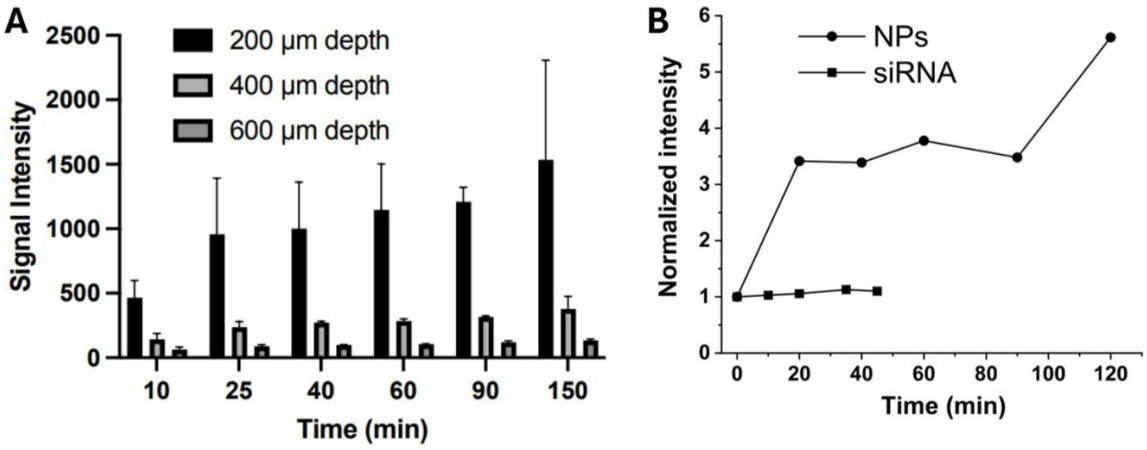

Figure 16 *– Trend of the Cy3 signal intensity analyzed at different timepoints after treating the rabbit nasal tissue with siRNA:TMC NPs (siRNA:TMC 1:20 w:w ratio) or free Cy3-siRNA. (A) Cy3 signal monitored at different depths after the permeation of the NP formulation (sample excited at 1000 nm). The standard deviations were calculated from a replicate of the measurements. (B) Comparison of Cy3 signal variations after treating the rabbit nasal tissue with siRNA:TMC NPs or free Cy3-siRNA, measured at 200 µm (sample excited at 950 nm) and 150 µm (sample excited at 1000 nm) of depth from the surface, respectively. The signal at each timepoint has been normalized with respect to the signal at the beginning of the penetration experiment.*

4. DISCUSSION

The immunostaining experiments performed by the two-photon microscope used to analyze the rabbit nasal mucosa confirmed that there are anatomical features that significatively distinguish the olfactory region from the respiratory one. More precisely, these experiments pointed out the similarities between different species such as humans and other mammals including rabbits. Indeed, here we demonstrated the existence of neuroepithelium characterizing the olfactory epithelium, which was already identified by the in-depth study of the human nasal mucosa mentioned in literature [36].

To detect the neuronal structure in the olfactory region, two different olfactory antigens were selected as tags: the Olfactory Marker Protein (OMP) and the Olfactory Receptor, family 10, subfamily R, member 2 (OR10R2). Two different primary antibodies were used to specifically bind the selected tags, and they could be visualized thanks to the labeling of secondary with Alexa Fluor™ 647, a near-infrared-fluorescent dye. This aspect is relevant, since this dye can be excited at 820 nm originating a typical emission spectrum, while at the same wavelength the auto-fluorescence signal typical of the non-targeted area of the tissue is avoided, therefore any interferent signal could be obtained.

OMP is a small cytoplasmatic protein characterizing the nasal mucosa of vertebrates, since it is expressed in mature olfactory receptor neurons, specialized in the detection of odorant stimuli [15]. Even if the role of this protein is not yet completely clear, some studies have shown that it is

activated in the early stage of olfactory transduction[15]. Two important features of this protein make it an ideal element to analyze the characteristics of the nasal mucosa exploiting, as in this case, immunostaining techniques: the first is its specificity, since it is widely expressed in the chemosensory systems [21,22]; the second consists in its phylogenetic conservation, meaning that its expression pattern is similar among the vertebrate species [23]. Moreover, even if the olfactory epithelium is composed of several types of different cells, none of them express OMP, which is just expressed in mature olfactory neurons [15,21,22].

The second specific antigen selected as a tag for the neurons in the olfactory region was OR10R2, that belongs to the Odorant Receptor (OR) protein family, consisting of G-protein coupled receptors of a considerable size that are selectively expressed in olfactory sensor neurons in vertebrates [16]. It is located in the superficial part of the olfactory neurons, *i.e.,* at the level of the cilia exploited by the neuron to capture the olfactory signals from the external environment [24–26]. The images acquired by the two-photon microscope exploiting the two antigens cited above were completely in line with the description of the olfactory nasal mucosa found in literature, in which the olfactory neurons are described as bipolar structures having the soma localized in the middle portion of the nasal epithelium [15]. The olfactory region is characterized by the extensive presence of neurons, whose amount gradually decreases moving towards the respiratory region. Our findings corroborate others reported in literature and performed on human nasal mucosa [36], showing that the neuronal structures present at the level of the olfactory mucosa extend through the lamina propria towards the brain.

Moreover, the microscope analysis highlighted that in the olfactory region it is possible to identify different types of cells organized in different layers: basal, intermediate and apical, as reported for humans [36]; however, the distinction between the three layers cannot be considered net as it is in humans, since it is less evident as reported for other species such as rodents [36].

The respiratory region as well was characterized by microscopy; in this case, the selected tag was β IV tubulin and the secondary antibody used to bind the primary antibody against this antigen was labeled with Alexa Fluor™ 488, a green-fluorescent dye.

β IV tubulin is an ubiquitous structural protein characterizing the microtubules and it is present in mammals in all the ciliated cells, including the respiratory epithelial cells and the olfactory neurons [17]. It is characterized by an aminoacidic sequence that is considered one of the most highly conserved in evolution, since among all the species the sequence is almost the same [17]; this aspect makes the antibody used in this work specific also against rabbit's tissue, even if it was originally designed to recognize the antigen just in mouse and human. Importantly, all the isotypes of β tubulin are present in olfactory cilia, while just two (among which the IV isotype) can be found in the respiratory epithelial cells [27].

The images acquired by the two-photon microscope reflected what is described in literature; the respiratory region appeared as a multi-layer of cells that express cilia in their superficial part, giving rise to a compact layer of cilia each having an experimental measured dimension of ~ 9 µm, consistent with the size reported in literature which is approximately 5-10 µm [28].

In this work, it was demonstrated that the number of cilia is significantly higher in the respiratory region than in the olfactory one. A certain number of cilia was also detected in the olfactory epithelium. Indeed, these are the cilia expressed by the mature Olfactory Receptor Neurons (ORN) which contribute to the transduction of the odor stimulus into a generator potential that travel to the olfactory bulb [15] and they are non-motile, so not involved in the muco-ciliary clearance [7].

The mucociliary clearance, consisting in the interaction between the nasal mucus and the ciliary beating, is potentially responsible for the early removal of the administered compound from the absorption site [4]. For this reason, to allow the brain absorption of the intranasally administered drug, it is important to avoid its deposition on the respiratory region of the nasal mucosa. Indeed, for nose to brain delivery purposes, the administered drug should be delivered to the olfactory part, giving that the olfactory neurons represent a direct connection between the nasal mucosa and the olfactory bulb localized in the brain [15]. In this way, the brain absorption of the administered formulation as such or the released drug can be optimized, thus the active compound can be absorbed from the neuron and directly delivered to the brain through the nose to brain pathway.

The e*x vivo* studies performed on a central and therefore transitional region of the rabbit nasal mucosa by two-photon microscopy pointed out that the siRNA-loaded NPs were able to adhere and penetrate across the nasal mucosa layer. The siRNA TMC NP formulation indeed, showed a well-defined tendency to interact with the surface of the mucosa as evidenced by the fact that the formulation formed aggregates possibly as a result of the interaction with the physiological nasal secretions and mucins in particular. As expected, the NP formulation turned out to be more mucoadhesive than the free Cy3-siRNA under a continuous aqueous flow simulating the physiological mucociliary clearance activity. Indeed, the naked Cy3-siRNA was washed away after 10 minutes, while the formulation reached the same minimum value after 30 minutes. Furthermore, the images acquired with the two-photon microscope to visualize the nasal mucosa treated with siRNA-loaded TMC NPs after 30 minutes of washing confirmed the presence of Cy3 used to label siRNA. These results are in agreement with those already shown in literature [29], showing the remarkable mucoadhesive properties of TMC.

The Z-scans of the nasal tissue obtained from permeation experiments showed that siRNA:TMC NPs favor the penetration of the Cy3 fluorescence in the tissue via preferential channels. Moreover, the penetration in the tissue increased over time, and 60 minutes after the treatment Cy3 emission signal was detected at 620 µm from the surface. This was probably due to the presence of TMC that

is characterized by well-known absorption enhancing properties attributed to its positively charged quaternary amino group on C-2 position that can electrostatically interact with anionic groups belonging to epithelial cells' surface glycoproteins and tight junctions [30,31]. Thus, TMC can open the tight junctions [32] improving the passage of the NPs or the cargo as such across the tissue exploiting a paracellular transport [30]. The mechanism behind the TMC ability of opening the tight junctions has been widely explored and it emerged that several elements are involved in the permeation enhancing. First, the binding between TMC and the tight junctions consists of an electrostatic interaction between the positively charged TMC and negatively charged sites on the tight junctions [33]. Then, the epithelial permeability can be enhanced because of the interaction between chitosan and claudin-4, the principal protein conferring to the tight junctions their characteristic barrier properties [34]. This mechanism was demonstrated through *in vitro* immunofluorescence staining experiments by Zhang *et al.* [34]. Moreover, it has been proposed that TMC could also improve the permeation of compounds across the epithelial barrier by interacting with the transmembrane protein occludin and altering its conformation, as reported by van der Merwe *et al.* [33]. The efficacy of TMC as penetration enhancer has already been confirmed in *ex vivo* studies done by Amidi *et al.* [35], that observed the penetration profile of protein-loading TMC nanoparticles across rat's nasal mucosa by confocal laser scanning microscopy. After treating the tissue with either the TMC nanoparticles or the raw cargo used as reference, the group confirmed the presence of nanoparticles inside the cytoplasmatic compartment of cells, while any signal was detected using the raw protein.

Similarly, in this study, the non-formulated Cy3-siRNA turned out to be less mucoadhesive than the formulated one. In addition to this, the results from this work allowed us to hypothesize a better permeation profile across the mucosal tissue when the NP formulation was exploited as drug delivery system compared to the raw Cy3-siRNA.

Finally, it must be underlined that the studies shown in this work aiming at analyzing the mucoadhesion and mucopenetration profile of chitosan nanoparticles, were done on a generic part of the nasal mucosa that is likely a transitional region between the olfactory and the respiratory region. However, considering the anatomical and physiological differences between the two mentioned areas, further studies are required to assess the difference in terms of adhesion and permeation across both one and the other regions.

5. CONCLUSION

The immunostaining study carried out in this work allowed to in depth understand the anatomical features distinguishing the olfactory from the respiratory region. The imaging analysis confirmed the anatomical description of the nasal mucosa reported in literature and allowed to increase the knowledge about the characteristics of the nasal tissue. Indeed, the characterization of the nasal mucosa done by the two-photon microscope pointed out that there is not an ideal net separation between the respiratory region to the olfactory one, but there are structures, such as cilia, common to both. Therefore, the main differences consist in the concentration, organization and function that those structures have in the different areas of the nasal epithelium. The studies performed to assess the drug adhesion to the tissue and its penetration across it with and without the use of a nanocarrier, highlighted the importance of intranasally administering drugs by suitable delivery systems, such as nanoparticles, to enhance mucoadhesion and guarantee the penetration across the mucus layer and the absorption through the tissue.

REFERENCES

1. Suman JD. Current understanding of nasal morphology and physiology as a drug delivery target. *Drug Deliv Transl Res*. 2013;3(1):4-15. doi:10.1007/s13346-012-0121-z
2. Ghori, Muhammad U., Mahdi, Mohammed H., Smith, Alan M. and Conway BR. Nasal Drug Delivery Systems: An Overview. *Am J Pharmacol Sci*. 2015;3(5):110-119. http://eprints.hud.ac.uk/id/eprint/26635/
3. Samaridou E, Alonso MJ. Nose-to-brain peptide delivery – The potential of nanotechnology. *Bioorganic Med Chem*. 2018;26(10):2888-2905. doi:10.1016/j.bmc.2017.11.001
4. Marttin E, Schipper NGM, Coos Verhoef J, Merkus FWHM. Nasal mucociliary clearance as a factor in nasal drug delivery. *Adv Drug Deliv Rev*. 1998;29(1-2):13-38. doi:10.1016/S0169-409X(97)00059-8
5. Monteiro-Riviere NA, Popp JA. Ultrastructural characterization of the nasal respiratory epithelium in the rat. *Am J Anat*. 1984;169(1):31-43. doi:10.1002/aja.1001690103
6. Sonvico F, Clementino A, Buttini F, et al. Surface-modified nanocarriers for nose-to-brain delivery: From bioadhesion to targeting. *Pharmaceutics*. 2018;10(1):1-34. doi:10.3390/pharmaceutics10010034
7. McClintock TS, Khan N, Xie C, Martens JR. Maturation of the olfactory sensory neuron and its Cilia. *Chem Senses*. 2020;45(9):805-822. doi:10.1093/chemse/bjaa070
8. Morrison E, Menco B. *Morphology of the Mammalian Olfactory Epithelium: Form, Fine Structure, Function and Pathology*.; 2003. doi:10.1201/9780203911457.ch2
9. Pereira ME, MacRi NP, Creasy DM. Evaluation of the rabbit nasal cavity in inhalation studies and a comparison with other common laboratory species and man. *Toxicol Pathol*. 2011;39(5):893-900. doi:10.1177/0192623311409594
10. Esquinas P, Botero L, Patiño MDP, Gallego C, Iregui C. Ultrastructural comparison of the nasal epithelia of healthy and naturally affected rabbits with pasteurella multocida A. *Vet Med Int*. 2013;2013. doi:10.1155/2013/321390
11. Villamayor PR, Cifuentes JM, Quintela L, Barcia R, Sanchez-Quinteiro P. Structural, morphometric and immunohistochemical study of the rabbit accessory olfactory bulb. *Brain Struct Funct*. 2020;225(1):203-226. doi:10.1007/s00429-019-01997-4
12. Phan TG, Bullen A. Practical intravital two-photon microscopy for immunological research: Faster, brighter, deeper. *Immunol Cell Biol*. 2010;88(4):438-444. doi:10.1038/icb.2009.116
13. König K. Multiphoton microscopy in life sciences. *J Microsc*. 2000;200(2):83-104. doi:10.1046/j.1365-2818.2000.00738.x

14. von Andrian UH, Mempel TR. Homing and cellular traffic in lymph nodes. *Nat Rev Immunol*. 2003;3(11):867-878. doi:10.1038/nri1222
15. Dibattista M, Al Koborssy D, Genovese F, Reisert J. The functional relevance of olfactory marker protein in the vertebrate olfactory system: a never-ending story. *Cell Tissue Res*. 2021;383(1):409-427. doi:10.1007/s00441-020-03349-9
16. Mombaerts P. Molecular biology of odorant receptors in vertebrates. *Annu Rev Neurosci*. 1999;22:487-509. doi:10.1146/annurev.neuro.22.1.487
17. Jensen-Smith HC, Ludueña RF, Hallworth R. Requirement for the βI and βIV tubulin isotypes in mammalian cilia. *Cell Motil Cytoskeleton*. 2003;55(3):213-220. doi:10.1002/cm.10122
18. R&D Biosystems. Protocol for Making a 4 % Formaldehyde Solution in PBS. 2013;(44):529449.
19. Guareschi F, Del Favero E, Ricci C, et al. Cyclosporine A micellar nasal spray characterization and antiviral action against SARS-CoV-2. *Eur J Pharm Sci*. 2024;193:106673. doi:10.1016/j.ejps.2023.106673
20. Sandri G, Saporito F, Ferrari F, Bonferoni MC, Rossi S, Caramella C. In vitro evaluation of a protective nasal spray: Measurements of mucoadhesion and reconstructive barrier properties towards a tracheobronchial reconstruct. *J Drug Deliv Sci Technol*. 2015;30:368-374. doi:10.1016/j.jddst.2015.09.013
21. Hartman BK, Margolis FL. Immunofluorescence localization of the olfactory marker protein. *Brain Res*. 1975;96(1):176-180. doi:10.1016/0006-8993(75)90593-4
22. Monti-Graziadei GA, Margolis FL, Harding JW, Graziadei PP. Immunocytochemistry of the olfactory marker protein. *J Histochem \& Cytochem*. 1977;25(12):1311-1316. doi:10.1177/25.12.336785
23. Keller A, Margolis FL. Immunological studies of the rat olfactory marker protein1. *J Neurochem*. 1975;24(6):1101-1106. doi:10.1111/j.1471-4159.1975.tb03883.x
24. Koshimoto H, Katoh K, Yoshihara Y, Mori K. Distribution of putative odour receptor proteins in olfactory epithelium. *Neuroreport*. 1992;3(6).
25. Koshimoto H, Katoh K, Yoshihara Y, Nemoto Y, Mori K. Immunohistochemical demonstration of embryonic expression of an odor receptor protein and its zonal distribution in the rat olfactory epithelium. *Neurosci Lett*. 1994;169(1):73-76. doi:10.1016/0304-3940(94)90359-X
26. Menco BPHM, Cunningham AM, Qasba P, Levy N, Reed RR. Putative odour receptors localize in cilia of olfactory receptor cells in rat and mouse: a freeze-substitution ultrastructural study. *J Neurocytol*. 1997;26(10):691-706. doi:10.1023/A:1018554029186

27. Woo K, Jensen-Smith HC, Ludueña RF, Hallworth R. Differential synthesis of β-tubulin isotypes in gerbil nasal epithelia. *Cell Tissue Res*. 2002;309(2):331-335. doi:10.1007/s00441-002-0591-2

28. Beule AG. Physiology and pathophysiology of respiratory mucosa of the nose and the paranasal sinuses. *GMS Curr Top Otorhinolaryngol Head Neck Surg*. 2010;9:Doc07. doi:10.3205/cto000071

29. Pardeshi C.V., Belgamwar V.S. Improved brain pharmacokinetics following intranasal administration of N,N,N-trimethyl chitosan tailored mucoadhesive NLCs. *Mater Technol*. 2020;35(5):249-266. doi:10.1080/10667857.2019.1674522

30. Kotzé AF, Lueßen HL, de Boer AG, Verhoef JC, Junginger HE. Chitosan for enhanced intestinal permeability: Prospects for derivatives soluble in neutral and basic environments. *Eur J Pharm Sci*. 1999;7(2):145-151. doi:10.1016/S0928-0987(98)00016-5

31. Kotzé AF, Lueßen HL, de Leeuw BJ, de Boer (A)Bert G, Coos Verhoef J, Junginger HE. Comparison of the effect of different chitosan salts and N-trimethyl chitosan chloride on the permeability of intestinal epithelial cells (Caco-2). *J Control Release*. 1998;51(1):35-46. doi:10.1016/S0168-3659(97)00154-5

32. du Plessis LH, Lubbe J, Strauss T, Kotzé AF. Enhancement of nasal and intestinal calcitonin delivery by the novel Pheroid™ fatty acid based delivery system, and by N-trimethyl chitosan chloride. *Int J Pharm*. 2010;385(1):181-186. doi:10.1016/j.ijpharm.2009.10.031

33. Van Der Merwe SM, Verhoef JC, Verheijden JHM, Kotzé AF, Junginger HE. Trimethylated chitosan as polymeric absorption enhancer for improved peroral delivery of peptide drugs. *Eur J Pharm Biopharm*. 2004;58(2):225-235. doi:10.1016/j.ejpb.2004.03.023

34. Zhang J, Zhu X, Jin Y, Shan W, Huang Y. Mechanism study of cellular uptake and tight junction opening mediated by goblet cell-specific trimethyl chitosan nanoparticles. *Mol Pharm*. 2014;11(5):1520-1532. doi:10.1021/mp400685v

35. Amidi M, Romeijn SG, Borchard G, Junginger HE, Hennink WE, Jiskoot W. Preparation and characterization of protein-loaded N-trimethyl chitosan nanoparticles as nasal delivery system. *J Control Release*. 2006;111(1-2):107-116. doi:10.1016/j.jconrel.2005.11.014

36. Borgmann-Winter K, Willard SL, Sinclair D, et al. Translational potential of olfactory mucosa for the study of neuropsychiatric illness. Transl Psychiatry. 2015;5(3):e527-e527. doi:10.1038/tp.2014.141

GENERAL CONCLUSION

GENERAL CONCLUSION

The research work illustrated in this Doctoral Thesis aimed at exploring and demonstrating the remarkable versatility of the intranasal (IN) route for the administration of drugs having a preventive or a therapeutic role against a wide range of diseases. Moreover, it was shown that IN administration can be exploited both for topical and systemic treatments, when drug absorption is required. In addition, even if this aspect was not developed in this work, the nasal route also represents a safe and efficient choice for the administration of vaccines. In addition to vaccines, that are preventive therapies *par excellence*, also products aimed at acting as barrier against inhaled pathogens can be intranasally administered. It is noteworthy that nasal barrier products have become dramatically important during the pandemic period to counteract SARS-CoV-2 infection's spread.

The advantages of IN administration have been widely illustrated in this thesis, as well as its limitations. Nanotechnology was exploited in this work to overcome the main issues characterizing the nasal delivery, comprehending the early removal from the deposition site caused by the mucociliary clearance and the need to bypass the superficial mucus layer to reach the epithelial absorption site. In addition to this, nano-systems were exploited to encapsulate and stabilize complex drugs and improve their bioavailability.

In particular, a biocompatible nano-sized drug delivery system consisting of polyethylene glycol 1000 succinate (TPGS) micelles was developed and optimized to encapsulate the poorly soluble peptide drug cyclosporine A (CSA) to enhance its efficacy via nasal administration. The chemical/physical features and the prolonged stability over time make TPGS micelles extremely suitable for IN administration of peptide drugs. Indeed, it was demonstrated that the extremely low particle size combined to the almost neutral PEGylated surface allowed the micelles to efficiently deal with the mucus layer overlying the nasal mucosa and rapidly penetrate across it to reach the epithelium.

The IN treatment with CSA-loading micelles turned out to be extremely versatile, since it was tested in two completely different pathological contexts, namely upper airways viral infections and neurological inflammatory disorders.

Indeed, the IN treatment with CSA formulated as micelles was proposed for both counteract early SARS-CoV-2 infection that mainly affects the upper airways, and as a prevention against neuroinflammation that is a remarkable key factor in the development of neurodegenerative diseases and depression. The efficacy against viral infection was confirmed *in vitro* and the results, combined with those obtained on an *ex vivo* model of nasal mucosa to simulate the IN administration, confirmed the promising antiviral activity of intranasally administered CSA encapsulated in micelles. Considering these promising results, the fundings of this work could be integrated with further in vivo safety and efficacy test, which could be also useful to clarify whether

the antiviral activity depends on a local effect or if it requires the absorption of the drug. This detail indeed, still needs to be clarified since the antiviral efficacy of the treatment was just assessed *in vitro*.

In addition to this, the neuroprotective properties of CSA-loaded TPGS micelles were confirmed *in vivo* on an LPS- injected mice model of neuroinflammation; in this case, micelles not only demonstrated to be suitable for IN administration, but also, turned out to be safeand suitable for Nose-to-Brain delivery of the peptide drug, that was not able to provide any noticeable effect when administered orally. However, the use of a mouse model as done in this Doctoral Thesis could be challenging, since the mouse's nasal anatomy is dramatically different from the human one. More precisely, since effective Nose-to-Brain delivery strongly depends on the ability of the drug to be precisely administered on the olfactory region of the nasal mucosa, the extremely limited area of the mouse's nasal mucosa could have limited the absorption surface and therefore the delivery to the brain. Fors this reason, in a future perspective, a most suitable animal model could be exploited to improve the translatability of data from the animal to the human and improve the predictability of the behavior of the micellar formulation once administered in human nose. For this purpose, a suitable candidate could be a rabbit model, since here we have demonstrated a remarkable similarity between rabbit's and human nasal mucosa.

In the context of a Nose-to-Brain delivery, the role of the olfactory epithelium appeared to be crucial and still poorly understood for lack of relevant *in vitro* and *ex vivo* models.

The immunohistochemical study of rabbit nasal mucosa performed in the context of this Doctoral Thesisdemonstrated the possibility to isolate the olfactory region of the animal nasal epithelium that is anatomically and histologically in close connection with the Central Nervous System (CNS). The presence of olfactory neurons potentially able to intake drug molecules and drive them to the brainhas been confirmed by the two-photon microscope analysis of the olfactory area of the tissue. Theseresults open to the possibility of exploiting this *ex vivo* model to better understand the fate of molecules, appropriately formulated and delivered with a nasal device allowing for deposition on the olfactory mucosa.

This has been demonstrated preliminary, through *ex vivo* experiments with the rabbit nasal mucosa performed using a trimethyl chitosan nanoparticle formulation encapsulating siRNA developed by another research group (Prof. Ravin Narain, University of Alberta, Edmonton, Canada). These results confirmed the crucial role that nanotechnology plays in Nose-to-Brain delivery. Indeed, the results included in the Doctoral Thesis demonstrated the chitosan-based polyplexes superiority not only in terms of interaction with the nasal mucosa but showed a remarkable enhancement penetration across the nasal epithelium in comparison with the non-formulated nucleic acid.

In conclusion, the administration of drug-encapsulating nano-sized drug delivery systems by IN

route represents an innovative and extremely versatile way to reach a topical, systemic or brain delivery of complex and challenging drugs including peptides, unstable or poorly bioavailable molecules.